The Hong Kong Polytechnic University

Department of Electronic and Information Engineering

DISTRIBUTED OPTICAL FIBRE SENSING SYSTEM BASED ON BRILLOUIN SCATTERING

MAO YUAN

A thesis submitted in partial fulfillment of the requirements for

The Degree of Doctor of Philosophy

August 2013

CERTIFICATE OF ORIGINALITY

I hereby declare that this thesis is my own work and that, to the best of my knowledge and belief, it reproduces no material previously published or written, nor material that has been accepted for the award of any other degree or diploma, except where due acknowledgement has been made in the text.

..... (Signed)

Mao Yuan ..... (Name of student)

ABSTRACT

Fiber optic sensing systems offer many advantages comparing with it electric counterpart such as small size, light weight, free from electromagnetic interference, easy to be multiplexed and ability of remote sensing over long distances. Systems based on the Brillouin optical fibre time domain analysis (BOTDA) technique enable simultaneous distributed strain and temperature measurement over a moderate range with high spatial resolution. They have found applications in many different areas.

The performance limitation of current BOTDA systems is addressed in this thesis. The factors limiting both the spatial resolution and the sensing range are analyzed. A scheme for measuring acoustic lifetime of different type of fibres has been proposed and results obtained. Coding technique and phase modulation are shown to be effective to enhance the signal to noise ratio of a BOTDA system and enable the realization of distributed sensing with high spatial resolution. The impact of optical pulse coding techniques on phase modulated Brillouin optical time domain analysis (BOTDA) systems is evaluated theoretically and experimentally.

Theoretical and experimental studies have been carried out to analyze and

compare the performance of BOTDA systems employing simplex coded and complementary coded pump pulses. Results obtained through the study show that both schemes demonstrate significant enhancement to SNR performance of the BOTDA systems. Key factors affecting the performance of a distributed sensing system with complementary code are identified. Using complementary coded pump pulses with pulse duration of 0.1ns, strain sensing over 20m of single mode fiber with 1 cm spatial resolution has been realized.

PUBLICATIONS ARISING FROM THE THESIS

Yuan Mao, Jie Li, and Chao Lu, “Coupling Characteristics between the Fundamental and High-order modes in a Photonic Crystal Fibre with a Filled Hole”, OECC 2009.

Jie Li, **Yuan Mao**, Chao Lu, Hwa Yaw Tam, and P. K. A. Wai, “Polarizing Properties of Photonic Crystal Fibers with High-Index Cladding Defects”, Journal of Lightwave Technology, Vol. 28, Issue 11, pp.1608-1614, 2010.

Li, J., **Mao, Y.**, Lu, C., Tam, H. Y., & Wai, P. K. A. “Polarization Splitting of Photonic Crystal Fiber With Hybrid Guidance Mechanisms”, Photonics Technology Letters, IEEE, Vol. 23, Issue 18, pp.1358-1360,2011.

Fernandez, A., **Mao, Y**., Lu, C., & Chi, J.“Combination of phase modulation and coding for SNR enhancement in distributed Brillouin sensors. Electronics letters, Vol. 47, Issue 8, pp.509-510, 2011.

Mao, Y., Guo, N., YU, K., Tam, H., & Lu, C.“1cm spatial resolution Brillouin optical time domain analysis based on bright pulse Brillouin gain and complementary code”, IEEE Photonics Journal, Vol. 4, Issue 6, pp.2243-2248,2012.

ACKNOWLEDGEMENTS

I would like to express my gratitude to my parents first. They have been giving me the unconditional love for every moment of my life. They offer so much understanding and support during my PhD period. Without all those understanding and support it is impossible for me to reach this achievement. I would like also thank my other family members. Their love really gives me great power and courage.

I would like to show my deepest gratitude to my supervisor, Professor Chao Lu. I can not imagine how I can achieve this moment without his help. At the beginning of my project I had just finished my bachelor degree. I had very little research experiences. Professor Chao Lu gave me many suggestions and directions. And he is always there to help when I face difficulties in my research. The methods of analyzing and solving problem I learnt from Professor Lu not only helps me to finish this project, they will also benefit me in the future. I would like also thank Professor Luc Thevenaz, my supervisor during a half year exchange program at EPFL, Switzerland. I learnt a lot about BOTDA from Professor Luc Thevenaz. He has also shared many valuable experiences with me and gave me a lot of suggestions on my research.

I would like to also thank my fellow researchers here. I would like to thank Dr. Hu Juanjuan, Dr. Arnaud Fernandez, and Dr. Li Jie for their instructions and helps when I start this project. I want to thank Dr. Yu Kuanglu and Mr. Guo Nan for working with me together on this project. I also appreciate other members of the group for their help and supports.

I also want to say thanks to my friends for their friendship and encouragement when I face difficulties. It is really important to me because it not only helps me to finish my PhD but also gives me so much memorable happy time for the past years.

TABLE OF CONTENTS

LIST OF ABBREVIATIONS

Abbreviation	Full Expressions
AD	analog/digital
AEOM	electro optic amplitude modulator
ASE	amplified spontaneous emission
BEDS	Brillouin echo distributed sensing system
BFS	Brillouin frequency shift
BOCDA	Brillouin optical correlation-domain analysis
BOFDA	Brillouin optical frequency-domain analysis
BOTDA	Brillouin optical time domain analysis
BOTDR	Brillouin optical time-domain reflectometry
CW	continuous wave
DFB	distributed feedback
DGD	differential group delay
EC-LD	external cavity laser diode
EDFA	Erbium doped fiber amplifier
EOM	electro-optical modulator
FBG	fiber Bragg grating
FDM	finite difference method
FEM	finite element method
FFT	fast Fourier transform
FUT	fiber under test
FWHM	full width at the half maximum
HB	highly birefringent
HF	holey fiber
HIC	high index cores
IFFT	inverse fast Fourier transform
MEM	multipole expansion method
MOF	microstructured optical fiber
PBG	photonic bandgap
PCF	photonic crystal fiber
PC	polarization controller
PD	photodetector
PEOM	electro-optic phase modulator
PPG	pulse pattern generator
PS	polarization scrambler

PWM	plane wave method
RF	radio frequency
RTO	real-time oscilloscope
SBS	stimulated Brillouin scattering
SMF	standard single mode fiber
SNR	signal of noise ratio
SOP	states of polarization
SPM	self phase modulation
SRS	stimulated Raman scattering
TEC	thermoelectric cooler
TIR	total internal reflection
TMM	transfer matrix method

LIST OF FIGURES

CHAPTER 1. INTRODUCTION

In this chapter, a brief introduction to optical sensing techniques is given. Motivations, objectives and organization of the thesis are presented.

1.1 Introduction

The history of optical fiber can be dated from the year 1966, when Charles Kao published the very first paper on optical fibers [1]. Since then, significant amount of research has been carried out in the area of fiber optics and the results have changed our everyday life dramatically. Nowadays we can watch online high quality videos, have video calls with our family members and friends, and share large multimedia files via the internet. All of these are not possible without the huge bandwidth provided by the optic communication systems based on optical fiber. Besides communication, optical fibers are also widely used for optical fiber sensors and fiber lasers. The sensors made of optical fibers often have small size, light weight. They are free from electromagnetic interference and can be easily multiplexed. They can also be used for remote sensing over long distances. Because of these advantages, optical fiber sensing systems have found increasing applications in military, in aviation industry, in the oil industry and construction industry.

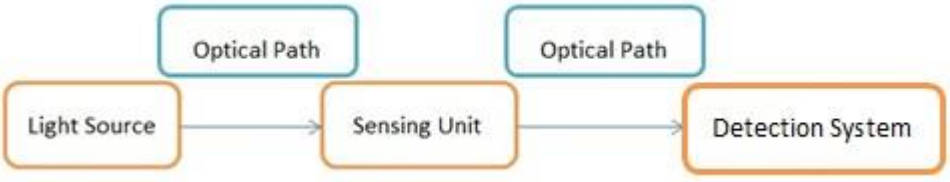

Figure 1-1 Schematic diagram of typical optical sensing system

An optical fiber sensing system may be defined as a system through which physical, chemical, biological or other quantities interact with light guided in an optical fiber or guided to an interaction region by an optical fiber to produce an optical signal related to the parameter of interest [2]. It is a good candidate for operating in harsh conditions or in applications that are inaccessible using alternative technologies. An optic sensing system is in general comprised of a light source, the sensing unit, and the detection system. In a fiber optic sensing system the optical channel is an optical fiber. Generally there are two different ways that a fiber can be used directly as the sensing unit. The first approach is by carrying out some special treatments on the fiber. For example we can write Fiber Bragg Gratings (FBGs) into the fiber at the sensing points. The spectrum of the light reflected back by the FBGs is sensitive to temperature and strain. By carefully designing the system and measuring the spectrum of the reflected light and compare it with the reference signals, we can measure the parameters of interest. We can also write Long Period Gratings (LPGs) in the optical fibers. The LPGs can couple the core modes into forward propagating cladding modes and the cladding modes are much more sensitive to the environmental parameters than the core modes. We can also side polish the fiber to fabricate the D-shaped fiber, it has evanescent wave into the air and therefore it is also very sensitive to the environmental changes. The disadvantage of using these

methods is that all the treatments are relatively complicated and will make the fiber more fragile. The other method is to directly use the untreated fiber as the sensing unit. The intensity, phase or polarization state of the light guided by the fiber can be effect by some external parameters due to a particular optic effect which affect the properties of the fiber. The advantage of this method is that the fiber is untreated. The system cost can be lower and the system will be more robust.

The optical fiber sensors can be classified as point sensors and distributed sensors. Single point sensors such as FBG based sensor can be used for strain, temperature, pressure, magnetic or electric field and chemical sensing. However, when a large number of points must be measured, many fibers must be used to connect the sensing heads, leading to a complex system. Therefore there have been significant amount of research interest in distributed fiber sensors, which can be used to measure a large number of sensing elements over a single fiber.

Distributed optical fiber sensing allows extracting the values of the measurand, as a function of position, along the length of the sensing fiber. Generally, distributed sensing techniques are based on some kind of light scattering mechanism occurring inside the fiber. Optical time domain reflectometry (OTDR) technique [3] based on Rayleigh scattering allows

location of losses introduced by micro bending to be measured. In 1985, *Dakin et al* developed a temperature measurement technique using Raman scattering [4]. Since the technique is relatively simple, systems based on Raman scattering have been used widely for measuring temperature in tunnels. However the scattering intensity is about 30 dB lower than the Rayleigh scattering. As a result, long measuring time is typically required. Brillouin scattering technology, which requires much more complex interrogating system than FBG and Raman-based distributed sensors, can be used to measure strain as well as temperature simultaneously along the fiber. Unlike Raman scattering based sensor, optical fiber sensors based on Brillouin scattering use wavelength for measurement and do not need calibration of the optical fiber loss. Comparing with Raman scattering, the detected signal power is also much larger. All these have made Brillouin scattering based sensing an attractive candidate for distributed sensing systems.

Brillouin scattering, named after the French physicist Léon Brillouin, occurs when light in a medium interacts with time dependent optical density variations and changes its frequency and path. This phenomenon is predicted by Léon Brillouin in 1922 [5]. It is believed that Lenoid Mandelstam has recognized the possibility of such scattering in 1918 but he only published his

work in 1926 [6]. So this effect is also named Brillouin-Mandelstam scattering. The effect was experimentally verified by French scientists Gross [7], R. Lucas, and P. Biquard [8] and two American scientists P. Debye and F. W. Sears 8-10 years after Léon Brillouin's prediction [9]. In their results there are two frequency shifted components and one un-shifted component in the scattering spectra. However at that time the frequency difference is too small to be resolved by the equipment available. Thus it was' not possible for researchers to study it in more detail until 1960, when Theodore H. Maiman invented the first laser. Since then, new equipments such as high resolution interferometers become available. More accurate measurement of frequency, intensity and line-width of the scattering become possible. The developments of the technology also made the measurement of the acoustic velocity and bulk modulus possible. The research in this field has since developed very fast. After Charles Kao published his paper on optical fiber [1] researchers began to be interested in Brillouin scattering in optical fiber. In 1972, E. P. Ippen and R. H. Stolen observed the Brillouin effect in optical fiber for the first time [10]. They reported the stimulated Brillouin scattering (SBS) effect in optical fiber and predicated that this phenomenon may limit the amount of power that can transmit through a fiber. It has since been shown that SBS in optical fiber is one of the major limiting factors limiting the performance of an optical

communication system [11]. To solve this problem, optical fiber has been specially designed to enhance the SBS threshold in order to lower the SBS in the fibers [12]. Other techniques have also been proposed to suppress the SBS effect [13].

Although in most of the situations the effect Brillouin scattering in optical fiber should be reduced, research studies have shown that the Brillouin effect can also be used for Brillouin-optical amplifiers [14], fiber lasers [15][16] and narrowband tunable filters [17]. It has also been shown that the group velocity of light can be controlled in optical fiber using the stimulated Brillouin scattering [18][19]. In addition to all these, an important application of stimulated Brillouin scattering effect is distributed sensing. It enables distributed strain and temperature measurement over moderate range with high spatial resolution.

1.2 Motivation and Objectives

For many years optical communication and sensing research have been two parallel research areas. However, if we look at them closely, there are many similarities between the two systems. Both optical communication and sensing systems are generally comprised of transmitters, optical channel, and receivers. In an optic communication system, with the knowledge of the received signal and the effect of the optical channel, the detection system will try to estimate the

signal sent out by the transmitter accurately. In the sensing system, with the knowledge of the signal transmitted at the transmitter and the signal received at the receiver, the detection system tries to estimate the change in the optical channel in order to obtain information about the parameters to be measured. Because of these, many techniques used in optical communication systems should be able to be employed in optical sensing systems. This may help to significantly improve the performance of the sensing systems.

On the other hand, many problems need to be addressed in the distributed sensing system based on Brillouin scattering when the number of sensing point is large, i.e. the spatial resolution is high and the total sensing length is long. The most critical problem is the low signal power. In a Brillouin scattering based optical distributed sensing system, the critical power of the pump light is inverse proportion to the total length of the sensing fiber. When the sensing length is long, the pump power must be very low to avoid the pump depletion. The scattered signal power will be low in this situation. Meanwhile, the pulsewidth of the pump pulse should be very short in order to achieve high spatial resolution, which will in turn reduce the interaction between the pump and probe light. As a result, the back-scattered signal will be weak. The worst situation is when both high spatial resolution and long sensing length are required. In this

case the signal will be very weak and the signal to noise ratio will be very poor even when EDFAs are used to amplify the backscattered signal. The signal processing is difficult in this case.

Because of all these, it is a very promising idea to study the use of techniques commonly used in communication system in Brillouin distributed sensing system. In particular, the use of coding technique which is widely used in the communication system in order to improve the signal to noise ratio of the sensing system is to be investigated.

1.3 Major Contributions

In this thesis, a detailed study of distributed sensing system based on Brillouin scattering is carried out. In particular, the research focus has been on Brillouin optical time domain analysis (BOTDA) systems. The main noise sources of the system are identified. The backscattered signal is studied carefully in order to find out methods to improve the performance of the system. The Brillouin lifetime in different types of optical fiber are measured. Although the spatial resolution of a BOTDA system has already broken the limitation of 1m resolution determined by the lifetime of the acoustic wave, a detail study of the acoustic lifetime can help us to obtain a better Brillouin signal. No detailed study in this aspect has been reported before.

By using a coding technique named complementary code, high spatial resolution distributed sensing over long sensing fiber has been realized. The coding and decoding process of the complementary code have been studied and it is demonstrated that signal to noise ratio of the system can be improved greatly. At the same time, the acquisition time can be reduced using the coding technique as well. There are two main reasons for the time reduction. The first reason is that the signal to noise ratio is improved and less average is needed to obtain a signal for required strain/temperature accuracy for given spatial distribution along the fiber. The second reason is that comparing with other coding techniques less pulse sequences are needed when complementary coding technique is used.

1.4 Organization of the Thesis

After a brief introduction including objectives, contributions and organization of the thesis, Chapter 2 introduces some optic effects which are commonly used in optical fiber sensor systems. They include Doppler effect, Sagnac effect, and Photoelectric effect. Scattering in optical fibers is discussed at the end of the chapter which is the main mechanism for realizing distributed optical sensing.

Chapter 3 provides some background for distributed sensing system. The

history of the research in the area, background theories of Brillouin scattering in optical fibre and its application in distributed sensing are discussed. Four typical Brillouin sensing techniques are introduced.

In Chapter 4, main challenges for achieving high spatial resolution over a long sensing fiber are highlighted. Techniques for realizing it are described. The performance limitations in the BOTDA systems are analyzed and possible solutions are discussed. An experimental setup for measuring acoustic lifetime of different type of fibre is proposed and measurement results are presented.

Chapter 5 presents the work on using coding technique to improve the performance of distributed sensing system based on Brillouin scattering. Discussion on the property of the code used as well as the results obtained for high spatial resolution distributed Brillouin sensing using phase modulation and code techniques are presented in detailed.

Finally in Chapter 7, conclusions are given and suggestions for future work are presented.

CHAPTER 2. OPTICAL EFFECTS IN OPTICAL FIBER SENSING SYSTEMS

In this chapter, different optical effects which are useful in the study of distributed optical sensing system based on Brillouin scattering are introduced. They include optical Doppler effect, photoelectric effect, electro-optical effect and linear and nonlinear scattering effects. Understanding these effects can helps to understand the mechanism of Brillouin scattering in an optical fiber and sources of noises in the BOTDA systems.

In an optical sensing system, the measurand can be any environmental parameters that may affect an optic signal. These parameters include temperature, strain, bending, and pressure. The optic signal guided by a fiber is either modulated by the measurands inside the fibre or outside the fibre at a sensing head through many kinds of optic effects. These optical effects include: optical Doppler effect, Sagnac effect, photoelectric effect, electro-optic effect, magneto-optical effect, and scattering including Raman scattering and Brillouin scattering.

There are two different groups of scattering effects in the optical fiber, the linear scattering and the nonlinear scattering. The linear scattering effect includes the elastic scattering such as Rayleigh scattering and inelastic scattering such as spontaneous Raman scattering and spontaneous Brillouin scattering. The Nonlinear scattering includes stimulated Raman scattering and stimulated Brillouin scattering. The time delay of the scattered light can be determined by using time domain techniques. So the scatterings can be potentially used to enable distributed sensing, which is very powerful since every single point along the fiber can be treated as a sensing unit. These scatterings, which are particularly important since they are potentially useful in distributed optical sensing system, will be discussed in more detail at the end of this chapter.

2.1 Optical Doppler Effect

The Doppler effect, name after the physicist Christian Doppler who observed this effect, is the change in frequency of a wave for an observer moving relative to the source of the waves.

In classical physics, the relationship between observed frequency f and emitted frequency f_0 is given by [20]:

$$f = \left(\frac{v + v_r}{v + v_s} \right) \bullet f_0 \tag{2.1}$$

here v is the velocity of waves in the medium, v_s is the velocity of the source relative to the medium, and v_r is the velocity of the receiver relative to the medium.

Because light is essentially an relativistic object and it has no medium, it is impossible to find absolute velocities as in the case of a material wave. Relativistic Relativity must be taken into account for the optical Doppler effect. Fortunately, it is even easier to find the relativistic Doppler effect than the classical one.

Assume the observer and the sources are moving away from each other with a relative velocity v. We consider the problem in the reference frame of the

source. Suppose one wavefront arrives at the observer. The next wavefront is then at a distance $\lambda = c/f_s$ from the observer (here λ is the wavelength, f_s is the frequency of the wave the source emitted, and c is the speed of light). Because the wavefront moves to the observer with a velocity of c and the observe escapes with a velocity v, the next wavefront will meet the observer at the time:

$$t = \frac{\lambda}{c - v} = \frac{1}{(1 - v/c) f_s} \tag{2.2}$$

Due to the relativistic time dilation, the observer will measure this time to be:

$$t_0 = \frac{t}{\gamma} = \frac{\frac{1}{(1 - v/c) f_s}}{\frac{1}{\sqrt{1 - v^2/c^2}}} = \sqrt{\frac{1 + v/c}{1 - v/c}} \bullet \frac{1}{f_s} \tag{2.3}$$

The corresponding frequency is:

$$f_0 = \frac{1}{t_0} = \sqrt{\frac{1 - v/c}{1 + v/c}} \bullet f_s \tag{2.4}$$

The corresponding wavelength is:

$$\lambda_0 = \sqrt{\frac{1 + v / c}{1 - v / c}} \bullet \lambda_s \tag{2.5}$$

Using Doppler effect, we can use the fiber to make a fiber optic vibration or acoustic sensor[21]. By using the Doppler's effect in flexible and expandable light waveguide, Kageyama *et al.* demonstrated a vibration/acoustic sensor with a resolution higher than nanostrain and a frequency range from 1 kHz to 1MHz. Based on Doppler effect, other applications such as ultrasonic detection [22], debonding detection for composite structures [23], and damage assessment in composite laminates [24] have also been reported.

2.2 Photoelectric Effect

Photoelectric effect is a phenomenon in which electrons are emitted from matter after the absorption of energy from electromagnetic radiation such as X-rays or visible light. Photoelectric effect takes place with photons with energies of about a few electronvolts. If the photon has sufficiently high energy, compton scattering (~keV) or pair production (~MeV) may take place [25][26][27].

The photons of a light beam have a characteristic energy determined by the frequency of the light. In the photoemission process, if an electron within some material absorbs the energy of one photon and thus has more energy than the

work function (the electron binding energy) of the material, it is ejected. If the photon energy is too low, the electron is unable to escape the material. Increasing the intensity of the light beam increases the number of photons in the light beam, and thus increases the number of electrons emitted, but does not increase the energy that each electron possesses. Thus the energy of the emitted electrons does not depend on the intensity of the incoming light, but only on the energy of the individual photons. (This is true as long as the intensity is low enough for non-linear effects caused by multi-photon absorption to be insignificant.)

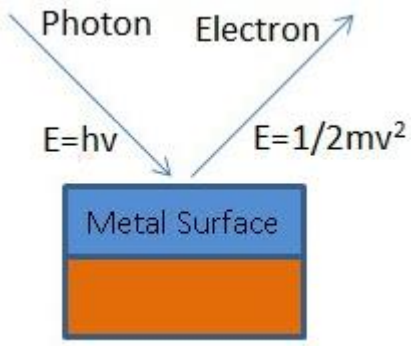

Figure 2-1 Electrons emitted from matter after absorbing energy from photons

2.3 Electro-optic Effect

The electro-optic effect happens when the optical properties of the material are changed due to a slowly varying electric field. The electro-optic effect includes Electro-absorption, Franz-Keldysh effect, Quantum-confined Stark

effect, Pockels effect, and Kerr effect. The electro-absorption refers to the change of absorption constants with the electric field. The Franz-Keldysh effect is the electro-absorption effect in some bulk semiconductors. The Quantum-confined Stark effect is the change happens in some semiconductor quantum wells. The Pockels effect refers to the refractive index change linearly proportional to the electric filed, which only happen in a few crystalline solids. The Kerr effect means the refractive index of the material changes proportional to the square of the electric field, i.e. the electric power.

2.4 Scattering

Scattering is a general physical process in fiber optics. It happens when the light is forced to deviate from a straight trajectory by one or more localized non-uniformities in the medium through which the light propagate. The scattering is particularly important in optical fiber sensors, especially due to its ability of achieving distributed sensing. The scattering can happen anywhere along the fiber and the backward scattered light from different position can be easily distinguished using time domain techniques. Rayleigh scattering is widely used in optic time-domain reflectometer (OTDR). Both Raman and Brillouin scattering can be used to realize distributed sensing system. The distributed sensing system based on Raman scattering is only sensitive to temperature

change while the one based on Brillouin scattering found applications in both temperature sensing and strain sensing.

Light is an electromagnetic wave. The scattering of the light may be linear or nonlinear depending on the intensity of the light propagating in the medium.

2.4.1 Linear Scattering Effects

Light scattering is mainly due to the in-homogeneities of the optical properties of the medium. When the medium is homogenous, the light will always propagate in its original direction. When the medium is no longer homogeneous, the light will be scattered due to density fluctuations of the media since the optical properties are modified [29]. In the linear case, the in-homogeneous of the medium is independent of the electromagnetic field $\vec{E}$ and the polarization also remains linearly dependent on $\vec{E}$. There are two types of linear scattering: elastic scattering and inelastic scattering. Elastic scattering means the light is scattered without frequency shift because in the scattering process the phonons maintain their energy. Elastic scattering includes spontaneous Rayleigh scattering and Rayleigh-wing scattering. Inelastic scattering means there are frequency shift due to the energy transfer between the photons and phonons. The inelastic scattering includes spontaneous Raman scattering and spontaneous Brillouin scattering. In the spontaneous Raman

scattering the energy transfer occurs between the photons and the molecular fluctuations density (optic phonons). In the spontaneous Brillouin scattering the energy transfer occurs between the photons and the pressure fluctuations density (acoustic phonons). The frequencies of different scattering are shown in Figure 2-2.

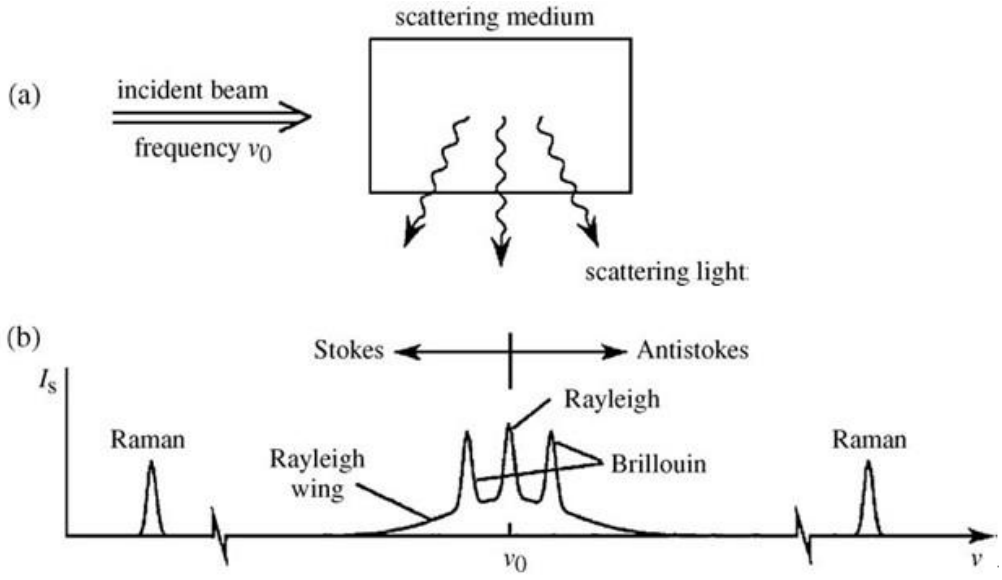

Figure 2-2 Linear scattering

2.4.1.1 Elastic Scattering Effect

Elastic scattering effect mainly contains Rayleigh and Rayleigh-wing scattering. Spontaneous Rayleigh scattering (or Rayleigh-center scattering) is the scattering of light from non-propagating density fluctuations. Therefore, this scattering does not involve any frequency shift due to Doppler effect, and the involved scattering center is fixed. Rayleigh scattering can be described as

scattering from entropy fluctuations. It is widely used in optic time domain reflectometer (OTDR). Spontaneous Rayleigh-wing scattering (i.e., scattering in the wing of the Rayleigh line) is generated by fluctuation in the orientation of anisotropic molecules. Because the molecular reorientation process is quite rapid, Rayleigh-wing scattering has a broad spectrum width.

The Elastic scattering is a scattering where the light is scattered with no frequency shift. In particle physics during the elastic scattering process, the kinetic energy of the incident particles is conserved. Only the direction of the propagation is modified.

In optics, when a photon penetrates into a medium composed of particles whose sizes are much smaller than the wavelength of the incident photon, Rayleigh scattering will happen and this process is elastic. During this process the energy of the incident photon, and therefore the wavelength, is conserved and only the direction of the propagation is changed. Figure 2-3 shows a typical picture of Rayleigh scattering in optical fibers. A light beam from a 630nm laser is injected into a spool of fiber. Ideally the light will be confined well inside the fiber. However part of the light is scattered mainly due to the Rayleigh scattering. This is the reason why we can see the red light from the fiber.

Figure 2-3 Rayleigh scattering in optical fiber (The picture is taken in our lab)

2.4.1.2 Inelastic Scattering Effect

Besides elastic scattering, the inelastic scattering can also occur inside the optic fiber. The inelastic scattering happens when the optic density is large enough that there will be energy transfer among the photons and the phonons. If the energy transfers from the photons to the phonons, the frequency of the scattering photon will be lower than the original photon and this process is known as Stokes process and the scattered photon is called Stokes wave. On the other hand if the energy transfers from the phonons to the photons, the scattered photon will have a higher frequency and it is called anti-Stokes wave.

Raman scattering or the Raman effect is the inelastic scattering of a photon discovered by C.V. Raman in liquids and by Grigory Landsberg and Leonid

Mandelstam in crystals [30][31]. When light is scattered from an atom or molecule, most photons are elastically scattered (Rayleigh scattering), such that the scattered photons have the same energy (frequency) and wavelength as the incident photons. However, a small fraction of the scattered light (approximately 1 in 10 million photons) is scattered by an excitation, with the scattered photons having a frequency different from, and usually lower than, the frequency of the incident photons. The excitation comes from the motion of the atom or molecule and the frequency difference depends on this motion. Since the motion of the atom or molecule is related to the temperature of the material, this frequency shift also depends on the temperature of the material. So Raman scattering can be employed to realize temperature sensing.

Brillouin scattering, named after Léon Brillouin, occurs when light in a medium (such as water or crystal) interacts with time dependent density variations and changes its energy (frequency) and path [5]. The density variations may be due to acoustic modes, such as phonons, magnetic modes, such as magnons, or temperature gradients. As described in classical physics, when the medium is compressed, its index of refraction changes and the lights path necessarily bends. The amount of the frequency shift depends on the density variations, which can be changed by temperature, strain, and magnetic

field. So Brillouin scattering can be used to sense temperature and strain.

From a quantum point of view, Brillouin scattering is an interaction of light photons with acoustic or vibrational quanta (phonons), with magnetic spin waves (magnons), or with other low frequency quasiparticles interacting with light. The interaction consists of an inelastic scattering process in which a phonon or magnon is either created (Stokes process) or annihilated (anti-Stokes process). The energy of the scattered light is slightly changed, that is decreased for a Stokes process and increased for an anti-Stokes process. This shift, known as the Brillouin shift, is related to the energy of the interacting phonon and magnon and thus Brillouin scattering can be used to measure phonon and magnon energies. The Brillouin shift is commonly measured using a Brillouin spectrometer based on a Fabry-Pérot interferometer.

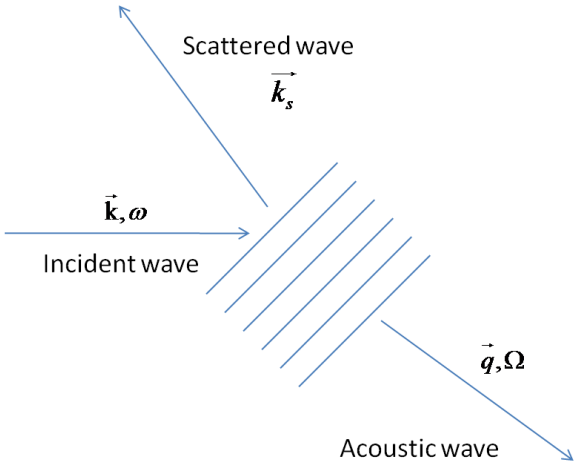

Figure 2-4 Incident wave, scattered wave and acoustic wave in Brillouin scattering

In a standard single mode fiber the light wave can only have two directions, the forward and the backward. Thus normally only the backward scattering can happen (Figure 2-5).

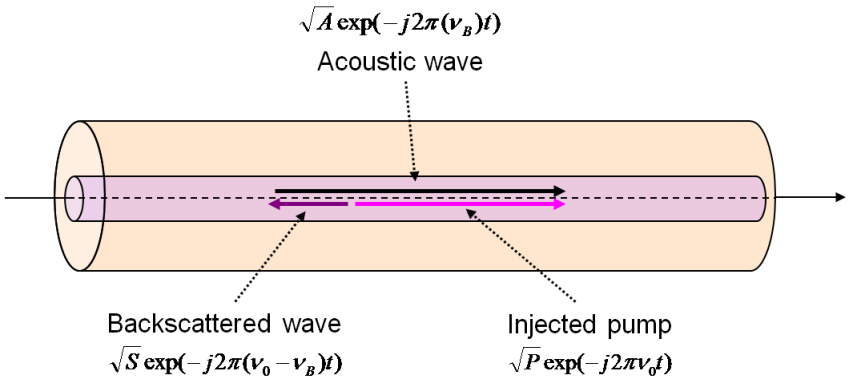

$$\nu_B = \Omega_B/2\pi = 2nv_A/\lambda_p$$

Figure 2-5 Brillouin scattering in Optical fibers

2.4.2 Nonlinear Scattering Effects

When a high optic power is applied on a dielectric medium such as the optical fibers the susceptibility of the material becomes dependent on the magnitude of the electromagnetic fields and the nonlinear effects will happen. As a result the induced polarization $\vec{P}$ is a combination of linear part $\vec{P_L}$ and nonlinear part $\vec{P_{NL}}$. In our case, we only consider the linear part $\vec{P_L}$ and the third order nonlinear part $\vec{P_{NL}^3}$:

$$\vec{P} = \vec{P_L} + \vec{P_{NL}^3} \tag{2.6}$$

The third order nonlinear part $\overrightarrow{P_{NL}^{3}}$ is responsible for most of the non-linear effects in fibers: stimulated Raman scattering, stimulated Brillouin scattering, and four-wave-mixing, self-phase modulation and modulation instability.

2.4.2.1 Stimulated Raman Scattering

Stimulated Raman scattering (SRS) is an optic effect which happens when an optical wave interact with the molecular fluctuations of the material. Similar to the spontaneous Raman scattering discussed before, the stimulated Raman scattering can also be described as the scattering of light from optical phonons. The different between spontaneous Raman scattering and SRS is in spontaneous Raman scattering the light is from normal light source and the power is weak so the vibration of the molecular is mainly due to the thermal motion of the molecule. On the other hand, in stimulated Raman scattering, the light is from a high power laser. The power is so strong that it can drive the molecule to vibrate. That means the vibration of the molecule is stimulated by the electromagnetic field of the strong laser light.

Raman scattering is an inelastic scattering, unlikely the case of elastic scattering such as Rayleigh scattering within which the scattered photons have the same energy and wavelength as the incident photons, the scattered photons

can have a frequency different from, and most of the time smaller energy than the incident photons. In Raman scattering the frequency change (energy change) is due to the vibrational or rotational energy of a molecule. The principle of Raman scattering is shown in Figure 2-6. From a quantum point of view, the scattering is the incident photon interacts with the molecule. The molecule can have the same energy level before and after the scattering. In this case the scattering is elastic and the typical example is Rayleigh scattering. The vibrational state of the molecule can be changed. So there is energy transfer during the scattering and in this case the Raman scattering happens. Because the energy is conserved, when the molecule have higher energy level after the scattering the scattered photon will have a smaller energy and its frequency will be down shifted. In this case the scattering is called Stokes scattering. On the other hand when the molecules have lower energy level after the scattering the scattered photon will have a higher energy and its frequency will be up shifted and the scattering is called anti-Stokes scattering.

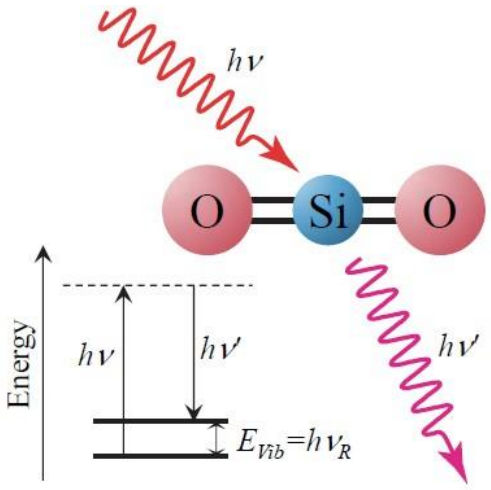

Figure 2-6 Principle of Raman scattering in the optic fiber

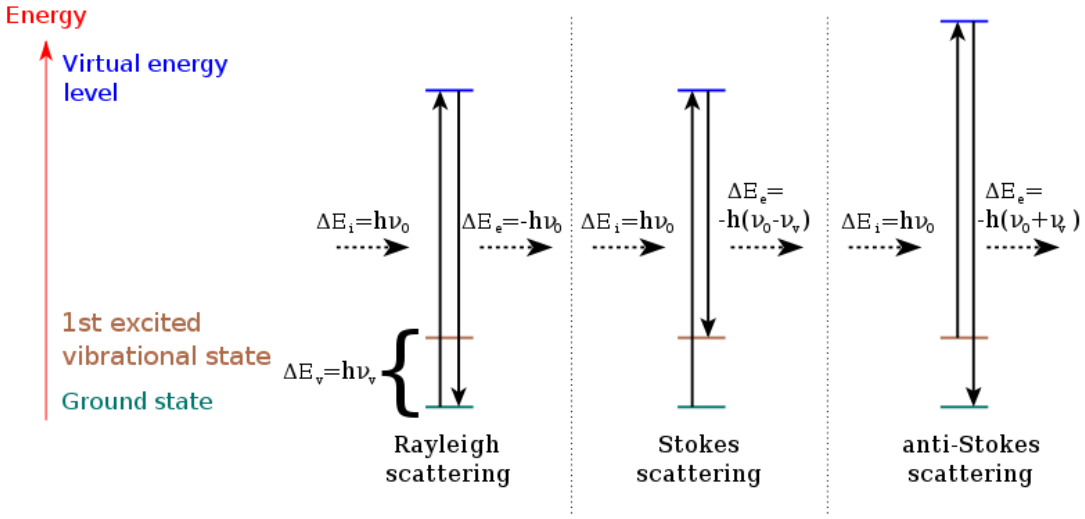

Figure 2-7 Rayleigh scattering and Stokes and anti-Stokes Raman scattering

2.4.2.2 Stimulated Brillouin Scattering

Figure 2-8 illustrates the SBS process in optical fibers [32]. The two counter-propagating light wave: pump wave which is generally stronger and the probe wave which is often weaker will interfere with each other. Since the

frequencies of these two waves are slightly different from each other, the interference pattern of them is sinusoid as shown in Figure 2-8. The energy density of the pattern is also sinusoid. The refractive index of the fiber will be modulated into sinusoid distribution due to the Electro-optic effect. The sinusoid distribution of the refractive index along the fiber will act as a fiber Bragg grating which is moving at the velocity of the sound because the interference pattern of the two propagating wave will move at this speed. The moving fiber Bragg grating will scatter part of the pump energy into the probe wave and this will in turn enhance the interference.

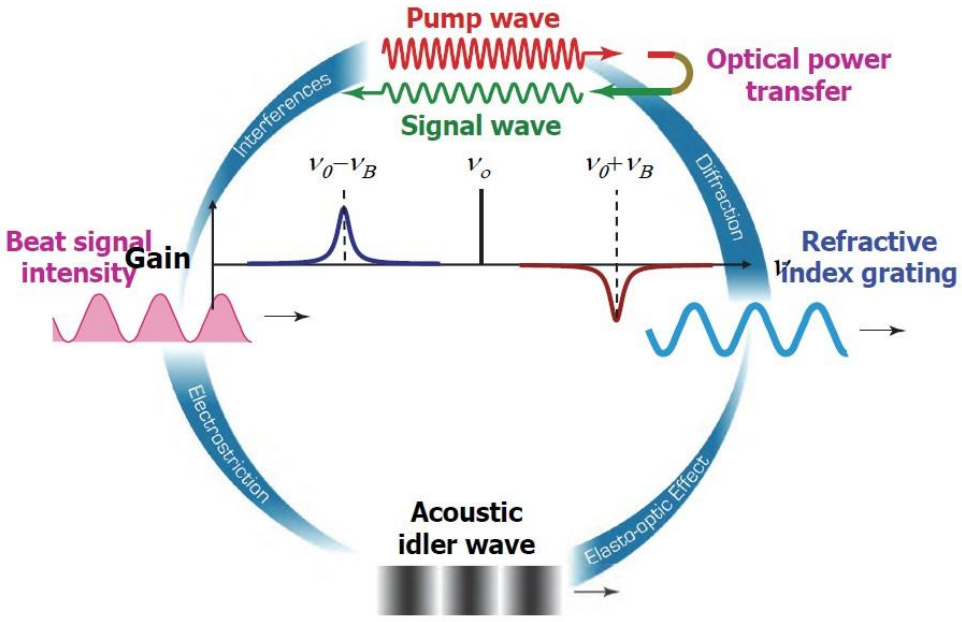

Figure 2-8 Schematic representation of SBS [32]

Due to different source of the probe wave, there are two different types of

SBS. In the first type the probe wave is generated by the spontaneous Brillouin scattering. In this case the probe wave is weak. To generate a strong interference pattern, a strong pump wave is needed. So this type of SBS only happens when the pump power is stronger than certain power level, i.e. the Brillouin threshold of the optical fiber. For the second type, we inject another light which is coherent with the pump light and has a frequency $\Delta\nu_B$ higher or lower than the pump wave. ($\Delta\nu_B$ is the Brillouin frequency shift of the fiber). This is the method we use in BOTDA systems. It is worth note that in BOTDA systems we need to have a strong pump power to achieve longer sensing distance however the pump power must be smaller than the Brillouin threshold to avoid the first type SBS. This is because the first type SBS will contain information from the whole Brillouin spectrum, which is a strong source of noise in the case of BOTDA systems.

From a classical point of view, the scattering occurs because the index of the medium changes when it is compressed. From a quantum point of view, Brillouin scattering is an interaction of light photons with acoustic or vibrational quanta (the phonons). The interaction consists of an inelastic scattering process and thus energy transfer so the energy of the scattered light is slightly changed. The energy is increased for a Stokes process and decreased for an anti-Stokes

process. This energy change is also treated as frequency shift of the scattered light, which is known as Brillouin shift.

The quantity of the energy change is equal to the energy of the interacting phonon. So by measuring the Brillouin frequency shift, which is always done by using a Brillouin spectrometer based on a Fabry-Pérot interferometer, we can measure the energy of the phonons.

In a standard single mode fiber, as shown in Figure 2-9, because the light waves can propagate in only two directions, the forward and the backward directions, normally only the backward scattering can occur.

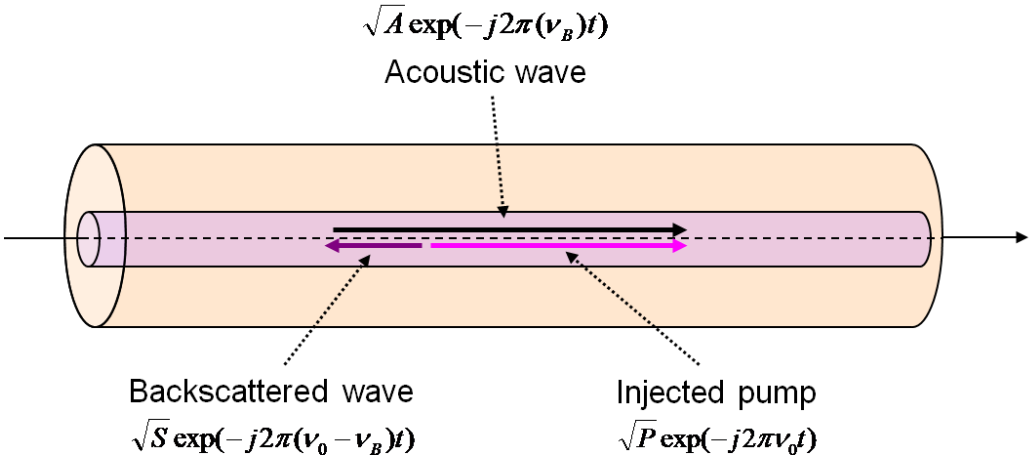

Figure 2-9 Brillouin scattering in Optical fibers

Here we assume that the electrical field of the incident light is described as

$$\mathbf{E}(z,t) = E_0(z,t)e^{i(\mathbf{k}\cdot\mathbf{r}-\omega t)} + c.c. \tag{2.7}$$

Taking a typical component of the thermally excited density fluctuation within the interaction region to be given by

$$\Delta\rho(\mathbf{r},t) = A(z,t)e^{i(\mathbf{q}\cdot\mathbf{r}-\Omega t)} + c.c. \tag{2.8}$$

For an isotropic and inhomogeneous medium, an additional polarization is brought in for the reason of the fluctuation of the dielectric constant. Since $\varepsilon = 1+\chi$, the fluctuation in the susceptibility is then given by $\Delta\chi = \Delta\varepsilon$. So the total polarization is given as

$$\mathbf{P} = \varepsilon_0\chi^{(1)}\mathbf{E} + \varepsilon_0\Delta\boldsymbol{\chi}\mathbf{E} = \mathbf{P}_0 + \Delta\mathbf{P} \tag{2.9}$$

where $\Delta\mathbf{P} = \varepsilon_0\Delta\varepsilon\mathbf{E}$.

From equations(2.7), (2.8) and (2.9) we can derive:

$$\nabla^2\mathbf{E} - \frac{1}{(c/n)^2}\frac{\partial^2\mathbf{E}}{\partial t^2} = -\frac{\gamma_e}{\rho_0 c^2}[(\omega-\Omega)^2 A^* E_0 e^{i((\mathbf{k}-\mathbf{q})\mathbf{r}-(\omega-\Omega)t)} + (\omega+\Omega)^2 A E_0 e^{i((\mathbf{k}+\mathbf{q})\mathbf{r}-(\omega+\Omega)t)}] + c.c. \tag{2.10}$$

When light travels in optical fibers, the propagation can be described by the perturbed wave equation directly derived from Maxwell equations:

$$\nabla^2 \mathbf{E} - \frac{1}{c^2}\frac{\partial^2 \mathbf{E}}{\partial t^2} = \mu_0 \frac{\partial^2 \mathbf{P}}{\partial t^2} \tag{2.11}$$

In an isotropic and inhomogeneous medium the equation becomes:

$$\nabla^2 \mathbf{E} - \frac{1}{(c/n)^2}\frac{\partial^2 \mathbf{E}}{\partial t^2} = \mu_0 \frac{\partial^2 \Delta\mathbf{P}}{\partial t^2} \tag{2.12}$$

From equations (2.8) and (2.12) we will have:

$$\begin{aligned}\nabla^2 \mathbf{E} - \frac{1}{(c/n)^2}\frac{\partial^2 \mathbf{E}}{\partial t^2} = -\frac{\gamma_e}{\rho_0 c^2}[&(\omega-\Omega)^2 A^* E_0 e^{i((\mathbf{k}-\mathbf{q})\mathbf{r}-(\omega-\Omega)t)} \\ &+ (\omega+\Omega)^2 A E_0 e^{i((\mathbf{k}+\mathbf{q})\mathbf{r}-(\omega+\Omega)t)}] + c.c.\end{aligned} \tag{2.13}$$

It is clear that the presence of the acoustic wave leads to new spectral components at frequency $\omega - \Omega$ and $\omega + \Omega$, which corresponds to the Stokes wave and the anti-Stokes wave respectively.

Consider the momentum and energy conservations we have the relationship:

$$\overrightarrow{k_s} = \vec{k} \mp \vec{q} \tag{2.14}$$

$$\omega_s = \omega \mp \Omega \tag{2.15}$$

Here $\overrightarrow{k_s}$ is the wave vector of scattered wave, $\vec{k}$ is the wave vector of

the injected pump, $\vec{q}$ is the wave vector of the acoustic wave. ω_s, ω and Ω are the angular frequencies for the scattered wave, injected pump, and the acoustic wave respectively. In the two equations above, "-" is for the Stokes wave and "+" is for the anti-Stokes wave.

The frequency and wave vector of the incident wave, acoustic wave, and scattered wave are related to each other by the relationships:

$$\omega = |\mathbf{k}| c / n \tag{2.16}$$

$$\Omega = |\mathbf{q}| V_A \tag{2.17}$$

$$\omega' = |\mathbf{k}'| c / n \tag{2.18}$$

The scattering for the Stokes wave is illustrated in Figure 2-10 and the scattering for the anti-Stokes wave is illustrated in Figure 2-11:

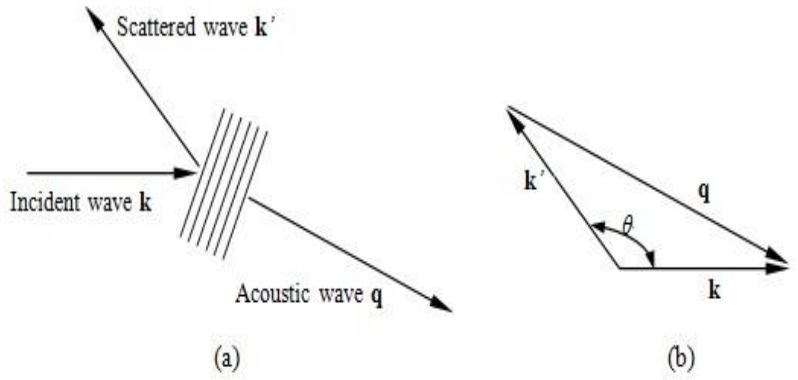

Figure 2-10 Illustration of Stokes wave generation

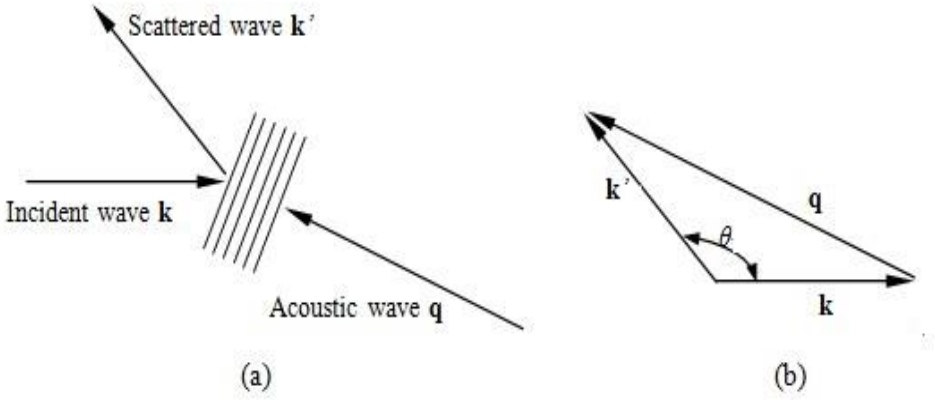

Figure 2-11 Illustration of anti-Stokes wave generation

Based on these equations we can calculate the Brillouin shift:

$$\upsilon_B = \Omega_B / 2\pi = 2nv_A / \lambda_p \tag{2.19}$$

here υ_B is the Brillouin frequency shift, Ω_B is the frequency of the acoustic wave, v_A is the speed of the acoustic wave in the optical fiber, and

λ_p is the wavelength of the injected pump.

CHAPTER 3. DISTRIBUTED OPTICAL FIBER SENSING SYSTEMS

In this chapter, commonly used distributed sensing techniques are discussed. The emphasis has been on distributed sensing techniques based on Brillouin scattering. Detection techniques for Brillouin Scattering based distributed sensing techniques are reviewed.

3.1 Optical Time-domain Reflectometer

Optical Time-Domain Reflectometer (OTDR) based on Rayleigh scattering is an optoelectronic instrument used to characterize an optical fiber. It has also been used for distributed sensing applications. In an OTDR system a series of optical pulses are injected into the fiber under test and back scattered light signals are received at the same end. The received light is due to Rayleigh scattering along the fiber or reflections along the fiber link such as near the connectors. The power of the reflected light is measured and integrated as a function of time. Since the signal from different position of the fiber takes different time to come back, the received signal can also be resolved as a function of fiber length. The strength of the Rayleigh scattering is linearly proportional to the power of the injected light. The OTDR can be used to measure the attenuation distribution of the fiber. By measuring the time different between the two strong reflections at the two ends of the fiber we can also use OTDR to measure the length of the fiber. If there is a break along the link, it can also be detected using the OTDR since there will be a strong reflection at the breaking point.

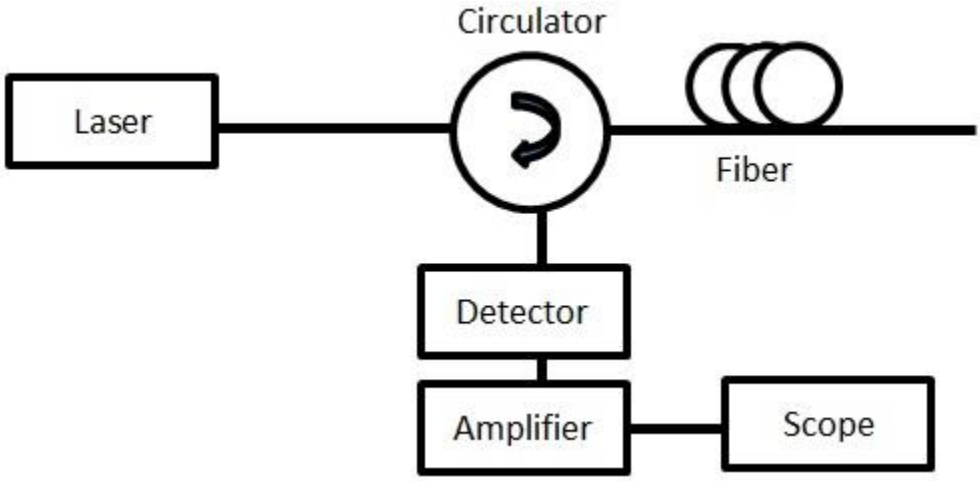

Figure 3-1 Experimental arrangement of the OTDR technology [3]

The concept of OTDR is first proposed by M. K. Barnoski and S. M. Jensen in 1976 [3]. The setup used by them is shown in Figure 3-1. The light from a pulsed injection laser was injected into the fiber using the lens. The backward signal is then detected by the detector and a scope. The time was related to the position of the fiber by the velocity of the light in the fiber. The result is then plotted as a function of the fiber length. The reflected signal contains the light scattered within the taper and fiber, and also the light reflected by the cleaved face at the far end of the fiber, which is a large pulse.

The technology became a very popular research topic and hundreds of papers have been published since then. Comparing with the first demonstration the spatial resolution is much higher and the speed of signal detection is much faster nowadays. Commercial OTDR is widely available and has been used

widely in industries and research labs to characterize optical fibers. Through introducing loss by pressure induced microbending, OTDR can easily be used as a sensing system.

By scanning the wavelength of the light source, the spectral of the Rayleigh backscatter along a certain length of fiber can be mapped. This spectral can be modulated by temperature. Based on this idea, D. K. Gifford *et al.* proposed a novel method to achieve distributed temperature sensing with high spatial resolution and 0.1℃ temperature measurement accuracy was realized [33]. Y. Koyamada *et al.* has also reported their result of using coherent OTDR to achieve distributed strain and temperature sensing in 2009 [34].

3.2 Raman Scattering Based Distributed Sensing

As introduced in Chapter 2, Raman scattering is also named Raman effect. It is an inelastic scattering of a photon. The spontaneous Raman scattering happens if the incident light is from a non-laser light source. Typically, the spontaneous Raman scattering is very weak. As a result it is very difficult to separate the weak in-elastical scattering light from the Rayleigh scattered light. If the incident light is a high power beam from a laser, SRS will happen. The SRS is much stronger than the spontaneous scattering and it can be used to achieve distributed temperature sensing. In 1985, J. P. Dakin *et al.* reported their

experimental results of distributed temperature sensing based on Raman scattering [35].

Compare to the distributed sensing systems based on Brillouin scattering, the Raman scattering based distributed sensing system can only measure the temperature distribution along the fiber. This, however, can be an advantage of Raman scattering based sensing system since it does not need to discriminate the change caused by strain and temperature along the fiber. If strain distribution is the measurand, then Brillouin sensors have to be used. The Raman sensors can also be used with the Brillouin sensing system to provide temperature distribution as a reference so that we can distinguish the temperature distribution and the strain distribution along the fiber.

Raman scattering can also be employed in the Brillouin sensing systems to avoid the pump depletion problem. In Brillouin sensing systems, especially the ones for long sensing range, the depletion of the pump power is a critical issue. The pump power becomes very small due to the attenuation and the Brillouin scattering. Using Raman amplification in the far end to amplify the pump power can help to avoid this problem and will result in a better Brillouin signal.

3.3 Brillouin Scattering Based Distribution Sensing

3.3.1 Brillouin Scattering

Another important distributed sensing technique is based on Brillouin Scattering. The characteristics of the optical fiber such as its refractive index and the density of the medium change when the temperature of the fiber is changed or a strain is applied onto the fiber. According to equation (2.19) we can see the Brillouin shift depends on the refractive index of the optical fiber n and the group velocity of the acoustic wave V_A. The group velocity of the acoustic wave in the solid is given by:

$$V_A = \sqrt{\frac{K}{\rho}} \tag{3.1}$$

where K is the bulk modulus of the silica and ρ is the average medium density of the fiber. The density ρ can be changed by either a temperature change or the strain applied onto the fiber. This will result in the shift of the Brillouin frequency. By analyzing the scattered light it is possible to resolve the temperature and strain distribution along the fiber. The dependence of the Brillouin frequency shift on temperature or strain is shown in Figure 3-2 [36].

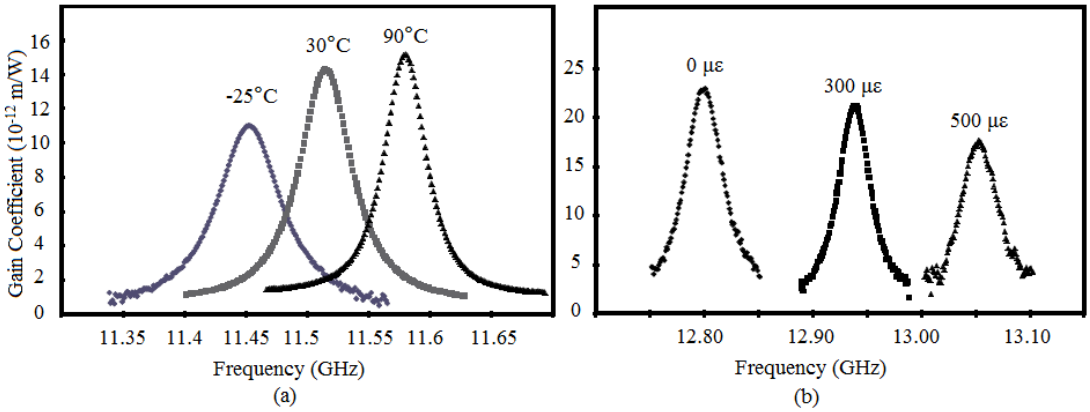

Figure 3-2 Brillouin spectrum for (a) different temperature (b) different strain [36]

By measuring the change of the Brillouin shift the temperature information along the fiber can be determined. This has provided the basis for Brillouin scattering based optical fiber sensing systems. To obtain spatial distribution information, a short optical pulse is transmitted along the fiber. Part of the pulse will be backscattered through the Brillouin effect. Since light scattered back at different part of the fibre will arrive at the receiver at different time, spatial distribution of the temperature and strain along a piece of fibre can be obtain by detecting the Brillouin scattering signal leading to a realization of distributed Brillouin fiber sensing system.

Three main performance parameters are important for assessing the performance of a distributed optical fiber sensing system: the accuracy of the measurand, the range of measurement and the spatial resolution. The accuracy of the measurand indicates the difference between the value measured and the

actual value. The range of measurement indicates the longest length of fiber before which we can still extract useful information from the output. The spatial resolution is defined as the smallest length of fiber in which sensible measurand can be detected.

3.3.2 Development of Distributed Sensing Based on Brillouin Scattering

The possibility of using SBS in an optical fiber for distributed sensing was first suggested by A. J. Rogers in 1986 [37]. This idea was analyzed in greater detail by D. Culverhouse *et al.* in 1989 [38]. Based on the analysis they proposed a method to realize a distributed temperature sensor. These have led to the first experimental demonstration of a distributed temperature sensor by Toshio Kurashima *et al.* in 1990 [39]. The reported sensing system can achieve a temperature measurement accuracy of 3℃ with a spatial resolution of 100m. Since then, there have been significant amount of research interest on distributed sensing systems based on Brillouin scattering and a lot of work has been done in the area. In the early experiments, bright pulse Brillouin gain/loss schemes were employed for distributed Brillouin sensing system [40][41].

In 1994, T. Horiguchi et al reported achieving 1m spatial resolution over an 11km fiber [42]. Another significant advance was realized when Nickles *et al*

proposed a novel setup using a single laser to generate the frequency difference between the pump and probe light by modulating the probe light using a LiNbO3 electro-optic modulator (EOM) driven by a microwave generator with a frequency near the Brillouin frequency shift [43]. By doing this, they can measure the temperature with an accuracy of 0.5K.

It was commonly believed that the spatial resolution of Brillouin techniques was limited to about 1m because of the fact that the observed Brillouin spectrum broadening when input pulse is shorter than 10ns. The pulse broadening reduces the accuracy of the measurand at sub-metric spatial resolution.

A breakthrough was made when Bao et al first observed the pre-activation of acoustic waves within the Brillouin resonance in 1999 [44]. This is qualitatively explained by Lecoeuche et al in 2000 [45]. This breakthrough enables a narrow output spactralwidth to be obtained even if the input pulse is shorter than 10ns. Then in 2005, Zou et al reported distributed measurements using pulse width down to 1.5 ns with the corresponding spatial resolution of 15cm [46]. In 2007, Brown et al presented a new scheme using dark-pulse pump signal which allows strong acoustic field excitation even when ultra-short dark-pulse width is used. By using dark pulses they built a sensor system with a spatial resolution of 20mm [47]. In the past few years much effort has been

made to enhance the performance of the BOTDA systems: to achieve a longer total sensing length or to obtain a higher spatial resolution. By using pre-amplification and employing Simplex code, M. A. Soto et al. achieved 120km total sensing length with 3.1°C/60με and 3m spatial resolution [48]. By using differential pulse-width pairs W.H. Li et al. demonstrated a BOTDA system with 10cm spatial resolution over kilometers of fibers [49]. Further improvement has been suggested by using a π-phase short pulse phase modulation on the pump and use the echo caused by the phase modulation for sensing [36][50] which is similar to pre-pumping using a dark pulse but with a magnitude twice as large, thus enables much more efficient realization.

Another achievement came from Hotate et al in 2000 [51]. They proposed an interesting technique based on the correlation control of two synchronous continuous frequency modulated waves. The resolution they reported was about 40cm, while the measurement range is 5.3m [52]. In 2006, they extended the measurement range to around 300m with a reduced spatial resolution of 20cm. More recently, in 2009, they managed to obtain $3\,\mu\varepsilon$ micro-strains and 0.08 degrees Celsius measurement accuracy for 31meter optical fiber.

Along with the development of BOTDA systems, the Brillouin optical time-domain reflectometry (BOTDR) was proposed just after the first

demonstration of the BOTDA system. It was first demonstrated by Kurashima in 1992 [53]. The principle of BOTDR is based on the OTDR technique but here the system uses spontaneous Brillouin scattering instead of Rayleigh scattering. BOTDR offers the advantage of single-end access. Comparing with the BOTDA technique, a spatial resolution of 1 m with measurement accuracy of ±0.003% has been achieved. However, the main advantage of BOTDA over BOTDR lies in the stimulated nature of the Brillouin interaction. Due to signal amplification in a system, for the same sensing length, the signal to noise ratio of the detected signal in a BOTDA system is much higher.

3.3.2.1 Brillouin Optical Time-domain Reflectometry (BOTDR)

Brillouin optical time-domain reflectometry (BOTDR) is a time domain technique. It was first developed by Kurashima in 1992 [54][55]. Two years later, K. Shimizu from the same group reported their results of using BOTDR to realize distributed strain and temperature sensing [56]. The configuration of their setup is shown in Figure 3-3. The system is based on the spontaneous Brillouin scattering. In the system, the light from a distributed feedback (DFB) laser is modulated using a pulse and the signal is then amplified before injecting into the fiber under test. The backscattered light due to the spontaneous Brillouin scattering is heterodyne detected using the reference light wave as the local oscillator signal (LD). Although at that time the spatial resolution of the

distributed sensing system was not studied, it is a very important work because it is the first demonstration of the technique and since then a lot of research has been carried out in the area and significant progress has been made.

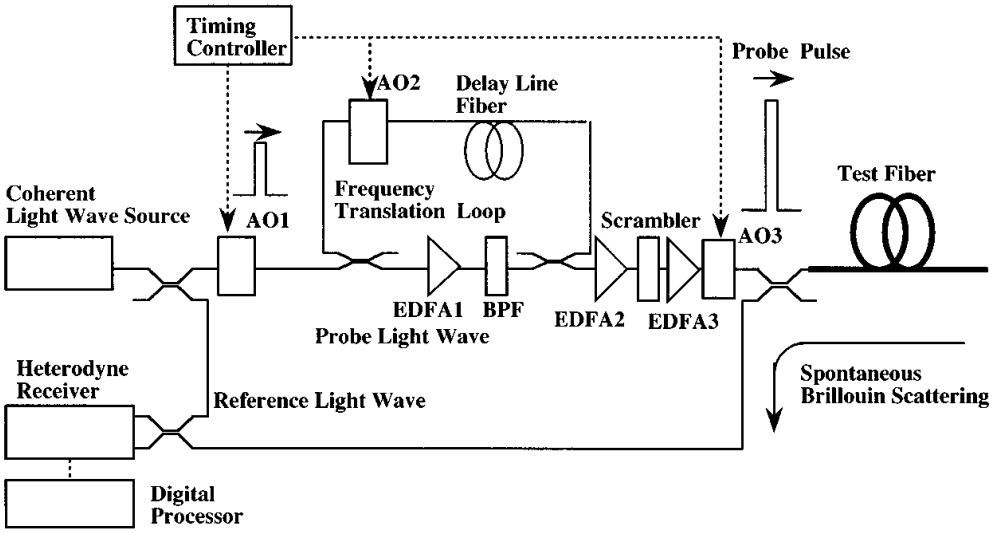

Figure 3-3 Configuration of the BOTDR system [56]

3.3.2.2 Brillouin Optical Time-domain Analysis (BOTDA)

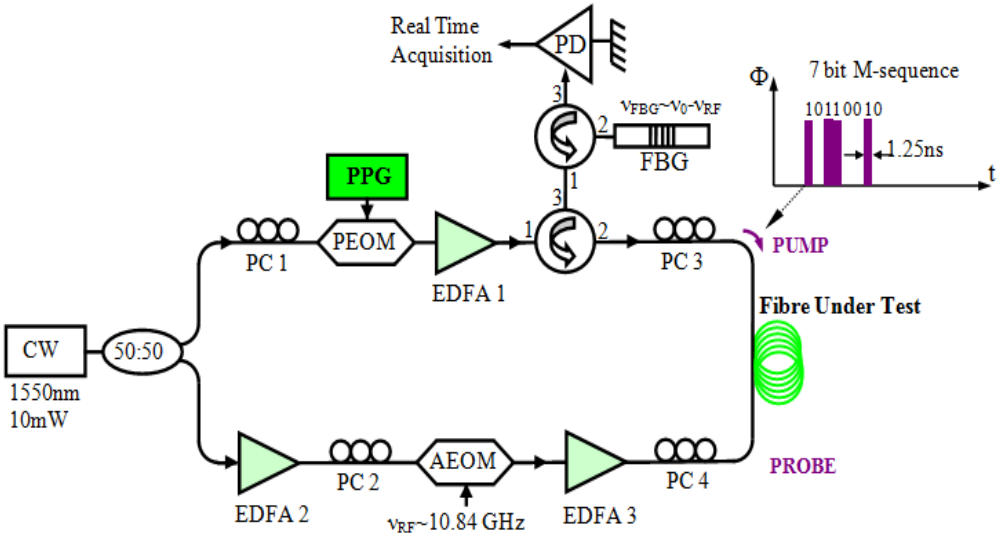

Figure 3-4 Experimental setup for BOTDA using phase modulated code sequences.

The typical BOTDA system is shown in Figure 3-4, the output from a continuous wave (CW) DFB laser signal is split through a 50:50 coupler to generate both the pump and the probe signals. An electro-optic modulator (EOM) driven by a pulse pattern generator (PPG) is employed to generate a custom phase or amplitude modulated pump signal at high repetition rate in the upper arm of the setup. In the lower arm, an electro-optic amplitude modulator (AEOM) driven by a sinusoidal wave signal at a frequency approaching the Brillouin frequency of the fiber under test (FUT) is used to generate the Stoke probe signal. Both pump and probe signal power will be adjusted respectively through an Erbium doped fiber amplifier (EDFA). The Stokes signal will be subsequently isolated, detected and analyzed through a narrow bandwidth FBG filter (~10GHz), a photodetector and a data acquisition and processing system (real time oscilloscope).

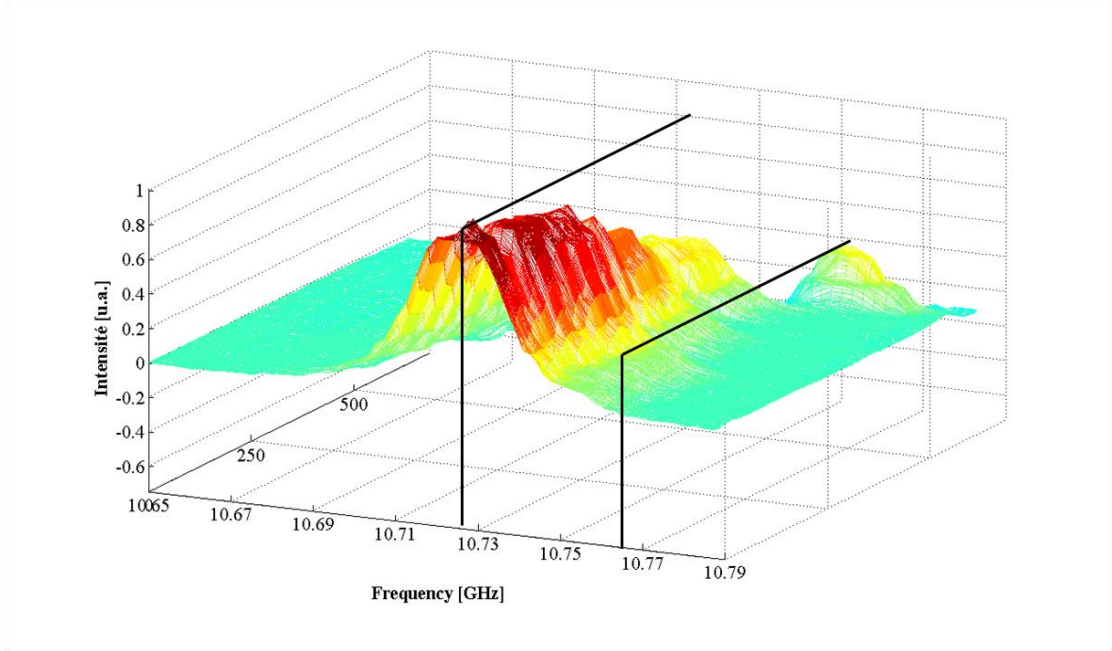

Figure 3-5 Typical result of the BOTDA experiment

The typical experimental result is shown in Figure 3-5. Most of the fiber under test is put under room temperature and the Brillouin frequency shift of the fiber is 10.73GHz as shown in Figure 3-5 and part of the fiber is put under higher temperature. The Brillouin frequency shift for the portion of fibre at higher temperature is 10.77GHZ. During the experiments we set the frequency of the RF source at a given value and then measure the reflected signal. This shall give us the Brillouin gain corresponding to the given frequency. By scanning the frequency of the RF source for the whole spectral span, Brillouin gain profile along the fiber is obtained. This is shown as a three dimensional spectral plot in Figure 3-5. The x axis represents the positions along the fiber, y

axis is the frequency, and z axis is the strength of the reflected signal i.e. the Brillouin gain. From this figure we can obtain the Brillouin gain/loss spectral for each point along the fiber. Based on this we can calculate the temperature or strain distribution of every single point along the fiber.

3.3.2.3 Brillouin Optical Frequency-domain Analysis (BOFDA)

Both BOTDR and BOTDA are time-domain approach, which means that a short pulse is sent along the fiber and the backward scattered light is detected with high temporal resolution and the spatial information is carried by the time different between the time the pulse is transmitted and when it is received. BOFDA carries out the measurement in the frequency domain to determine the transfer function of the fiber. Optical frequency domain reflectometry (OFDR) was first analyzed by Ghafoori-Shiraz *et al.* in 1986[57]. Ten years later Dieter *et al.* proposed Brillouin Optical Frequency Domain Analysis (BOFDA) [58][59].

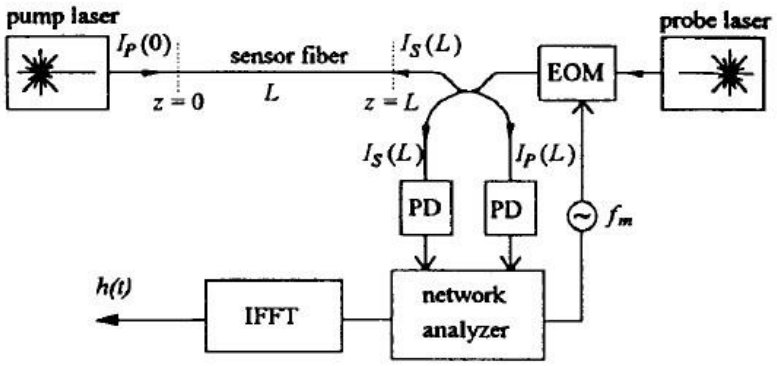

Figure 3-6 Typical configuration of a BOFDA system [59]

The configuration of a BOFDA system is shown in Figure 3-6. Unlike the time domain approach within which a short pulse is used, the frequency domain approach uses CW light for both pump and probe signals. The intensity of the probe light is modulated by an RF signal with a modulation frequency f_m. The received signal is then converted into digital signal by an analog to digital converter. The digital signal is fed to a signal processor which calculated the Inverse Fast Fourier Transform (IFFT). The IFFT is approximately the impulse response of the system.

The authors claimed that using BOFDA can improve the signal to noise ratio and achieve better dynamic range due to the use of inverse Fourier transform. They also claimed BOFDA can achieve higher temperature or strain resolution. However the main drawback of a BOFDA system is the measurement time. It is much longer compare to that of the BOTDA system.

3.3.2.4 Brillouin Optical Correlation-domain Analysis (BOCDA)

Brillouin optical correlation-domain analysis (BOCDA) is an approach proposed by Hotate *et al.* in 2000 [51]. The principle of the BOCDA system is that the probe's gain spectrum at certain position is determined by fiber Brillouin gain spectrum and the pump-probe beat spectrum. If the probe and pump signal is modulated in phase or frequency, a gain peak will appear at a position along the fiber where the two beams are highly correlated. The position of the gain peak can be tuned by changing the modulation signal.

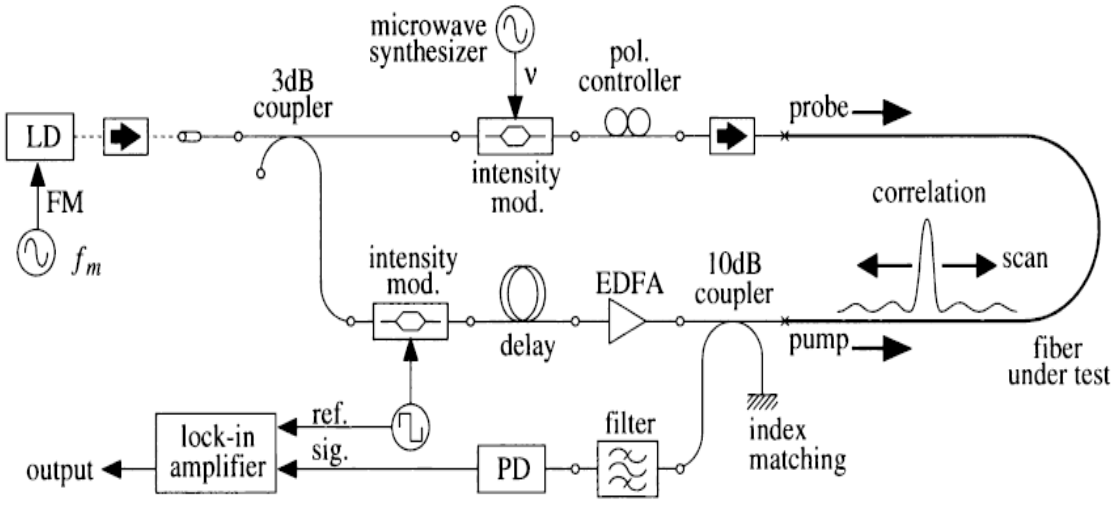

Figure 3-7 Setup of a BOCDA system [51]

Their experiments setup is shown in Figure 3-7. The light from the laser diode is modulated by a sinusoidal waveform of frequency f_m and then divided into two beams by a 3dB coupler. One beam is modulated by an intensity

modulator with a microwave frequency ν to generate two sidebands. The lower sideband with frequency $\nu_0 - \nu$ is used as the probe signal and counter-propagates with the other beam which is used as the pump signal. Polarization controllers and EDFAs are used to control the polarization state and power of the system. The reflected signal is then coupled out by and 10dB coupler and received by the PD. In this system, the gain spectrum is obtained by changing the microwave frequency ν and the distribution of the gain along the fiber is obtained by varying the FM frequency f_m.

Brillouin scattering in a BOCDA system can be generated locally along the fiber therefore pulsed light is no longer needed. So this technique offers the advantages including extremely high spatial resolution, strong backscattered signal, and free of the spectral broadening due to the short pulse used in other techniques. Using this technique, two years later Hatate *et al.* reported their achievement of 1-cm spatial resolution of distribution sensing [60]. In 2006 Kwang-Yong Song *et al.* demonstrated distributed sensing with 3mm spatial resolution based on BOCDA [52]. Applications based on BOCDA including aircraft structural health monitoring and crack detection have also been reported [61][62].

The drawback of BOCDA system includes the limitation of sensing range,

high complexity, and long measurement time. The sensing range is generally limited to several meters. The limitation is due to the relative phase shift between the two CW waves. The sensing range can be improved by stabilizing the probe and pump waves at different frequencies. The penalty is a reduction of the spatial resolution. The Brillouin scattering is generated locally and the position is switched by varying the modulation frequency f_m. Therefore it will take many steps to finish a scan along the whole fiber, which increase the complexity of the system and the measurement time.

CHAPTER 4. LIMITATIONS OF CURRENT BOTDA SYSTEMS

In this chapter, performance limitation of current BOTDA systems is discussed. A scheme for measuring acoustic lifetime of optical fiber is proposed. The result of acoustic lifetime of different types of optical fiber is presented.

4.1 Brillouin Signal

Before the limitations of a BOTDA system are discussed, the working principle of a BOTDA system and how the Brillouin signal is obtained are described briefly.

A typical Brillouin Optical Domain Analysis (BOTDA) system is shown in Figure 4-1.

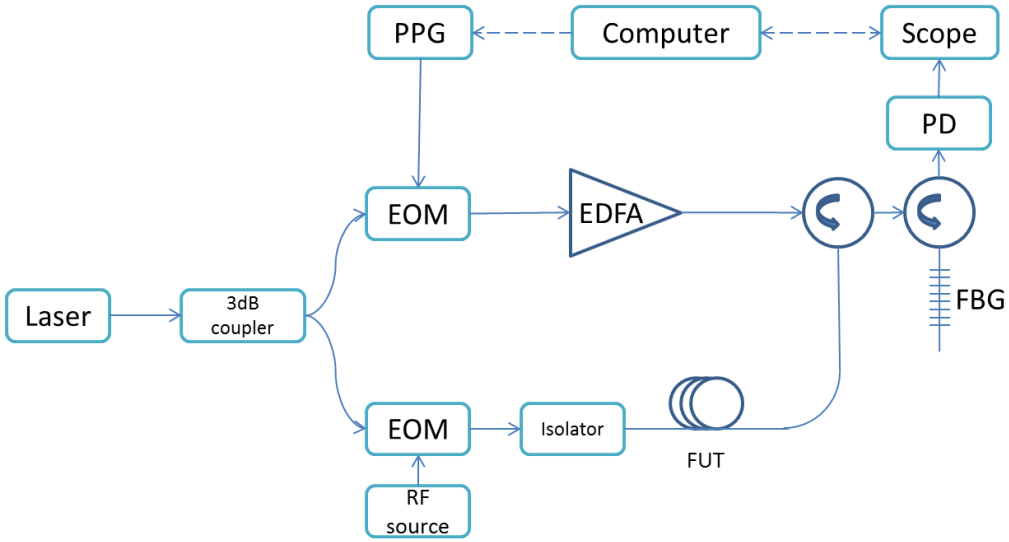

Figure 4-1 Typical experimental setup of BOTDA

The light from a narrow linewidth laser is split into two beams. The upper beam is modulated by an EOM which is driven by a pulse generator to form the pump pulse. The lower beam in modulated by another EOM driven by a radio frequency (RF) generator. The sideband of the modulated signal is then used as the Stokes light. The frequency difference is defined by the frequency of the RF

generator. The pump pulse and the Stokes light will counter-propagate in the fiber. The Stokes light will be amplified by the pump pulse based on the Brillouin gain profile at different point of the fiber. The probe signal is filtered out by an FBG filter and then detected by the photo detector. The Brillouin gain along the fiber is subsequently obtained.

The detected probe signal for one frequency step is shown in Figure 4-2.

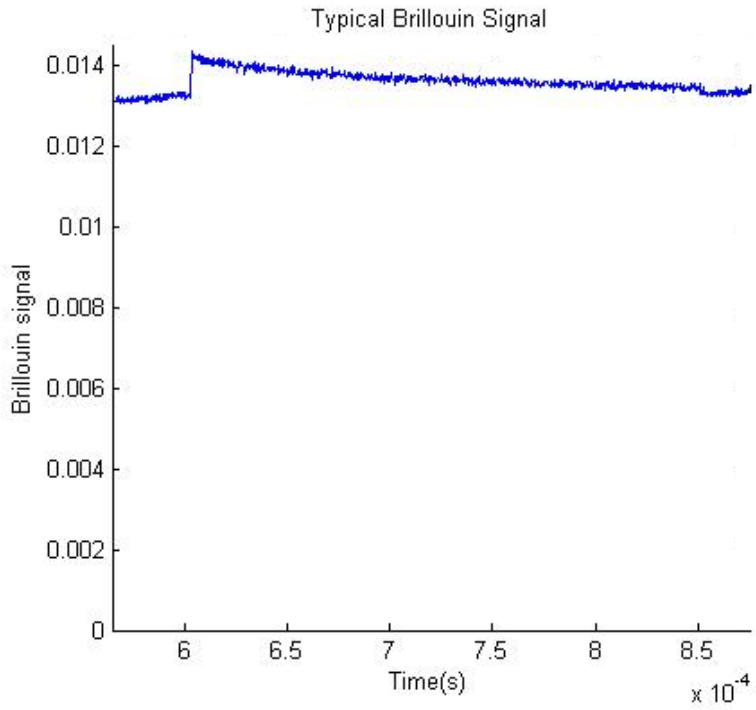

Figure 4-2 Brillouin signal from 25km G652D fiber

Because of the backscattered nature of Brillouin scattering, the light scattered at different point along the fiber will arrive at the photodetector at

different time. Thus in Figure 4-2, the time will be equivalent to the position along the fiber.

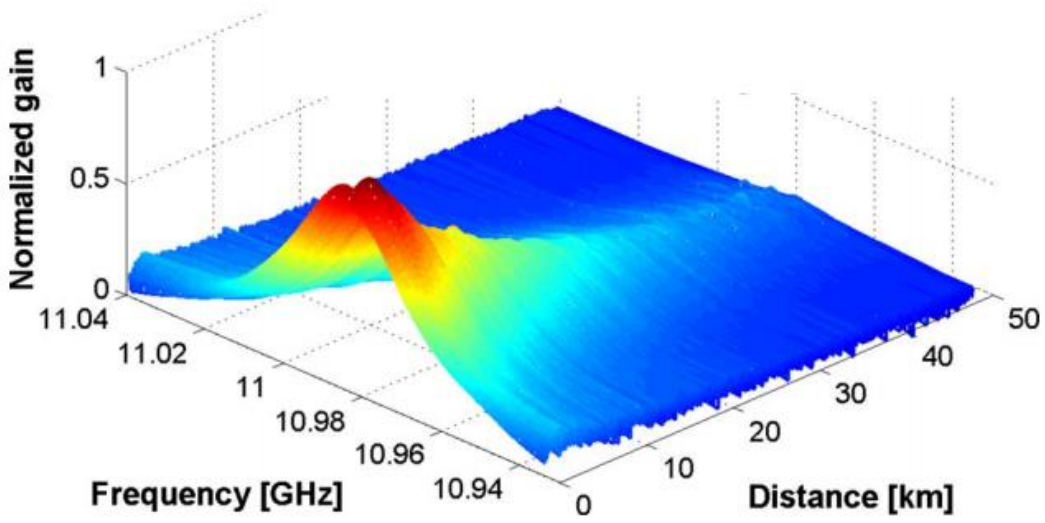

Figure 4-3 Typical Brillouin signal represented by a 3-D map

By tuning the frequency of the RF generator we can scan the Brillouin gain through changing the frequency difference between the pump and the probe signals. Combine all the signals measured for different frequency difference, we can draw a three dimensional plot with position, frequency, and Brillouin gain amplitude as the three axes as shown in Figure 4-3.

The signal shown in Figure 4-3 is for a 25km long G652D fiber. During the experiment the pump pulse is 20ns corresponding to a 2m spatial resolution. The frequency of the probe signal is set at 10.83GHz lower than the pump signal, which is the Brillouin shift of the G652D fiber. The probe signal is then detected

by a 125MHz photodiode and measured by a realtime oscilloscope (Picoscope 5203). From Figure 4-2 and Figure 4-3 we can see that key features of the signal include a DC component, an AC component, and the noise. The strength of the AC is decaying along the fiber because the energy of the pump pulse is decreasing while propagating along the fiber due to the fiber attenuation and at the same time some of the energy is transferred from the pump to the stokes signal. To be more easily detected, the signal should fulfill the following requirements. Firstly, the AC component which is the signal we need should be large enough. Secondly the noise should be small otherwise we can only detect noise. Thirdly the ratio of AC/DC should be large because the dynamic range of the ADC (analog-to-digital converter) of the realtime/sampling scope is fixed, which means if the AC/DC ratio is small, the measured result of the scope may not show the accurate value of the AC component due to the quantization noise of the ADC.

4.2 Spatial Resolution Limitation of the BOTDA Systems

In early experimental demonstrations bright pulse Brillouin Gain and bright pulse Brillouin loss schemes were used [40][41][63]. At that time it was believed that the spatial resolution is limited by the phonon life time of the Brillouin

process which is normally 10ns. So when we use Brillouin scattering to carry out distributed sensing, the pump pulse cannot be shorter than 10ns. Otherwise there will be no Brillouin scattering since the time duration of the light wave is too short to generate an acoustic wave strong enough to scatter the light. This will limit the spatial resolution of the distribution sensing system, which cannot be shorter than 1m under this limitation.

4.2.1 Frequency-domain Interpretation

The limitation to spatial resolution can be explained in both frequency domain and time domain. Based on frequency domain explanation the spectral width of the Brillouin scattered light is defined by the decaying speed of the acoustic wave. In the optical fibers the spectral width is generally wider than that of the bulk silica. This broadening is attributed to the properties of the fiber for example the doping type and concentration [64]. This is because the materials doped into the fiber can increase the decaying speed of the acoustic wave in the fiber and thus increase the width of the Brillouin gain spectrum. The typical width of the Brillouin Gain spectrum is around 27MHz. On the other hand, the pump pulse injected into the optical fiber will have a spectral width defined by the pulse width of the pump. The spectral width will grow gradually while the pulse width decreases. The effective gain spectrum of the Brillouin gain is the

convolution between the spectrum of the pump pulse and the Brillouin Spectrum of the optical fiber.

For BOTDA systems with low spatial resolution, the pulse width of the pump pulse is so wide (normally larger than 10ns) that its spectral width is much narrower than the Brillouin spectrum of the fiber. In this case the effective gain spectrum measured from the experiment is approximately the same as the Brillouin spectrum of the optical fiber. Then measured Brillouin gain spectrum can represent the real spectrum so we can measure the strain or temperature properly.

To achieve high spatial resolution, the pulse width of the pump pulse must be very short. For BOTDA systems with centimeter scale spatial resolution, the pump pulse can be as short as 100ps. This means the frequency spectrum of the pump signal will be broader than the Brillouin gain spectrum of the fiber. The measured effective gain spectrum will be limited by the fiber's Brillouin gain spectrum and this will limit the strain or temperature resolution. At the same time the peak value of the effective gain spectrum will also decrease thus it will result in a reduced SNR.

4.2.2 Time-domain Interpretation

The acoustic wave in the optical fiber is the movement of the materials. This movement has an inertial response with a time constant around 12ns. Which means it will take about 12ns to excite the acoustic wave when the pump and signal light wave are injected into the fiber. For pump pulses shorter than this time constant, the acoustic wave cannot be fully excited. The partly excited acoustic wave itself is weak and will result in a weak Brillouin scattering. When the pump pulses are extremely short, which is the case for the high spatial resolution BOTDA system, the Brillouin signal will be very small and lead to a much reduced SNR. In this case there will be a large error of the measurement result. This is also the reason people believe the best spatial resolution of the BOTDA system is 1m limited by the lifetime during the early years of development of this technology.

4.2.3 Break the Limitation of Spatial Resolution of the BOTDA System

As mansion before, the spectral width of the Brillouin signal becomes very large when the width of the pump pulse is very short. This is the main reason why during the early years of developments the researchers believed the spatial resolution limited by the acoustic lifetime at 1m. A remarkable progress was

made by X. Bao *et al.* in 1999. They reported that they can measure short pulses and narrow Brillouin spectrum simultaneously as shown in Figure 4-4 [44].

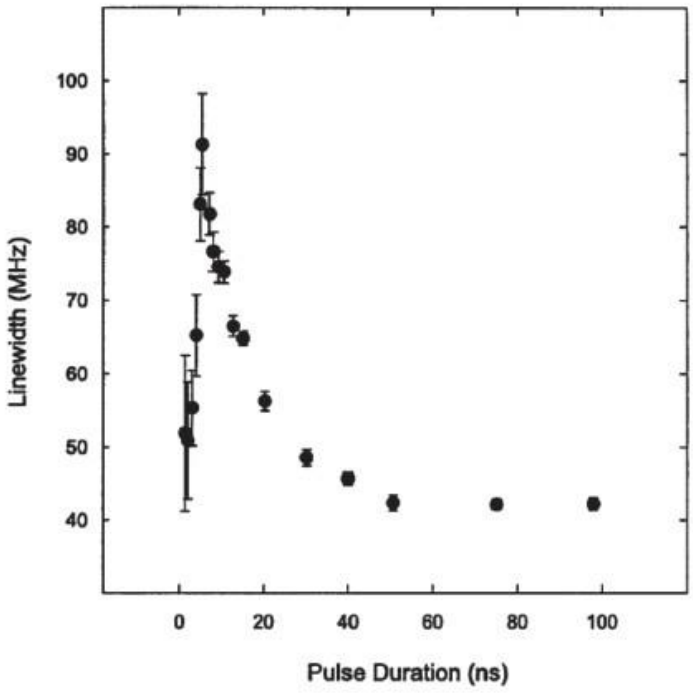

Figure 4-4 Short pulses and narrow Brillouin spectrum simultaneously [44]

As shown in Figure 4-4 the linewidth of the Brillouin spectrum increases while the pulse duration decreases at first as everyone expected. However, when the pulse duration is shorts than several nanoseconds the Brillouin linewidth drop quick while the pulse duration decreases and it come back to the linewidth with very long pulse finally.

Later this phenomenon is attributed to the low extinction ratio of the EOM they used. This means there is still some optical power when it is supposed to be

zero. Under this condition, when the duration of the pulse is longer than the acoustic life time the pump pulse can still excite the acoustic wave. Thus the Brillouin linewidth increases while the duration of the pump pulse decreases, just as discussed before. However, when the duration of the pump pulse becomes much shorter than the acoustic lifetime, the pump pulse cannot excite sufficient acoustic wave for the Brillouin scattering. It is the background power which excites the acoustic wave. Namely the acoustic wave is pre-excited by the leaking energy of the modulator. Then when the short pump pulse come, the acoustic wave remain its former state due to the inertial behavior of the material as shown in Figure 4-5. Since the Brillouin spectrum being measured comes from the leaking energy instead of the pump pulse, its linewidth is similar to that of the Brillouin spectrum generated by a continuous pump light.

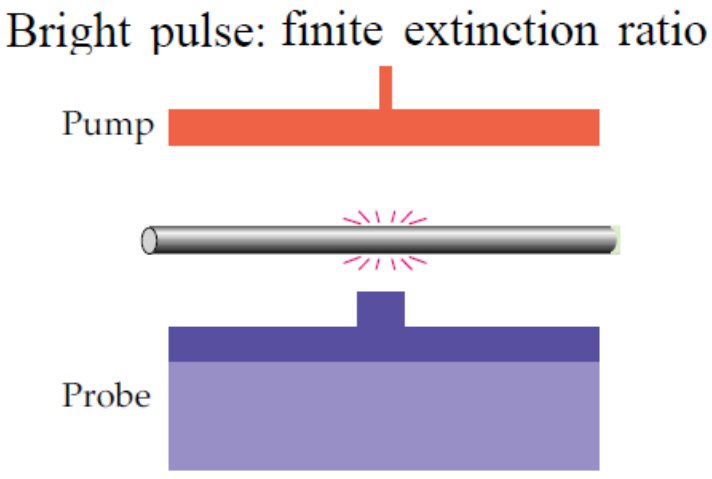

Figure 4-5 Finite extinction ratio

The discovery by X. Bao *et al.* shows that the limit of the acoustic lifetime can be break and the spatial resolution of the BOTDA system can be much higher the 1m spatial resolution limit. Later this discovery led to a novel technique to realize high spatial resolution distributed sensing which is called echo sensing. Echo sensing including the finite extinction ration methods, dark pulse methods, and the phase modulation methods. All of these techniques are trying to pre-excite the acoustic wave before the pump pulse is injected into the fiber. Then when the pump pulse goes into the fiber, the acoustic wave will almost maintain the same state as before due to the inertial behavior of the material.

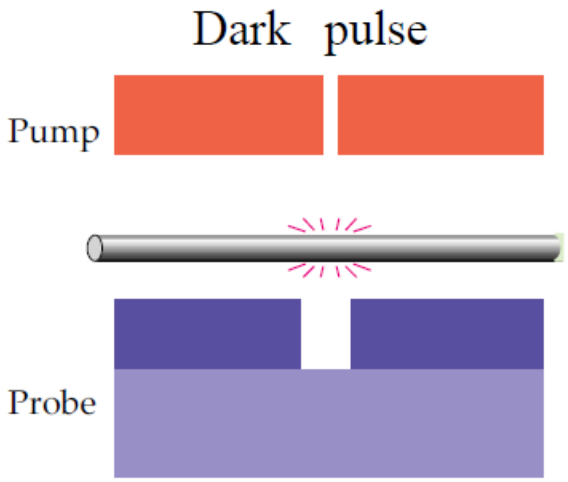

Figure 4-6 Dark Pulse

The dark pulse technique proposed by Brown *et al.* presented a new

scheme of using dark-pulse pump signal to enable strong acoustic field excitation even when ultra-short dark pulsewidth is used. Although the pulsewidth is very narrow, the optic power is in the outside of the pulse and the duration is long enough to generate sufficient acoustic wave for the scattering process.

Recently short pulse phase modulation on the pump has been suggested to further improve the BOTDA system performance. It can cause the same Brillouin loss as a dark pulse but with a magnitude twice as large, thus much more efficient realization [50][65].

In all these systems, when the length of the sensing fiber is long and the spatial resolution is high, the system performance will be limited by low SNR at the signal detection and processing system. This leads to a tradeoff between the total sensing length and the spatial resolution. We can only realize either a long range sensing system with low spatial resolution or high spatial resolution sensing system with short sensing length. To increase SNR of the system, code sequences instead of a single pulse can be used to modulate the pump of the BOTDA system [66]. The most popular code used is Simplex code that has been successfully used in OTDR systems before [67]. It has been suggested that the use of the code in a BOTDA system can significantly enhance its SNR [68][69].

Recently, a BOTDA fiber sensing system with 1m spatial resolution over a 50 km range was reported [70]. This was the first demonstration of the use of the simplex code in a BOTDA system. In the experiment, the SNR of the system is greatly enhanced by 10.3 dB when a 511-bits Simplex code was employed.

4.3 Limitations of the Sensing Range

We already discussed about the spatial resolution limitation. Now we will focus on the limitation of the sensing range and discuss the challenges we face while trying to realize high spatial resolution and long sensing range simultaneously. We will discuss the limitations on the sensing range.

In BOTDA systems, the pump power should be carefully adjusted, especially for long sensing length system. Generally, to realize a precise measurement, we need a Brillouin signal with high amplitude. The power of the pump pulse and probe signal launched into the sensing fiber should be high in order to obtain a large Brillouin signal. However there are mainly two problems if we launch high power pump pulse and probe signal into a long sensing fiber. The first problem is that the pump power will be limited by the modulation instability; Raman scattering, and the SBS power threshold. The pump pulse power should be smaller than those critical powers to avoid the depletion. The second problem is that the probe power is also limited by the depletion. If the

power of the probe signal is high, the Brillouin scattering will be very strong. This will lead to a potentially depletion of the pump power. Under this condition the pump power can be very small after a long fiber, which means the signal from the end part of the fiber is very small and the spectral measured from that part of fiber is shifted from the real value.

In any BOTDA system, no matter it is based on Brillouin Gain or Brillouin Loss, the power from the higher frequency light will be gradually transferred to the lower frequency light. The energy transfer will result in depletion. For BOTDA system with short sensing fiber, depletion is not a major problem. However, when the length of the sensing fiber increases, depletion will become a serious problem. The depletion of the pump power will affect the system from two aspects. Firstly the depletion of the power will cause the error in the spectral measurement near the end of the sensing fiber. Secondly it will reduce the signal amplitude near the end of the fiber and it will make the measurement even more difficult.

4.3.1 Depletion Due to Attenuation

If only fiber attenuation is considered when considering the pump power distribution along the fiber, the optical power in the optical fiber will be attenuated during the propagation by a factor of α. The power distribution of

the pump and signal light in the fiber is:

$$P_P(z) = P_{p0}e^{-\alpha z} \tag{4.1}$$

$$P_s(z) = P_{s0}e^{-\alpha(L-z)} \tag{4.2}$$

respectively. Here P_P and P_S are the power of pump and signal light, respectively, z is the distance between a given point and the starting point of the fiber, P_{P0} and P_{S0} are the initial pump and signal power injected into the fiber, α is the fiber loss factor and L is the total length of the fiber.

The local Brillouin signal amplitude depends on the Brillouin gain efficiency of the fiber g_B, the effective mode area A_{eff}, the local pump and signal power at the particular point P_P and P_S, and the pulse width of the pump pulse which corresponding to the spatial resolution of the system Δz:

$$\Delta P_s = \frac{g_B}{A_{eff}} P_P P_s \Delta z \tag{4.3}$$

From equations (4.1) (4.2) and (4.3) we will have:

$$\Delta P_s(z) = \frac{g_B}{A_{eff}} P_{p0}e^{-\alpha z} P_{s0}e^{-\alpha(L-z)}\Delta z = \frac{g_B}{A_{eff}} P_{p0}P_{s0}e^{-\alpha L}\Delta z \tag{4.4}$$

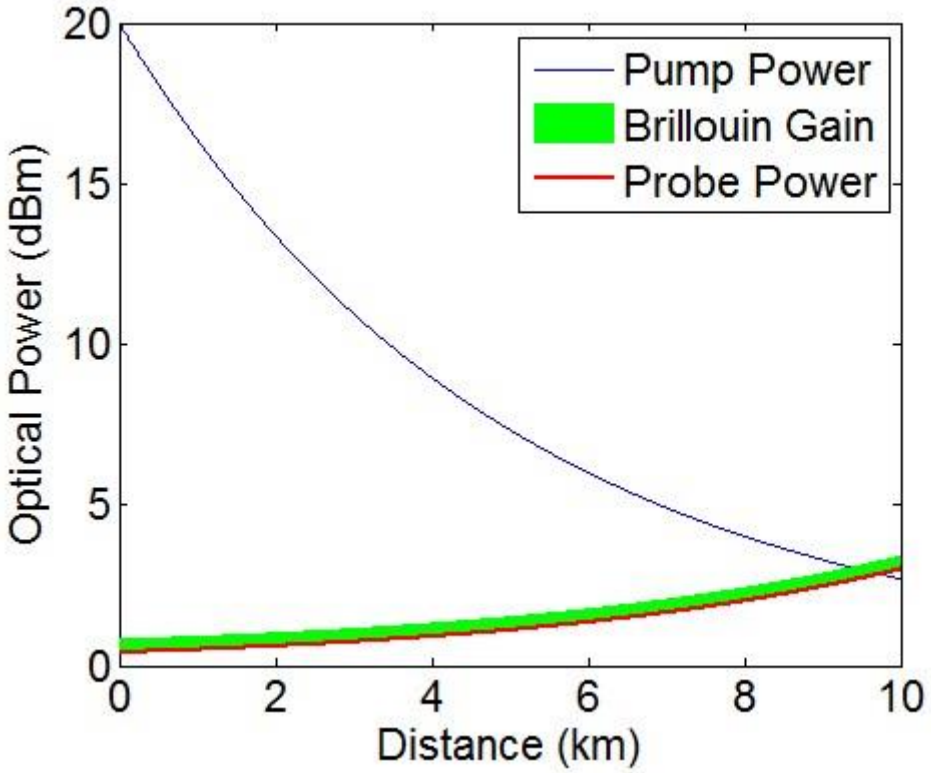

Figure 4-7 Brillouin gain (green area) and pump power (Blue line) and probe power (red line) along the fiber

From equation (4.4) and Figure 4-7 we know the signal is independent of the location z, which means for a given fiber and pump and signal power, the local Brillouin scattering power is uniform along the fiber. Equation (4.4) also indicates that the strength of the Brillouin Gain depends on the pump and probe power, the length of the fiber, and the attenuation of the fiber.

Unlike the uniform Brillouin gain shown in Figure 4-7, in the experiment the signal from the end of the fiber is smaller than that from the beginning of the

fiber. This is mainly due to the attenuation while the scattered signal propagating along the fiber. Although the Brillouin signal is independent of the position z along the fiber, as described by equation(4.4), the signal itself will also be attenuated while propagating along the fiber:

$$\Delta P_s(z) = \frac{g_B}{A_{eff}} P_{p0} P_{s0} e^{-\alpha L} \Delta z e^{-\alpha z}, \tag{4.5}$$

This means the signal from the end point of the fiber will become even smaller because it will experience the most loss since it will propagate in the fiber for the longest distance. Because of this, the signal from the end point is the most difficult to be measured. The following part of this chapter will focus mainly on signal from this point. To increase the Brillouin signal power as well as the SNR from this critical point we need to increase the power of the interacting waves. In addition, we need to choose a fiber with higher Brillouin gain efficiency g_B, or a smaller mode area A_{eff}. At the same time for distributed sensing with long sensing range, we also need to choose a fiber with very small attenuation α to get a high signal power at the critical point. For a given fiber if we want to obtain a larger Brillouin signal, we have to increase the initial pump and signal power P_{P0} and P_{S0}. However both of them can not be increased infinitely since the pump power will be limited by other nonlinear effects such

as modulation instability and forward Raman scattering and the probe power is limited by depletion and amplified spontaneous Brillouin scattering. So when the spatial resolution is high and the total sensing length is very long, the Brillouin signal will be very weak and the detection of such a weak signal becomes the main challenge of the measurement.

4.3.2 Modulation Instability

The modulation instability originates from Kerr effect and anomalous dispersion. It is a solitons self-building process and depends on the signal power, the larger the power, the stronger the effect of modulation instability. The critical peak power for the pump is:

$$P_{pcrit}^{MI} = \frac{4}{2\gamma L_{eff}} \tag{4.6}$$

Where γ is the fiber nonlinear coefficient, which is around $1W^{-1}km^{-1}$ in the standard silica optical fibers. For a fiber with a length of 25km its value is about 120mW. If the pump power is larger than this critical power it will be strongly depleted. Under the strong depletion condition the signal will become very small after a few kilometers of strong Brillouin scattering, as shown below.

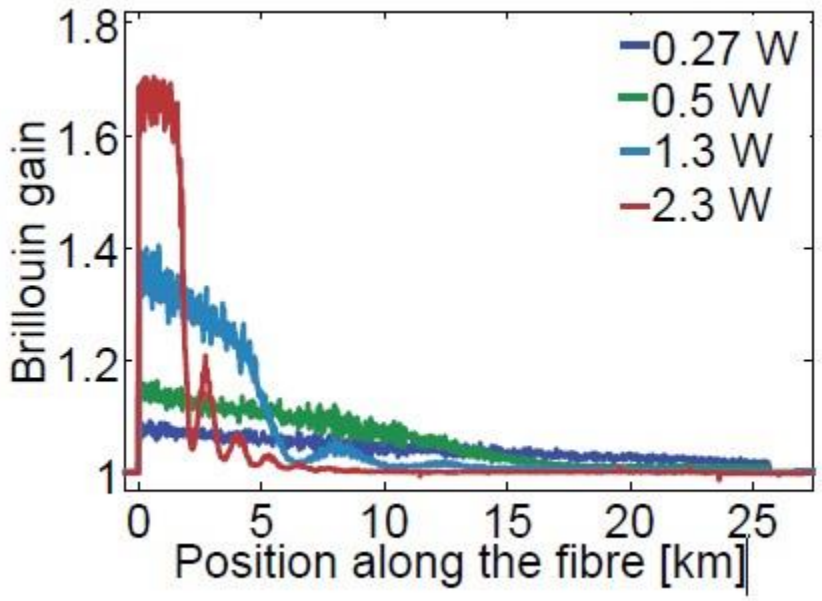

Figure 4-8 Brillouin distributed gain for different pump power in a 25km fiber [72]

Since the modulation instability originates from the Kerr effect and the anomalous dispersion, it can be totally eliminated if we use a dispersion shifted fiber which shows normal group velocity dispersion in 1550nm. However, this will increase the cost of the sensing system since dispersion shifted fiber is not ready available. Moreover, even if we replace the standard single mode fiber with a dispersion shifted fiber we can only eliminate the effect of modulation instability. There are still other nonlinear effects such as the Raman scattering which will limit the pump power at around 580mW. Under this consideration the pump power is limited at 120mW.

4.3.3 Depletion Due to the Probe Power

The other way to improve the response of the Brillouin sensing system is raising the probe power as mansion before. Here we will show that the probe power can not be increased infinitely either. As described in equation(4.4), the Brillouin signal strength depends on the probe power. A larger probe power means a stronger Brillouin signal and at the same time it means more energy transfer from the pump to the probe.

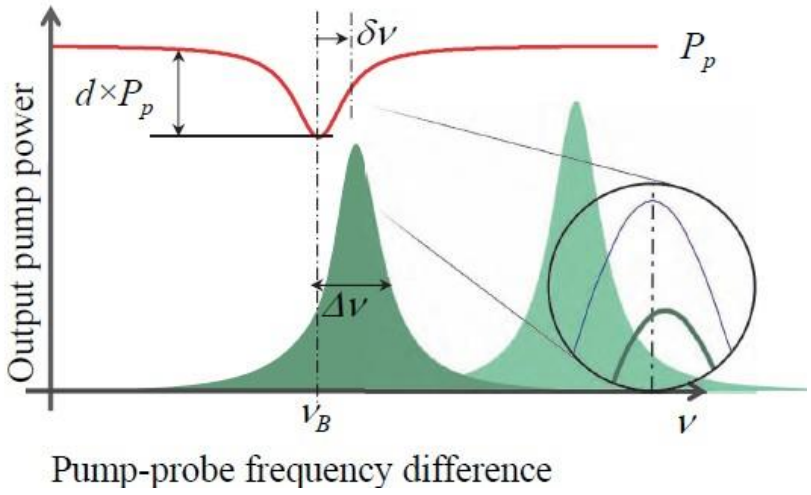

Figure 4-9 Effect of pump depletion by probe [72]

As shown in Figure 4-9, if the pump depletion is large due to the large probe power, the measurement of the spectrum at the far end of the fiber will not be correct. This means there will be a large error for the measurement of the Brillouin frequency as well as the temperature of strain. The limitation of the

probe power under this condition will be:

$$P_{CWcrit}^{SBS} = \frac{18A_{eff}}{g_B L_{eff}} \tag{4.7}$$

which is around 5mw in a long standard fiber.

4.3.4 Brillouin Power Threshold

The Brillouin power threshold of the fiber is:

$$P_{SBS} = \frac{21A_{eff}}{g_B L_{eff}} \tag{4.8}$$

where A_{eff} is the effective area of the fiber, g_B is the Brillouin gain coefficients, and L_{eff} is the effective length. In the BOTDA system the pump power should be smaller than this power threshold. Otherwise the pump pulse itself can stimulate the acoustic wave with or without the probe signal. This means if the pump pulse is larger than the power threshold we can have Brillouin signal even when the frequency different between the pump and probe is out of the Brillouin gain bandwidth of the fiber, which will reduce the measurement accuracy. From equation (4.8) it is clear that when the total length of the sensing fiber increases, the threshold of the stimulated Brillouin scattering in the fiber will decrease. This means in BOTDA systems if sensing fiber is long

the pump power should be small. The small pump power will result in very small Brillouin signal, which is very difficult to be detected.

4.3.5 Noise of the System

For a long sensing fiber the pump and probe signal power is limited to a very low level due to the SBS threshold, from equation (4.4) we know the Brillouin signal is very small when standard single mode fiber is used. To detect such a small signal, PIN or APD with electronic preamplifier can be used. In this case the performance of the system is limited by noise of the preamplifier. To further improve system performance, optical preamplifier can be used. In this case the main noise source is signal-ASE beating noise. In both cases signal to noise ratio (SNR) of the detected signal will be limited. To improve the SNR of the system, more averages have to be used to reduce the impact of noise, which will result in a much longer measurement time. Other methods include adding filters after the EDFAs to reduce the ASE noise, and using coding techniques to enhance the SNR by the coding gain.

4.3.6 Background Signal

From Figure 4-2 we can see that the detected Brillouin signal has a large DC component. In the experiment setup, the analog signal is converted to digital

signal through the ADC of the realtime oscilloscope. With a small Brillouin signal sitting on a large DC component and a limited number of effective bits for the ADC, signal to quantization noise ratio for the Brillouin signal will be low. To improve on this, DC component has to be removed.

A DC blocker can be used to remove the DC component effectively. However in a system with very high spatial resolution and long sensing range, it is difficult to realize this. High spatial resolution means we have to measure a high frequency signal. For example in a BOTDA sensing system with 1cm spatial resolution, the rising or falling edge of the detected signal should be less than 10ns, which corresponding to 1cm spatial resolution. The bandwidth of this signal is approximately 3.5GHz by the relationship:

$$BW = \frac{0.35}{\Delta t} \tag{4.9}$$

On the other hand the time duration of the signal from the starting point to the end point of the fiber is around $250\,\mu s$ corresponding to 25km fiber, as shown in Figure 4-2. This means the cut off frequency of the DC blocker cannot be higher than 4kHz. Unfortunately there is no commercial available DC blocker with a cut off frequency smaller than 4kHz and Bandwidth larger than 3.5GHz. So a large capacitor is needed to remove this DC component of the signal. For

the case shown in Figure 4-2, the AC/DC ratio can be improved by using a large capacitor after the photodetector to filter out the DC component of the received signal. The result is shown in Figure 4-10.

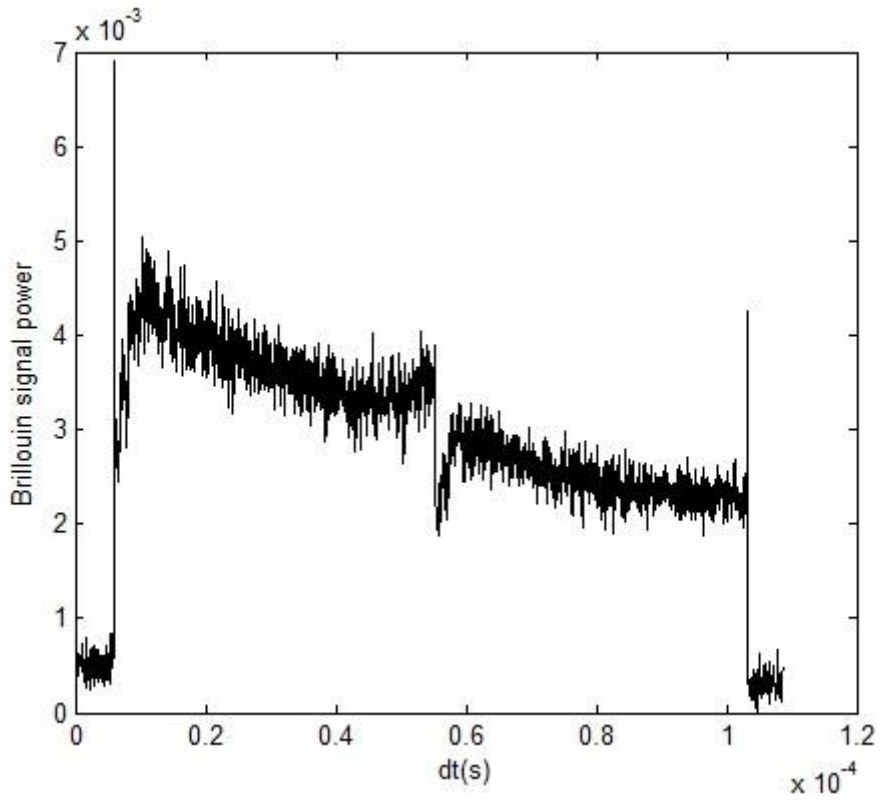

Figure 4-10 Brillouin signal with DC removed by a large capacitor

By comparing the results of Figure 4-2 and Figure 4-10, we can see the AC/DC ratio is enlarged greatly using the DC blocker. However, using the DC blocker to remove the DC components will introduce some distortion to the Brillouin signal.

Although this distortion can be reduced using a larger capacitor, it will be better to find methods to generate Brillouin signal with smaller DC component. We analyzed the setup carefully and find out that the sources of the DC component include the residual carrier frequency of the EOM which is used to generate the two sidebands to be used as the probe signal Brillouin scattering of the residual energy of the pump signal when it should be zero, the Rayleigh backscattering, and the ASE noise from the EDFAs. There is not much we can do about the Rayleigh scattering of the fiber, so here we focus on the modulators and EDFAs in the setup. The effect of these components on the experimental results and the possible ways to reduce these effects are studied.

4.3.6.1 Extinction Ratio of the Modulators

In the upper branch of the setup shown in Figure 4-1, an EOM driven by the pulse pattern generator is used to modulate the light from the cw laser with pulses. In practice the extinction ration of the modulator cannot be infinite. So there is always some power at the optical frequency of the pump propagating in the same direction of the pump pulse even when the pump should be zero. This leaked power and the cw probe signal can pre-excite the acoustic wave and it is reflected back all the time, which will contribute to the DC component of the detected signal. Moreover, it can interact with the probe signal and course more background noise, which will be discussed below.

In the lower branch an EOM driven by the RF source is used to generate two sidebands. The spectrum after the modulation is shown in Figure 4-11.

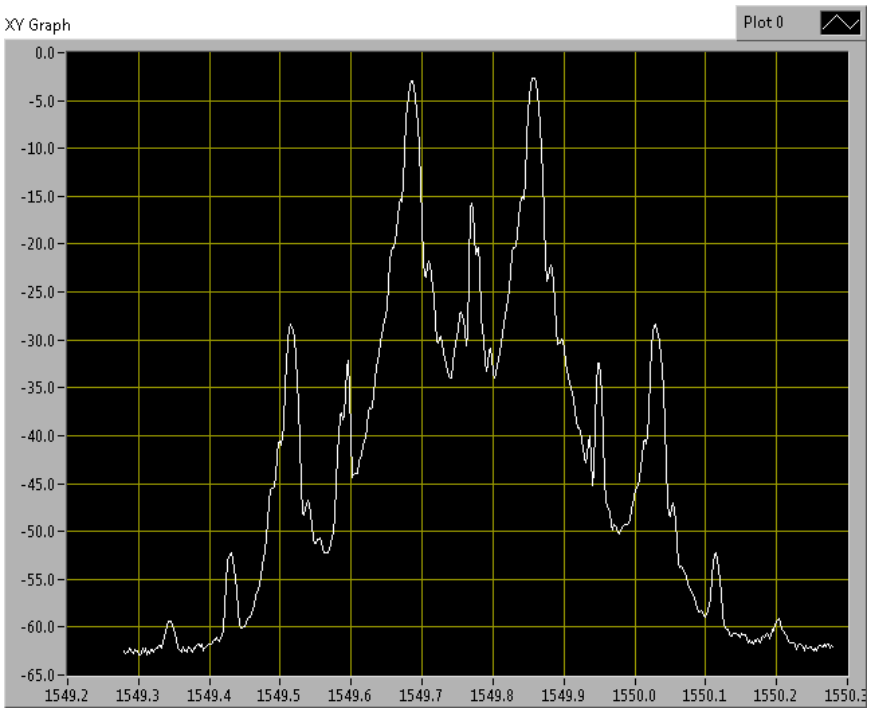

Figure 4-11 Spectrum of the modulated signal in the lower branch

In the EOM we carefully tune the bias voltage to the "null" point of the modulator. In this way the modulator works at the carrier-suppressed mode and modulated signal has a spectrum as shown in Figure 4-11. The center is the wavelength of the laser λ_0 . The energy of this frequency is suppressed. There are two main sidebands next to the carrier-frequency with a frequency around 11GHz, which is defined by the frequency of the RF source. Both of the sidebands are used as the probe light. The sideband with higher frequency will

experience Brillouin Loss while the sideband with lower frequency will experience Brillouin Gain. There are other frequencies due to the higher order harmonics with much less power and can be neglected here.

There are two advantages of using this approach. One advantage is that since the probe light is originated from the same laser as the pump, thus if there is a frequency drift of the laser, the frequency of the probe will drift with the pump frequency and their frequency different defined by the frequency of the RF source will not change. The system is more stable than the system using two lasers for pump and probe individually. The other advantage is the dual-probe can help to avoid the pump depletion as shown in Figure 4-12.

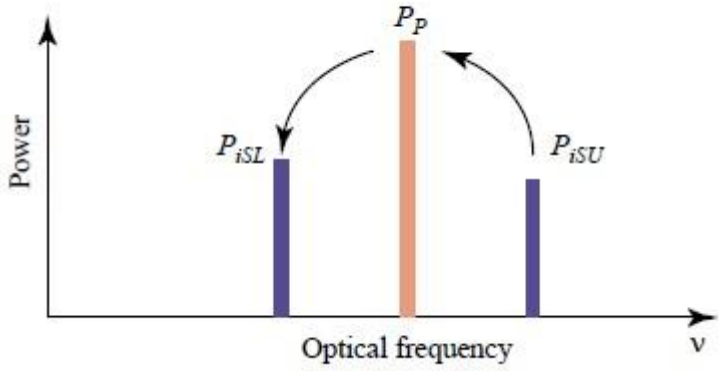

Figure 4-12 Effect on depletion of using the two sidebands method

In stimulated Brillouin scattering, the energy transfer is from the high frequency to the low frequency light. Part of the energy of the pump will transfer

to the probe signal while they counter-propagating inside the fiber. This will lead to a depletion of the pump power. This depletion will affect the measurement result as discuss before. However when there are two probes, while the energy of the pump transfer to the probe at lower frequency, it can be compensated by energy transfer from the probe with higher frequency to the pump. We then use a FBG to filter out one of the sideband and measure the signal of this particular frequency using a photodetector.

One problem in practical system of using the dual-probe method is that the residual energy at λ_0 can not be eliminated since the response of the modulator is not ideal. From the spectrum of the modulated signal shown Figure 4-11, there is still some power at the wavelength of the laser. Although the power of this frequency is much smaller than the power of the two probes, it will affect the response of the system.

This residual power has the same frequency as the pump light and they are from the same laser. They will interference with each other and form a stand wave along the fiber. Assume the electric field of the pump is $\overrightarrow{E_1} = E_1 e^{-i(\omega t - kz)}$ and the electric field of the residual power at carrier frequency in the probe is $\overrightarrow{E_2} = E_2 e^{-i(\omega t + kz)}$. We have the electric field of the interference pattern along the fiber:

$$\vec{E} = \vec{E_1} + \vec{E_2} = E_1 e^{-i(\omega t - kz)} + E_2 e^{-i(\omega t + kz)}, \tag{4.10}$$

where $E_1 = \left(\frac{2nP_1}{C\varepsilon_0 A_{eff}} \right)^{1/2}$ and $E_2 = \left(\frac{2nP_2}{C\varepsilon_0 A_{eff}} \right)^{1/2}$. P_1 and P_2 are the power of the pump in the zero state and the residual frequency from the probe, respectively.

The refractive index of the silica can be changed by the electric field of the light due to the elasto-optic effect:

$$\Delta n = \lambda \kappa E^2 \tag{4.11}$$

here κ is the coefficient of the elasto-optic effect.

So the refractive index along the fiber can be slightly modulated by the interference pattern of the two ligh and the amplitude of the modulation can be calculated as:

$$\Delta n = 4\lambda \kappa A_1 A_2 \tag{4.12}$$

Since the power P_2 is very small, the modulation is very weak. However this modulation exists all over the fiber because this two light exist in the whole fiber. The slightly modulation on the refractive index will then actually form a very long, weak FBG. The reflectivity of this FBG at λ_0 can be approximated

as [73]:

$$\begin{aligned} R(l,\lambda) &= \tanh^2\left(\frac{\pi\cdot\Delta n}{\lambda}\cdot l\right) \\ &= \tanh^2\left(\frac{4\pi\lambda\kappa E_1 E_2\cdot l}{\lambda}\right) \\ &= \tanh^2\left(4\pi\kappa E_1 E_2 l\right) \\ &\approx \left(4\pi\kappa E_1 E_2 l\right)^2 \\ &= (6.86*10^{-6}(P_1P_2)^{1/2}l)^2 \end{aligned} \tag{4.13}$$

which is linearly proportional to the optical power and to the square of the fiber length. When the length of the sensing fiber is extremely long, much pump power will be reflected back by the grating. Although the reflected light is at the frequency of λ_0, which is supposed to be filtered out by the filter before the photodetector, it will still affect the measurement since the filter used here can not have infinite suppression at this wavelength. So part of the reflected power still goes to the photodetector. When the power from the pump pulse is reflected, it will contribute to noise which is added to the Brillouin signal. When the power due to the finite extinction ration of the modulator is reflected back it will form the background energy and contribute to the DC component of the Brillouin signal shown in Figure 4-2. Although this power can be relatively small compare with the pump power, it is comparable with the Brillouin signal especially when the spatial resolution of the BOTDA system is very high since the width of the

pump pulse is very narrow and the Brillouin signal is also very small.

So in the BOTDA systems with a very high spatial resolution and long sensing range, in order to remove the DC component in the Brillouin signal as much as possible, we should pay extra attention to the two modulators used in the setup. We should bias the modulator in the pump branch at a proper position so that the extinction ration is large. Under certain conditions it will be very helpful to use a nonlinear loop mirror after this modulator to remove the DC component of the modulated signal. At the same time we should also pay extra attention to the modulator in the probe branch. It should also be biased at proper state in order to suppress the power at the carrier frequency λ_0 as much as possible. We can also put a FBG with very narrow bandwidth and central frequency of λ_0 after the modulator to reduce the residual power.

4.3.6.2 Noises from the EDFAs

Each EDFA used in the setup will generate Amplified Spontaneous Emission (ASE) noise. This noise is continuous in both spectral domain and time domain. So it will add noise to the final measured signal and contribute to the DC component in the Brillouin signal. In order to minimize this effect, a filter is suggested to be added after the EDFA. This will filter out the out of band noise while not affecting the detected signal.

4.3.6.3 The Coding Process

In the BOTDA systems employ coding technique, the coding and decoding process can also introduce some background signal to the Brillouin signal. For the complementary code used in our research, the distortion of the code sequence can introduce a large noise and background signal to the Brillouin signal, especially when long code sequences are used. This will be discussed in detail in next Chapter.

4.4 Experimental Study of a BOTDA System

4.4.1 Experimental BOTDA System

The schematic diagram of an experimental BOTDA system is shown in Figure 4-13.

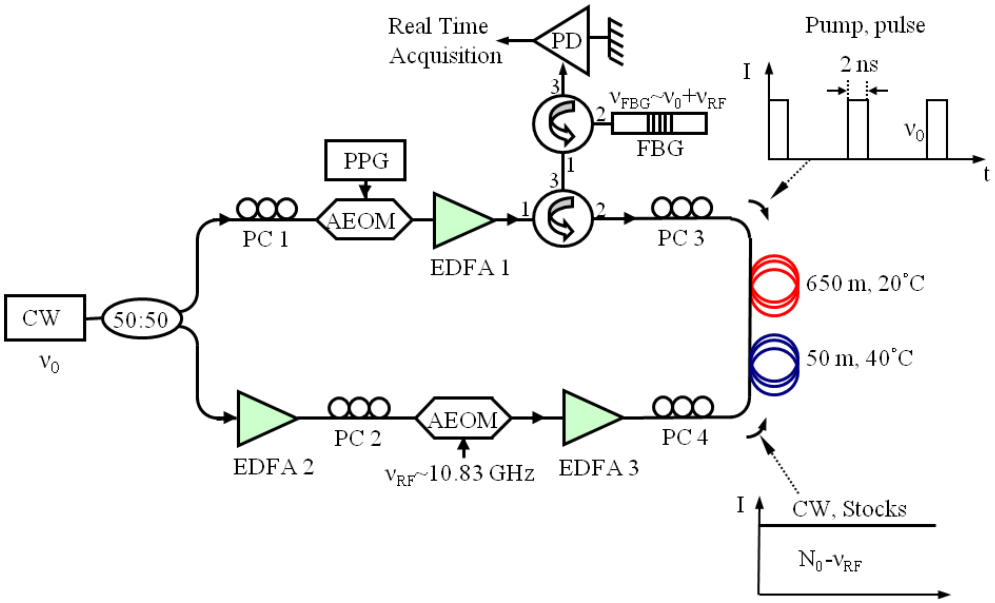

Figure 4-13 Our BOTDA setup with single pump pulse

The output from a continuous wave (CW) DFB laser signal is split into two beams through a 3dB coupler to generate both the pump and the probe signals. An EOM driven by a PPG is employed to generate pump pulse at high repetition rate in the upper arm of the setup. In the lower arm, an EOM driven by a sinusoidal wave signal at a frequency approaching the Brillouin frequency of the FUT is used to generate the Stoke probe signal. Both pump and probe signal power will be adjusted respectively through an EDFA. Polarization controller (PC) is used to optimize the polarization state of the light. PC1 and PC2 are used to modify the polarization state of the input light to maximize the efficiency of the two modulators. PC3 and PC4 are used to optimize the polarization state of the pump and probe signal to maximize the Brillouin scattering inside the FUT.

The Stokes signal is subsequently isolated, detected and analyzed respectively through a narrow bandwidth FBG filter (~10GHz), a photodetector and a real time oscilloscope.

4.4.2 Experimental Results of BOTDA System

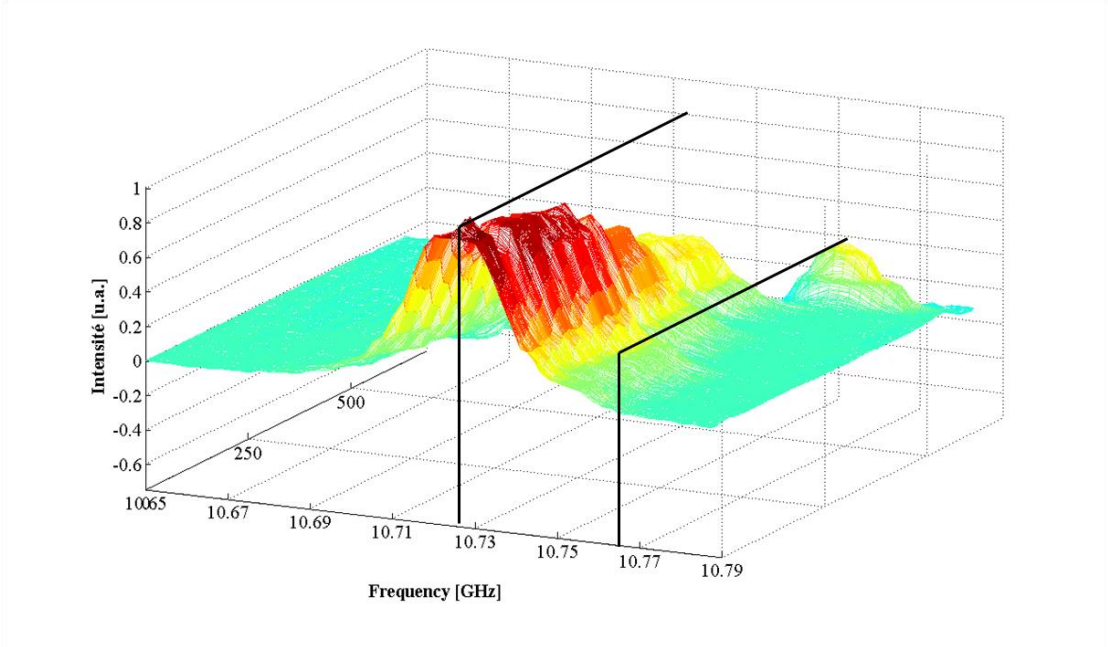

Figure 4-14 Experimental result of the BOTDA system

During the experiments we set the frequency of the RF source at a given value and then measure the reflected signal. The detected signal is the Brillouin scattering signal corresponding to the given RF frequency which defines the frequency difference between the pump and the probe signal. When the frequency of the RF source is scanned through the whole spectral span chosen by us according to required sensing range, we can map a three dimensional

spectral plot as shown in Figure 4-14. The x axis of the picture represents position along the fiber, y axis is the frequency, and z axis is the strength of the reflected signal. From this plot the Brillouin gain spectrum at each point along the fiber is obtained. This will in turn determine the temperature or strain distribution along the fiber.

In the experimental result shown in Figure 4-14, most of the FUT is put under room temperature with corresponding Brillouin frequency shift of the fiber at 10.73GHz as shown in Figure 4-14. For the part of the fiber put under higher temperature (72℃), the corresponding Brillouin frequency shift is 10.77GHZ. From this result we can also see that the signal is not flat. It means there is a strong fluctuation of the reflected signal. This fluctuation is due to the variation of the polarization state of the light during its propagation along the fiber although it has already been optimized by the PC before the light enters the fiber. To improve on this a polarization scrambler (PS) is employed to avoid the influence of the polarization change. The improvement in experimental results using the PS can be seen clearly from the experimental results shown in Figure 4-15.

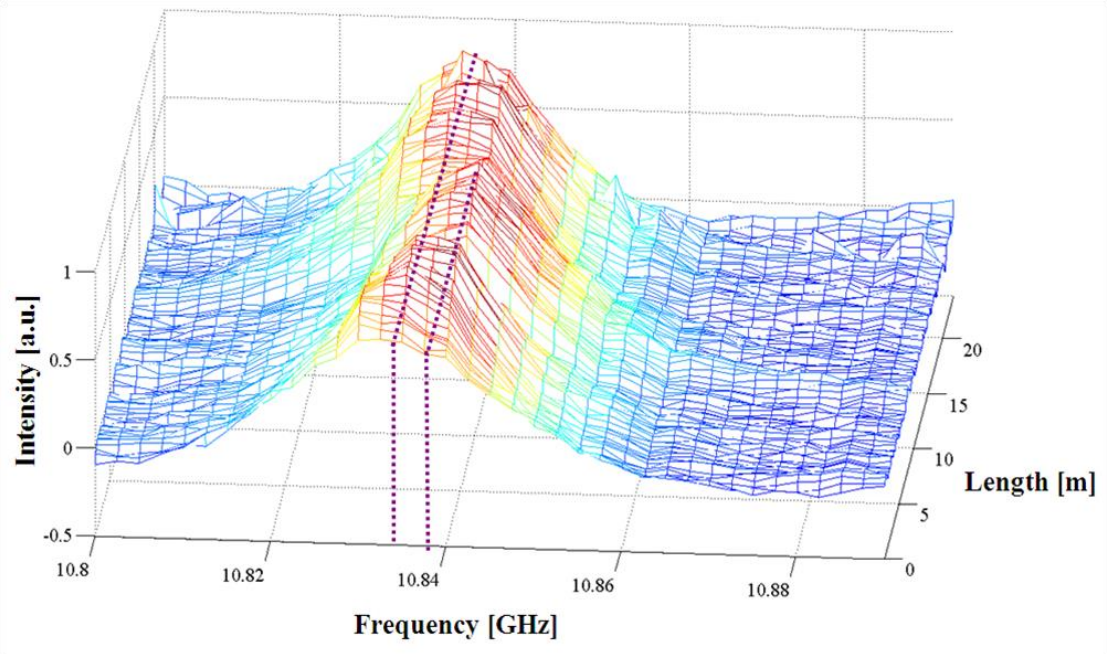

Figure 4-15 Result of BOTDA system using polarization scrambler

4.4.3 Effect of Polarization

When the pump and probe light propagating along a standard signal mode fiber their polarization state will change randomly. The Brillouin scattering is a polarization dependent effect. So when the pump and probe light are at the same polarization state the Brillouin signal is the largest. However when the pump and probe light are at orthogonal polarization states the Brillouin signal will be the smallest. This will cause a significant variation in the form of noise in the amplitude of the detected signal. To show noise caused by the polarization change, we carried out a series of experiments. First, we measure the backscattered Brillouin signal from a FUT with a total length of 10km (several

hundred meters of fibers between two segment of 5km fiber) using the setup shown in Figure 4-13. Then we replace the PCs with a polarization scrambler so that the polarization state of the pump pulse can be rotated randomly over all the possible states.

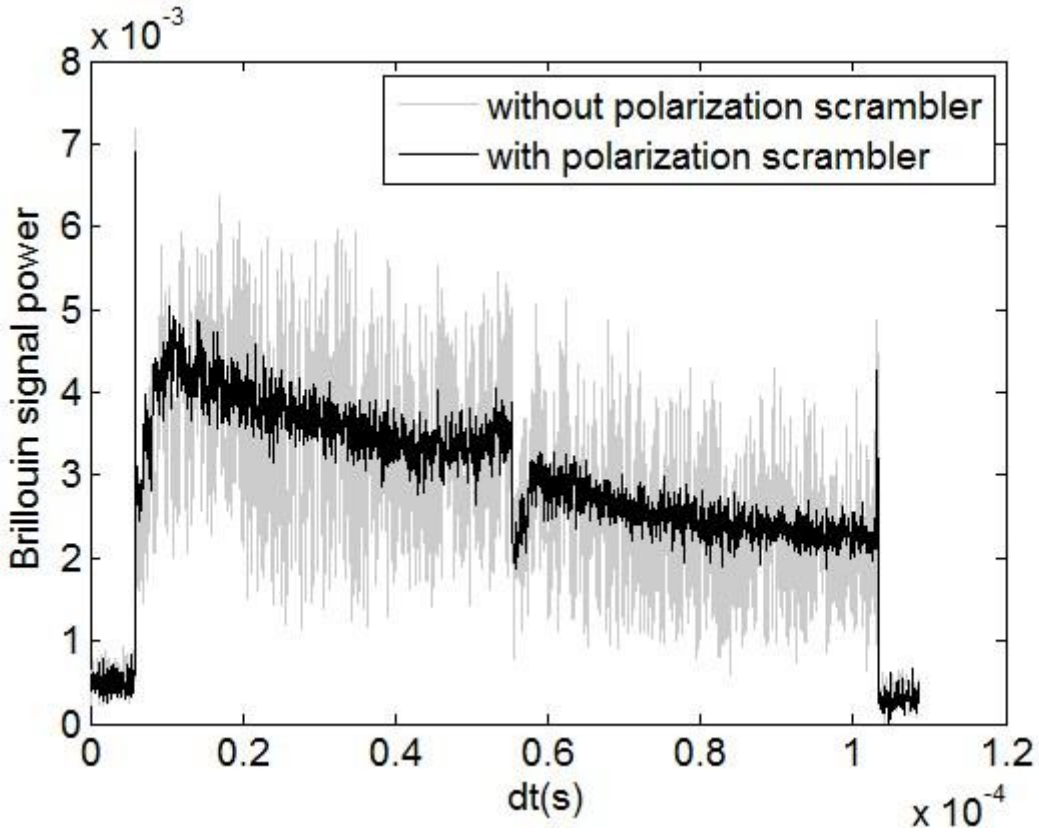

Figure 4-16 Brillouin signal without and with the polarization scrambler

The result is shown in Figure 4-16. The noise is very large in the Brillouin signal without polarization scrambler. When the scrambler is used, the signal at any point is the average among the signal from all possible polarization states.

The effect of the random change of the polarization state along the fiber is reduced and so the noise is reduced.

Besides this advantage, there are two main disadvantages associated with the use of polarization scrambler. The first disadvantage is that although it can reduce the noise induced by the polarization change along the fiber, the polarization scrambler will also introduce some noise to the system since it can not perfectly rotate the polarization state of the pump light over all the possible state with the same probability. The second disadvantage is that the measurement time will increase while using the polarization scrambler since we need to wait for the scrambler to rotate the polarization state of the pump light to all the possible states before calculating the average.

A more convenient method to handle the polarization problem is using a device named polarization switch. The polarization switch can switch the polarization state between two orthogonal polarization states. Using the polarization switch in our system, we can measure two Brillouin signals which are independently generated by two pump pulses with orthogonal polarization states. By averaging these two signals we can obtain the equivalent of the averaged Brillouin signal from pumps covering all the possible polarization state using the polarization scrambler.

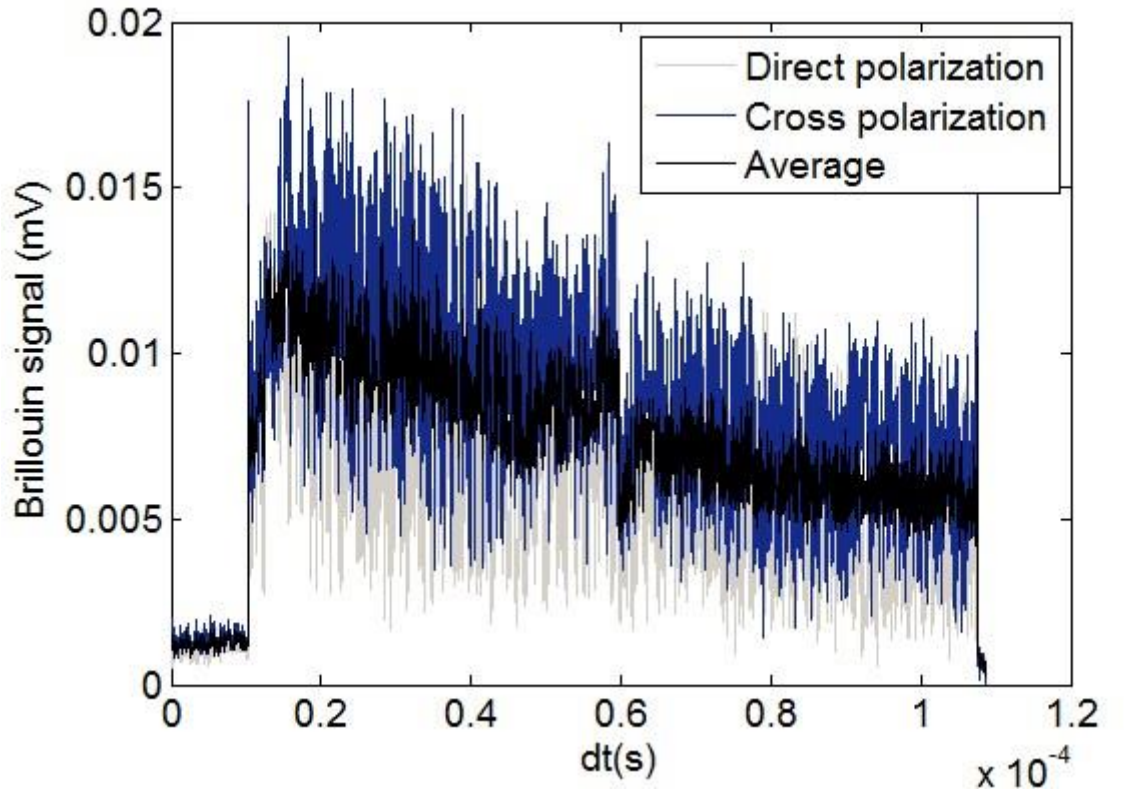

Figure 4-17 Effect of polarization switch

The result of using polarization switch is shown in Figure 4-17. For the two signals obtained with any of the two pumps with orthogonal polarization state the noise is large. This is similar to the results obtained without polarization scrambler shown in Figure 4-16. However the average between them has a much lower noise, similar to the result obtained with polarization scrambler shown in Figure 4-16.

Having the same effect of reducing the noise by using the polarization

scrambler, the system employing polarization switch can fully overcome the two disadvantages of using the polarization scrambler. It is important to reduce the measurement time for each frequency step especially in cases where the frequency range to be scaned is large (to measure large temperature/strain range).

4.5 Acoustic Lifetime in Optical Fibers

One important parameter characterizing a BOTDA system is the acoustic lifetime of a fiber. Although the spatial resolution of a BOTDA system has already broken the limitation of 1m resolution determined by the lifetime of the acoustic wave, a detail study of the acoustic lifetime can help us to obtain a better Brillouin signal.

In the backscattered signal of the BOTDA system, at the point where the Brillouin frequency changes caused by either temperature, strain, or variation of fiber type, the Brillouin signal of previous part of fiber will decay and a new signal corresponding to the new part of the fiber will be established. This decay will introduce a ‘tail’ to the Brillouin signal. It is important to understand this decaying behavior because by analyzing this behavior we can remove this tail of the signal during signal analysis.

It was shown in theory that the acoustic lifetime can be calculated by the Full Width at the Half Maximum (FWHM) of the Brillouin gain spectrum:

$$\Delta\nu_b = \frac{1}{2\pi\tau_A} \tag{4.14}$$

However, to our knowledge no experiment for measuring acoustic lifetime has been reported. Here we describe a scheme and present the results of measuring the Brillouin linewidth and the acoustic lifetime independently in several different types of fibers. Recently, a distributed fiber sensing system based on Brillouin Echoes Distributed Sensing (BEDS) was reported [74]. Using the technique the information of the strength of the acoustic wave can be obtained. According to the work, the decay of the signal near the fiber end indicates the lifetime of the acoustic wave in the fiber. Based on this, a series of experiments have been carried out to measure the acoustic lifetime for different types of fiber and the experimental results are compared with the theoretical value calculated using equation (4.14).

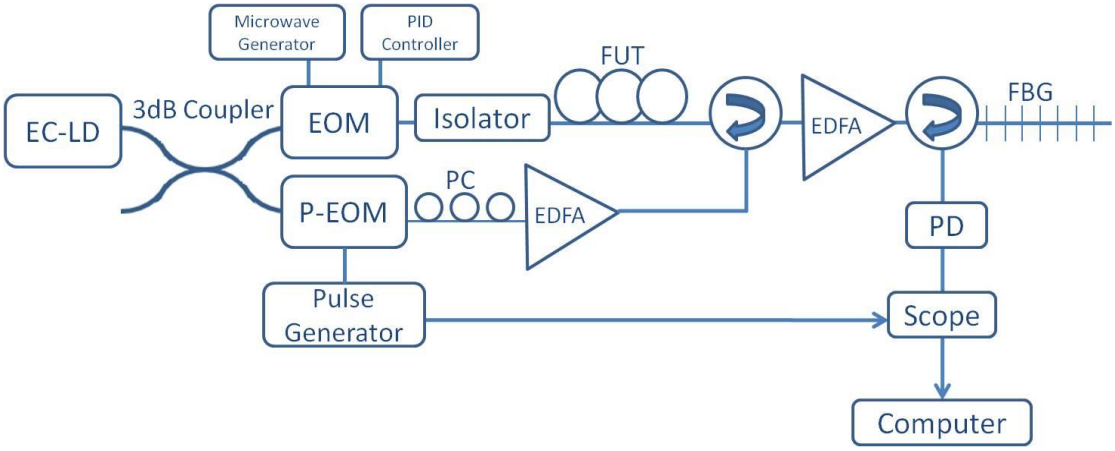

Figure 4-18 Setup for lifetime measurement

Figure 4-18 shows the experimental setup for the lifetime measurement. The light from a single frequency laser diode is spitted into two branches. One branch is modulated by an electro-optic modulator (EOM) to generate a sideband which works as the probe signal in the system. The EOM is driven by a RF signal from a microwave generator and the bias is controlled by a PID controller. The bias voltage is adjusted in such a way that the carrier frequency is suppressed and the RF frequency is the Brillouin frequency shift in the fiber under test (FUT). The other branch is modulated by a phase EOM (PEOM) and then amplified by an Erbium doped fiber amplifier (EDFA). The amplified light is the pump signal. The reflected signal due to Brillouin scattering in the FUT is then amplified by another EDFA and filtered by a FBG. A photodetector (PD) is then used to convert the optic signal into an electronic signal. The electronic signal is then measured using a real-time scope and the results are record by the

computer.

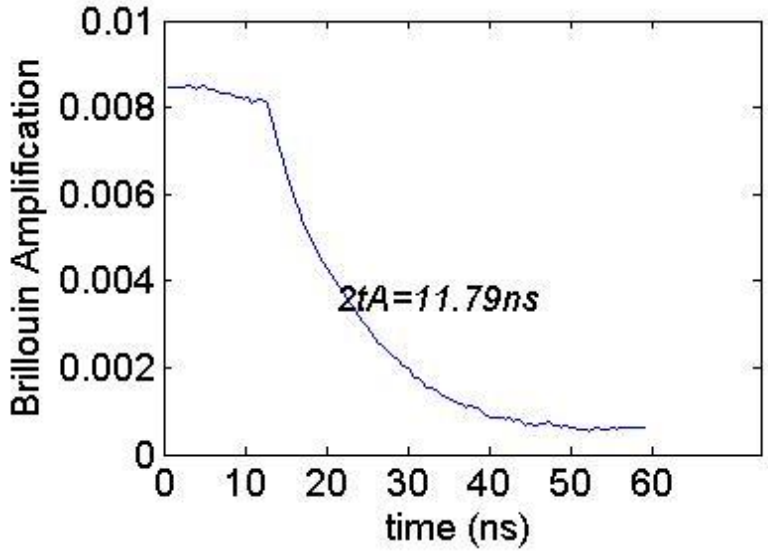

Figure 4-19 Decay of optic signal at the end of the fiber

Since the pump signal is a phase modulated pulse, due to an effect named second echo in the system, the local acoustic wave will decay exponentially at each point along the fiber.

$$A = A_0 \exp(\alpha t) \tag{4.15}$$

The received signal will be the integration of local signal from all the points along the fiber, which will be an exponential function with the same constant α . So the decay of the optic signal in the end of the fiber as shown in Figure 4-19 indicates the decay of the acoustic wave. By analyze the curve we can obtain a direct measurement of the lifetime of the acoustic wave in the optical fiber. In

the set up shown in Figure 4-18 when we tune the RF frequency of the microwave generator we can measure the response for different frequency shift. So we can measure the Brillouin gain spectral after scan the RF frequency of the microwave generator. We independently measured the lifetime and the Full width at half maximum of the Brillouin gain spectrum of six different step index fibers A, B, C, D, and E which showing different core size and different doping concentration. Fiber E is F-doped fiber. For each fiber we measured the lifetime five times and calculate the average value and standard deviation. The result is shown in Figure 4-20. In Figure 4-20 the x-axis is the FWHM of the Brillouin Gain Spectrum. The blue stars are the average value of the measured lifetime and the error bars show the standard division of the measurement. The red circles show the acoustic lifetime calculated using (4.15) from the measured FWHM Brillouin linewidth $\tau_A = \frac{1}{2\pi\Delta\nu_b}$.

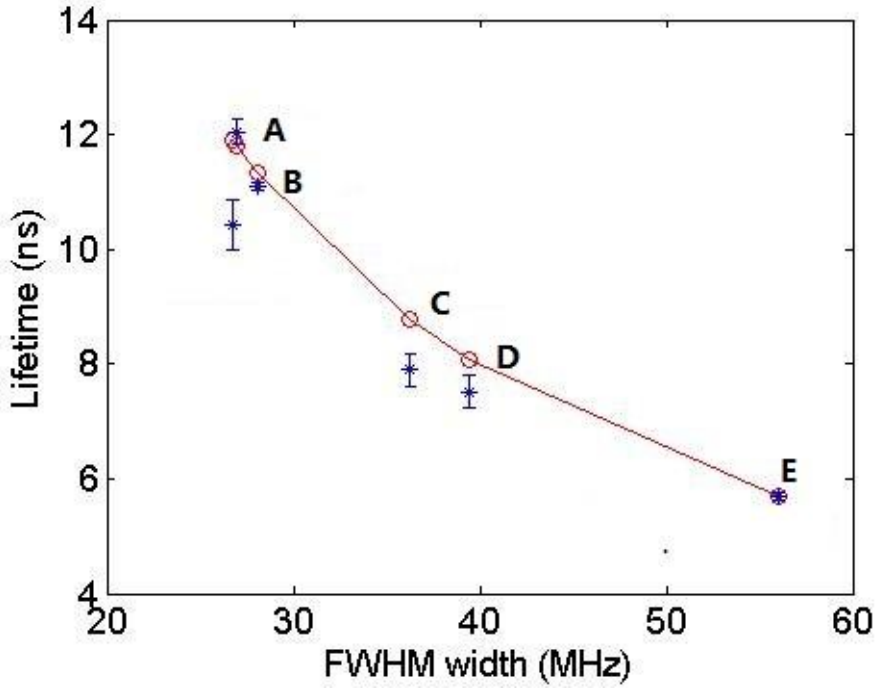

Figure 4-20 Lifetime versus FWHM of the Brillouin gain spectrum

From Figure 4-20, the measured value agrees well with the theoretical value. The experimental and calculated results for fiber A, B, and E match very well, while the experimental results for fiber C and D are smaller than the calculated value. It is worth noting that the F-doped fiber cannot guide the acoustic waves because the acoustic wave has a smaller velocity in the cladding. This explains why the acoustic wave has a much shorter lifetime in F-doped fiber.

In conclusion, using a BEDS setup, we measured the acoustic lifetime in six different optic fibers. By comparing our results with some theoretical results,

we verified that the acoustic lifetime in the optic fiber and the FWHM of the Brillouin gain Spectrum fulfill the relationship described by equation $\Delta v_b = \frac{1}{2\pi\tau_A}$.

CHAPTER 5. BOTDA SYSTEMS WITH PHASE MODULATED CODED SEQUENCES

In this chapter, BOTDA systems using phase modulated pump signal with coded sequence are studied. Experimental study shows that system performance can be improved significantly.

5.1 Brillouin Sensing System with Phase Modulated Coded Sequences

As discussed in Chapter 4, in a BOTDA system, there is always a tradeoff between total length of sensing fiber and the spatial resolution. Much research has been carried out to realize high spatial resolution over long sensing range. The main challenge in optimizing system performance has been the low SNR of the detected signal. In order to increase spatial resolution, a short pulse has to be used. However, this will result in low signal power and as a result a limited SNR for the detected signal.

For Brillouin process, the effective length of the sensing fiber is:

$$L_{eff} = \frac{1}{\alpha}\left(1 - e^{-\alpha L}\right) \tag{5.1}$$

Here α is the attenuation of the fiber and L is the physical length of the fiber. The power threshold of the system is:

$$P_{th} = \frac{21A_{eff}}{g_B L_{eff}} \tag{5.2}$$

Where A_{eff} is the effective area of the fiber, g_B is the Brillouin gain coefficient and L_{eff} is the effective length given by equation(5.1).

If the pump power is larger than the threshold, the reflected signal is mainly due to the SBS backscattering of the pump, not due to the interaction between the pump and the probe signal. So the detected signal contains other frequency in addition to the frequency of the probe signal. This will increase the noise and will limit the performance of the BOTDA system.

The total gain of the probe signal can be calculated by:

$$G_B = \exp\left(\frac{g_B P_p v_g \tau_p}{2A_{eff}}\right) \tag{5.3}$$

Here P_p is the pump power, v_B is the velocity of the acoustic wave, τ_p is the pulse width of the pump, and A_{eff} is the effective area. Since the spatial resolution is defined by the pulse width of the pump. If we have a long length of sensing fiber, to make sure the reflection is due to the interaction between the pump and probe signal we should have a large effective area A_{eff}. If we need high spatial resolution, the pulse width τ_p should be very small. From the equation above, we know the total gain is small when both long sensing fibre and high spatial resolution are needed. This will limit the SNR of the received Brillouin signal and makes Brillouin gain peak very difficult to be measured accurately.

To increase the SNR of the system and overcome the tradeoff, optical pulse coding technique (simplex code) was proposed [66]. It was shown that the use of the simplex code can greatly improve the performance of the optical time domain reflectometer (OTDR) system [67]. This technique has been applied to intensity modulated Brillouin fiber sensing system, and 1m spatial resolution over 50 km was realized by using the simplex-code [68][69][70]. In the experiment, the SNR of the Brillouin optical time domain analysis system is greatly enhanced with the use of a 511-bits Simplex code. Coding technique is a very promising method since it can improve the SNR by the coding gain while maintaining high spatial resolution and long sensing range [69].

Here, the use of phase modulated coded sequence on the pump signal is investigated. It is known that phase modulation can significantly reduce the SBS threshold, and the code sequence can also offer an improved SNR. Based on these techniques sensing system with high resolution and long sensing range can be realized potentially. Experimental demonstration has shown that sub-cm resolution can be achieved.

In the experimental setup as shown in Figure 5-1, the output from a continuous wave (CW) DFB laser signal is split through a 50:50 coupler to generate both the pump and probe signals. An electro-optic phase modulator

(PEOM) driven by a PPG is employed to generate a custom phase modulated pump signal at high repetition rate in the upper arm of the setup. In the lower arm, an electro-optic amplitude modulator (AEOM) driven by a sinusoidal wave signal at a frequency approaching the Brillouin frequency of the FUT is used to generate the Stoke probe signal. Both the pump and the probe signal power are adjusted using an EDFA. The Stokes signal is subsequently isolated, detected and analyzed through a narrow bandwidth FBG filter (~10GHz), a photodetector and a real time oscilloscope (Tektronix DSA72004) .

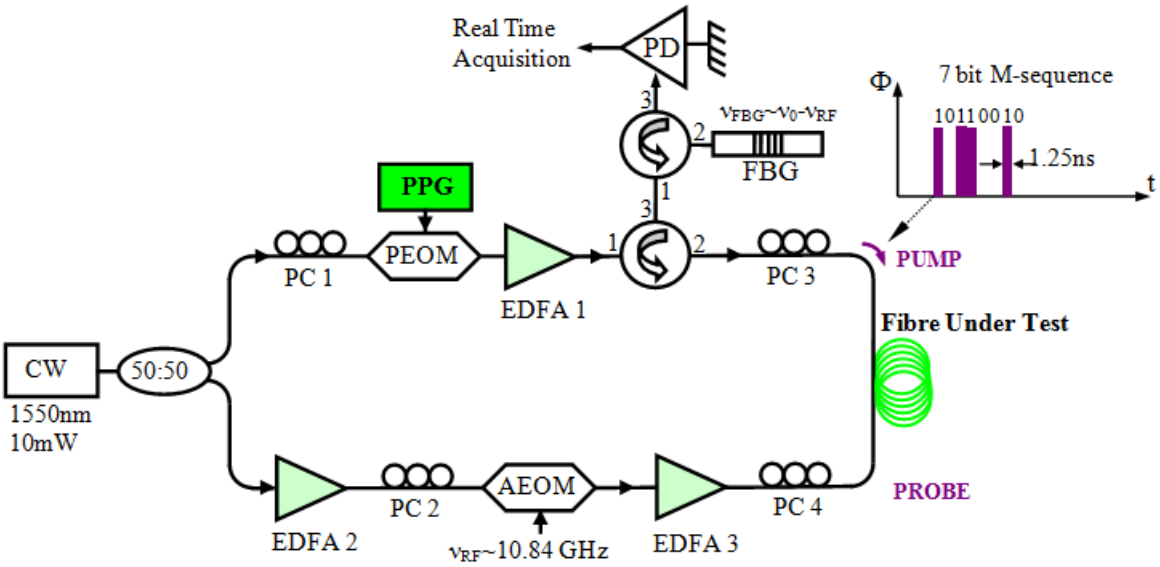

Figure 5-1 Experimental setup for Brillouin Optical Time Domain Analysis by using phase modulated code sequences.

The fiber under test consists of three sections, as shown in Fig.5-2. The total length is 20 meters, 6 meters of the fiber in the middle is put in an oven

with a temperature of 46℃ and the other two sections of the fiber are under room temperature.

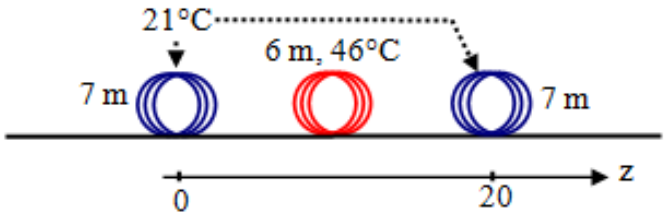

Figure 5-2 Fiber under test

The code sequence used for the experimental system is a 7 bit length m-sequence at 0.8GHz repetition rate. A 1.25ns phase pulsewidth allows a 12.5cm spatial resolution ($L_P = v_g \tau_p / 2$).

The coding technique does not give sensing information immediately. For *2n-1* bit m-sequence, we need to send successively *2n-1* codes, the detected amplified probe signal is stored and processed using a numerical matrix decoding technique. The decoding process can be expressed as:

$$
\begin{aligned}
R(t) &= S * \begin{bmatrix} R_1(t) \\ R_2(t) \\ \cdots \\ R_M(t) \end{bmatrix} \\
&= \begin{bmatrix} S_1'(t) & S_2'(t) & \cdots & S_M'(t) \end{bmatrix} * \begin{bmatrix} S_1(t) \otimes r(t) \\ S_2(t) \otimes r(t) \\ \cdots \\ S_M(t) \otimes r(t) \end{bmatrix} \\
&= \begin{bmatrix} S_1'(t) & S_2'(t) & \cdots & S_M'(t) \end{bmatrix} * \begin{bmatrix} S_1(t) \\ S_2(t) \\ \cdots \\ S_M(t) \end{bmatrix} \otimes r(t) \\
&= M * I * r(t)
\end{aligned}
\tag{5.4}
$$

Where, I is an M*M unit matrix. Figure 5-3 shows the sensing results for a 7 bits m-sequence. The results are compared with those obtained for single pulse and 3 bit coded pulse. We can clearly observe that the sensing result is improved with longer m-sequence. Comparing with room temperature a positive temperature shift of 25℃ induces a positive frequency shift of 17.5MHz at the peak Brillouin gain (1.4 MHz/℃).

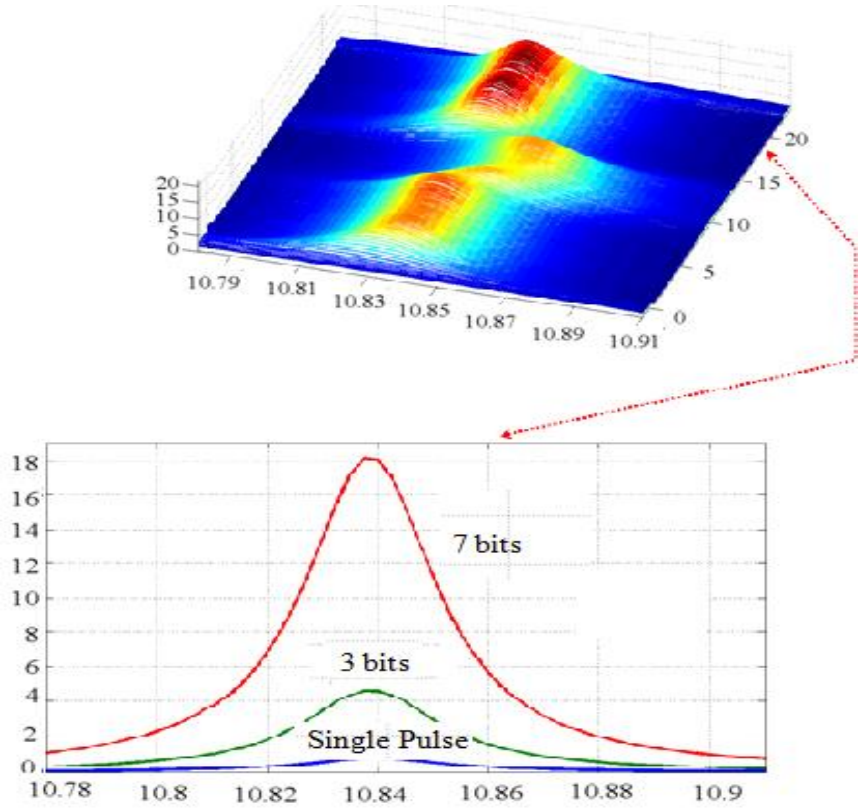

Figure 5-3 Experimental results for 7 bits m-sequence and comparison of different codelength

In order to demonstrate that higher spatial resolution can be achieved we measured the strain distribution along the fiber and the result is shown in Figure 5-4. In this experiment a 511 bit code is used. It is worth to note that for the same setup and pulsewidth, we can not get any meaningful result if coding is not used.

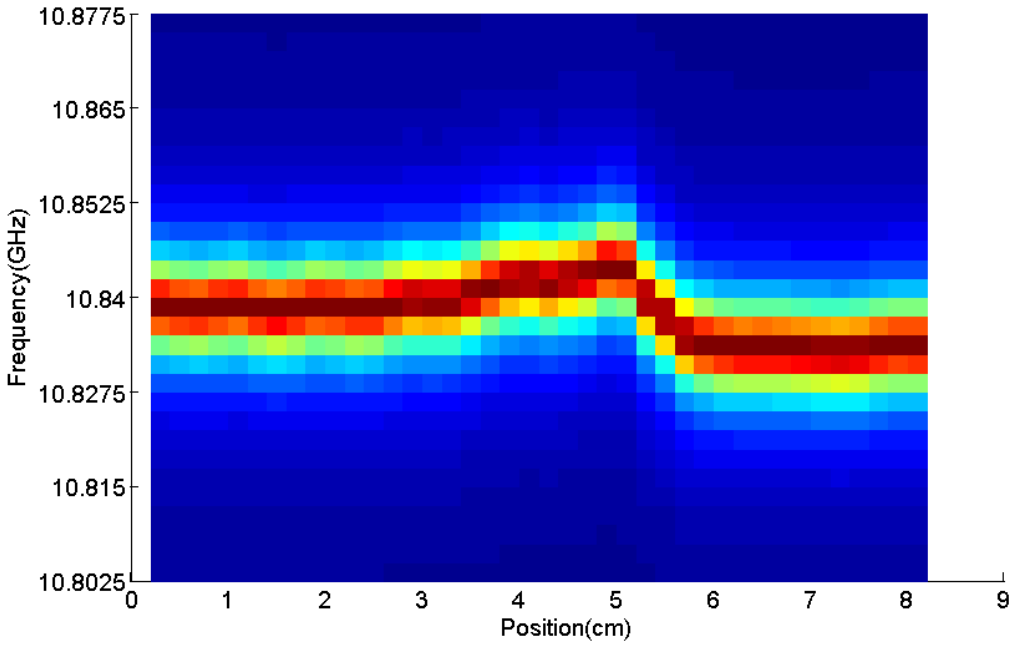

Figure 5-4 Strain distribution along the fiber under test

From Figure 5-4 we can see clearly that the resolution is about 1cm. The fiber in the left part is under a strain higher than the fiber in the right part. Its Brillouin frequency is higher than the right part. In the middle the fiber has the highest strain due to the fiber holders used in the experiment. The width of the fiber holder used in the experiment is around 1cm. In order to hold the fiber more steadily, large strength is applied to the fiber holder. All these can be seen from the figure. This means using our system we can measure a strain change over 1cm fiber. From the figure we can also see that the shift from a frequency to another occurs within 1cm.

5.2 Effect of Code Length on SNR Improvement

In the previous section, we demonstrated a Brillouin sensing system with high spatial resolution. The results show that the use of coding technique can improve the SNR of the system. The improvement in system performance depends on the length of the code used. Experiment is carried out to verify the effect of the coding length. The experimental results show significant SNR enhancement provided by an increasing length of the phase-coded pump with short code length (7 to 31 bits), thus allowing strain sensing over a 30 m standard fiber with 1 cm spatial resolution.

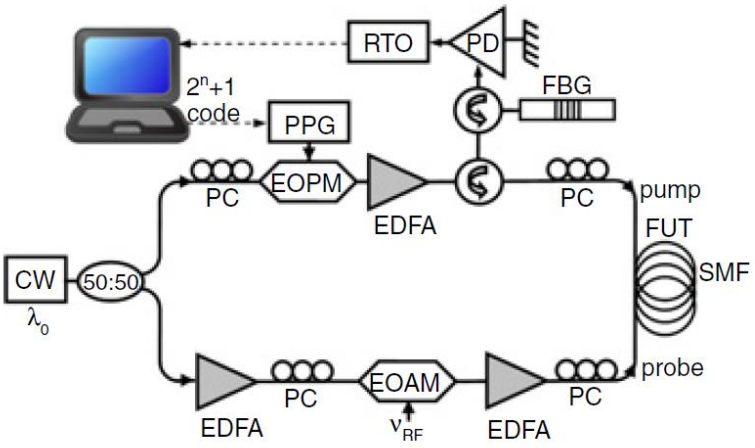

Figure 5-5 Schematic describing BOTDA experimental setup

The experimental setup is shown in Figure 5-5. A single CW-DFB laser signal (1550.1 nm) is split by a 50:50 coupler to generate the pump and probe

signals simultaneously. The DFB laser's linewidth is sufficiently narrow (<20 MHz) to allow a coherence time longer than the acoustic-wave build up time (T_a). In the upper arm of the setup, an PEOM driven by a PPG is employed to generate an adjustable 2^n-1 bit length phase-coded S-sequence at a high repetition rate of 10GHz thus allowing a 1cm spatial resolution. In the lower arm, an electro-optic amplitude modulator (AEOM) biased at the minimum of its power transfer function is modulated by a RF sin wave to generate the Stokes signal through a carrier suppression scheme. Sensing is realized by scanning the RF signal around the Brillouin frequency ($\nu_B = 10.84$ GHz) of the SMF used as FUT. A FBG – unchirped with a 3dB bandwidth equal to 10.2GHz – is placed prior to a DC-70 GHz photodetector (PD) to isolate the Stokes signal from the probe. To satisfy an optimum SNR at the detection stage, the polarization and power of both signals are respectively aligned and adjusted through PCs and EDFAs. Finally, the photodetected data are displayed and stored via a 20GHz bandwidth real-time oscilloscope (RTO)(Tektronix DSA72004).

The FUT is a 31.5m-long SMF with a strain coefficient of 0.046MHz/με. We deliberately applied a mechanical strain of 363 $\mu\varepsilon$ on the 30cm fiber sample located at one end of the FUT. Performance of phase S-coding scheme is evaluated through the acquisition of the frequency shift and

backscattered power as shown in Figure 5-6. The results are obtained by taking a series of 53 consecutive backscattered traces, each one separated by 2.5MHz, starting at 10.78GHz. Each trace is averaged 500 times.

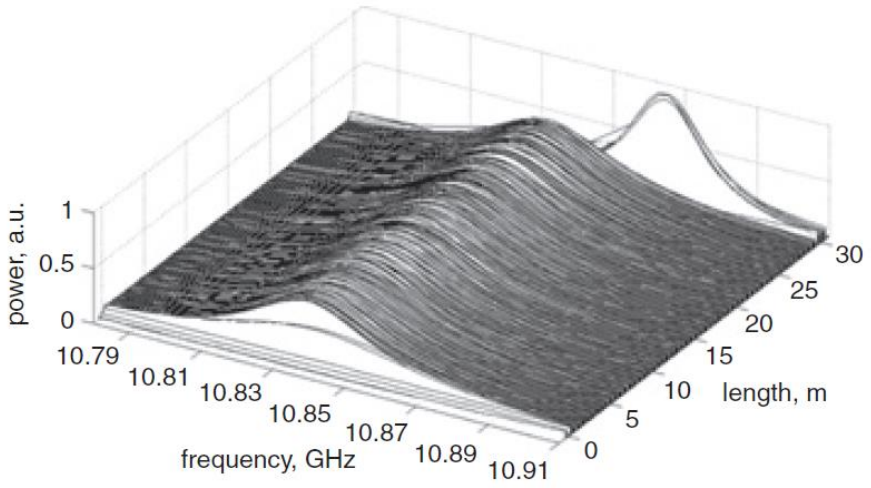

Figure 5-6 Brillouin gain spectrum against distance using 31 bit length phase-coded S-sequence

Figure 5-6 shows the BOTDA experimental results with a 31 bit length S-sequence. We can observe that power transfer between pump and probe takes place at any position along the fiber when the frequency offset between them is within the local Brillouin gain spectrum. The frequency showing maximum gain is called Brillouin frequency shift (BFS) and depends linearly on strain applied to the FUT. Remarkable results on SNR improvement owing to the S-coded pump are illustrated in Figure 5-7. We can see that, even with short code length

(7 to 31 bits), a phase-coded pump scheme produces a notably enhanced Brillouin gain when the length of the S-coded sequence is increased. The reason for such enhancement is the same as in the case of an intensity S-coded pump with moderate code length (127 bits) [70]. Moreover, experimental results show a SNR improvement of 3.1dB with an increasing code length L from 7 to 31 bits. This improvement follows the same analytical evolution as reported in earlier papers [67], it equals to:

$$(L+1)\big/(2L^{1/2}) \tag{5.5}$$

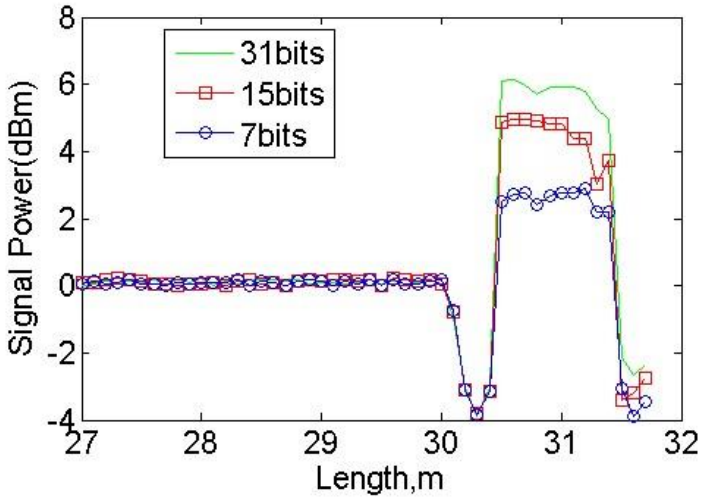

Figure 5-7 SNR enhancement of Stokes recorded trace for BFS of 10.867 GHz with increasing length of Simplex code (The signal power are normalized)

However, one can observe in Figure 5-7 the detrimental effect caused by the second Brillouin echo. The intensity change owing to a radical strain change is not clearly appearing on the decoded signal as it should be. This “bouncing”

transition originates from the decoding operation between a Brillouin echoed backscattered probe and decoding matrix which does not take into account the second Brillouin echo of the p-phase pump impulse response. An alternative solution can be found by implementing the numerical impulse response of a π -phase pulse into the decoding matrix. This will be an elegant way to numerically cancel the interfering effect of the second echo.

Finally, it is worth noting that decoding an S-sequence is time consuming, especially for long sequences (127 bits). We believe that a different coding scheme, such as the complementary code, can drastically reduce the computational effort. This is studied in the following section.

The experimental results above demonstrated that significant SNR enhancement is achievable through a new technique unifying phase coding and Simplex code in BOTDA sensing systems. Even with short code length ranging from 7 to 31 bits we have clearly observed a 1.4dB SNR improvement.

5.3 High Resolution BOTDA System Based on Bright Pulse Brillouin Gain and Complementary Code

In this section, we study the use of complementary code for improving the performance of Brillouin Optical Time Domain Analysis (BOTDA) systems experimentally. The results show that complementary code based schemes can provide significant enhanced SNR to the BOTDA system. Using complementary coded pump pulses the average time can be reduces significantly and so do the measurement time. The complementary coded pulses with individual pulse duration of 0.1ns allowed us to realize temperature sensing over 50m of single mode fiber with 1cm spatial resolution.

In Brillouin fiber sensing systems, there is always a tradeoff between total sensing length and spatial resolution. High spatial resolution and long sensing range simultaneously will result in low SNR. In the previous section we have already shown that the use of simplex code can help to improve the SNR of the Brillouin sensing systems. We have also shown that the improvement of the SNR depends on the length of the code used. By using a longer code length the SNR performance of the Brillouin sensing systems can be improved greatly. However, when the code length is very long, the acquisition time, memory

requirement and the time taken for the decoding process will increase significantly.

Another coding technique named complementary codes has also been used to improve the SNR of an OTDR system [67]. Compared with simplex codes, the acquisition time and memory space required are much less for the same length of the code. In this section, we study the performance of BOTDA sensing system using coded pump pulses. Unlike the study in [68][69][70], the focus here is phase modulated pump signal rather than intensity modulated pump signal based BOTDA. We compare the performance of simplex code and complementary code schemes. The results show that to achieve similar SNR performance complementary code based scheme will require less acquisition time, less memory space while offering similar decoding complexity compare with the simplex code based scheme. Meanwhile, complementary code allows easy trade off among SNR enhancement, acquisition time, memory space requirement and decoding complexity. Using complementary coded pulses with individual pulse duration of 0.1ns a strain sensing system over 50m of single mode fiber with 1 cm spatial resolution can be realized.

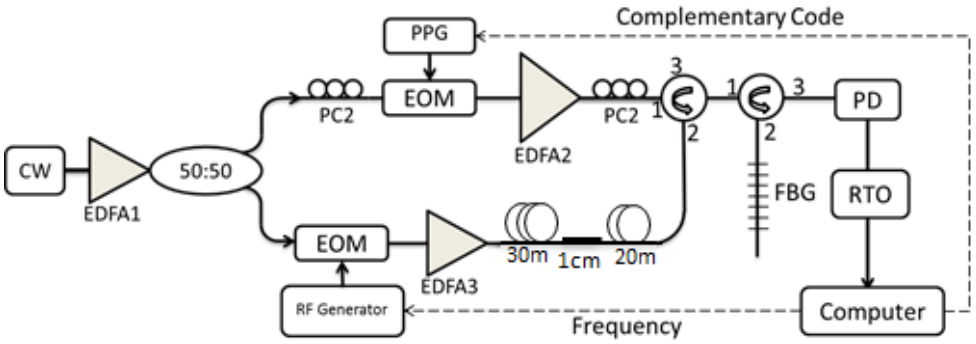

Figure 5-8 Configuration of the BOTDA sensing system

The schematic diagram of the experimental setup is shown in Figure 5-8. A continuous wave (CW) tunable laser operating at 1550nm is used. The linewidth of the laser is 100kHz, which is sufficiently narrower than that of the Brillouin spectral bandwidth. The output of the laser is amplified by an EDFA and then split through a 50/50 coupler to generate both the pump and the probe signals. One beam goes to the upper arm and is modulated by an EOM. The EOM is driven by a PPG which is controlled by a computer to generate a given length of complementary code. The bias voltage of the EOM is carefully tuned so that the modulator is biased at quadrature and is working at on-off key (OOK) modulation format. In the lower arm, the beam is modulated by another EOM driven by a sinusoidal wave signal generated by a RF generator. The frequency of the RF generator is controlled by the computer at a frequency approaching the Brillouin frequency shift of the FUT to generate the Stokes probe signal. Both the pump and the probe signal power are adjusted respectively through EDFAs

and their states of polarization (SOPs) are adjusted by two PCs to obtain maximum Brillouin scattering along the fiber and then injected into the FUT. The Stokes signal is subsequently isolated, detected and analyzed through a narrow bandwidth FBG filter (~2GHz), a PD and a Tektronix realtime oscilloscope (RTO). The data collected by the RTO are then processed by the computer with a decoding program to recover the spectra along the FUT and to calculate the temperature distribution along the FUT.

In our experiment, the FUT is a 50 meters long SMF. A hot spot with a length of 1cm is introduced to the FUT at the point 30 meter away from the start point of FUT. The temperature of the hot spot is controlled by a thermoelectric cooler (TEC).

When a pump pulse is launched into the sensing fiber of the BOTDA, the detected signal r(t) at each given time point represents the amplified probe signal from a particular spatial point along the fiber. The signal can be treated as the impulse response of the sensing system. When coded sequence is employed to modulate the pump, the acquired signal through the oscilloscope is the convolution of the coded pulse with the impulse response of the system, which can be expressed as $c(t) \otimes r(t)$, where c(t) is the code words and r(t) is the impulse response of the system. The impulse response is directly related to the

spatial resolution of the sensor system. A decoding process is required to recover the impulse response of the system and in order to obtain the distributed sensing information (strain or temperature) along the fiber. Different decoding algorithms are necessary for simplex code based scheme and complementary code based scheme.

For the case of m-bit simplex code, a group of M code pulses need to be launched sequentially to the fiber. The detected signal of the i-th code can be expressed as $R_i(t) = S_i(t) \otimes r(t)$, where $S_i(t)$ is modulated pump signal with i-th code sequence. In the decoding process, an S-Matrix is required, which are the rows of the M*M matrix $S = \left[S_1^{'}(t) \quad S_2^{'}(t) \quad \cdots \quad S_M^{'}(t) \right]$. The decoding process can be expressed as:

$$\begin{aligned} R(t) &= S * \begin{bmatrix} R_1(t) \\ R_2(t) \\ \cdots \\ R_M(t) \end{bmatrix} \\ &= \left[S_1^{'}(t) \quad S_2^{'}(t) \quad \cdots \quad S_M^{'}(t) \right] * \begin{bmatrix} S_1(t) \otimes r(t) \\ S_2(t) \otimes r(t) \\ \cdots \\ S_M(t) \otimes r(t) \end{bmatrix} \\ &= \left[S_1^{'}(t) \quad S_2^{'}(t) \quad \cdots \quad S_M^{'}(t) \right] * \begin{bmatrix} S_1(t) \\ S_2(t) \\ \cdots \\ S_M(t) \end{bmatrix} \otimes r(t) \\ &= M * I * r(t) \end{aligned} \tag{5.6}$$

Where, I is an M*M unit matrix. The last step in the equation is based on the definition of the Simplex code. According to the above equations, the signal can be increased by a factor of M^2 and the SNR can be improved by a factor of M when the decoding results are summed up.

For the case of complementary codes, two coded pulses A and B are launched into the fiber. One method to generate these two codes is known as appending. The rule is to use N-length code pairs to generate a 2N-length code pairs:

$$\left\{\begin{matrix} A \\ B \end{matrix}\right\} \rightarrow \left\{\begin{matrix} A|B \\ A|\overline{B} \end{matrix}\right\} \tag{5.7}$$

Where $\overline{B}$ denotes swapping the 1's and -1's in B. According to the calculation, the complementary codes have a very good correlation behavior:

$$A_k * A_k + B_k * B_k = \begin{cases} 2N, & \text{for } k=0 \\ 0, & \text{for } k \neq 0 \end{cases} \tag{5.8}$$

Where $"*"$ denotes the cross correlation of the two sequences.

Since in intensity modulation based BOTDA system, only unipolar optical intensity signals are available, in our experiment, four group of codes are used: A_1, A_2, B_1, and B_2 to generate A and B. Where:

$$i_{1,\ k}=\begin{cases}1 & i_k=1\\ 0 & i_k=\text{-}1;\end{cases} \tag{5.9}$$

$$i_{2,\ k}=\begin{cases}1 & i_k=\text{-}1\\ 0 & i_k=1\end{cases} \tag{5.10}$$

Where i=A or B.

So we have

$$\begin{cases}\mathrm{A}=\mathrm{A}_1-\mathrm{A}_2;\\ \mathrm{B}=\mathrm{B}_1-\mathrm{B}_2.\end{cases} \tag{5.11}$$

The detected signal can be expressed as the convolution between the code words and the impulse response of the system $R_i(t)=r(t)\otimes C_i(t)$, where $C_i(t)$ is the modulated pump signal. By calculating the cross correlation between the reflected signal and the original code words for each code and sum them up, the impulse response can be fully recovered. The decoding process can be expressed as in equation:

$$\begin{aligned}R(t)&=\left(R_{A,1}(t)\text{-}R_{A,2}(t)\right)*C_A(t)+\left(R_{\mathrm{B},1}(t)\text{-}R_{\mathrm{B},2}(t)\right)*C_B(t)\\&=\left(r(t)\otimes C_{A,1}(t)-r(t)\otimes C_{A,2}(t)\right)*C_A(t)+\left(r(t)\otimes C_{\mathrm{B},1}(t)-r(t)\otimes C_{\mathrm{B},1}(t)\right)*C_A(t)\\&=\left(r(t)\otimes C_A(t)\right)*C_A(t)+\left(r(t)\otimes C_{\mathrm{B}}(t)\right)*C_{\mathrm{B}}(t)\\&=r(t)\otimes\left(C_A(t)*C_A(t)\right)+r(t)\otimes\left(C_{\mathrm{B}}(t)*C_{\mathrm{B}}(t)\right)\\&=r(t)\otimes\left(C_A(t)*C_A(t)+C_{\mathrm{B}}(t)*C_{\mathrm{B}}(t)\right)\\&=2\mathrm{N}\cdot r(t)\end{aligned} \tag{5.12}$$

where N denotes the length of the code words.

According to the expression above, the signal processing can be employed to recover fiber impulse response with the spatial resolution of single bit using the raw signal. The signal power will be increased by a factor of 2N, and the noise will be increased by a factor of $\sqrt{2N}$. So the SNR can be improved by a factor of $\sqrt{2N}$ when N-bit complementary code is used.

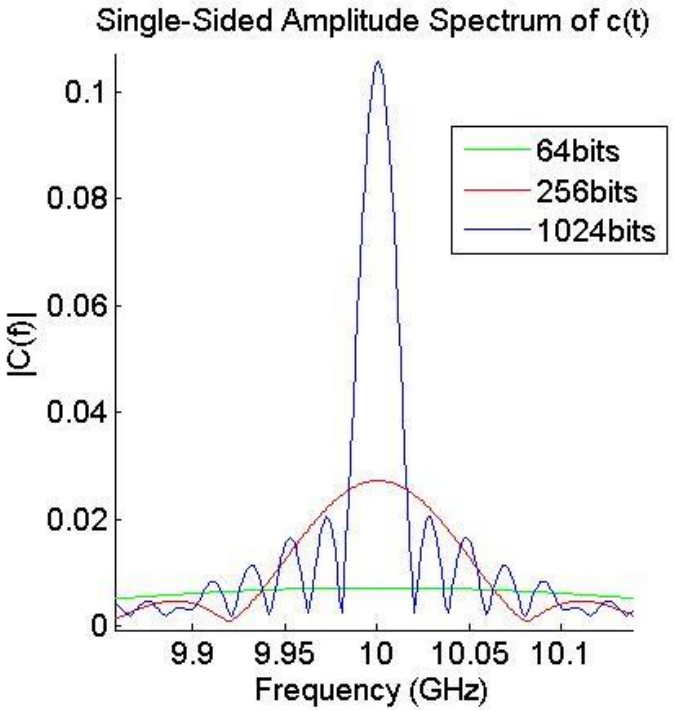

Figure 5-9 Dependence of the bandwidth of the pump pulse on the code length

Besides SNR enhancement, another advantage of using coding techniques is that we can enhance the spatial resolution of the BOTDA system. In a BOTDA system with single pulse, when the width of the pump pulse is very

short, the spectral width of the pump pulse becomes extremely wide. For a pulse shorter than 10ns to achieve a spatial resolution better than 1m, its spectral width is much wider than the Brillouin bandwidth. In this case the efficiency of the Brillouin scattering will be very low and the signal is too weak to be detected. By using coding technology, the spectral width of the pump pulse will be reduced. Figure 5-9 shows the relationship between the bandwidth of the pump pulse train and the length of the codes used. It shows that although the width of each bit of the code is shorter than 10ns, the spectral width of the pump pulse train is narrower than the Brillouin Gain spectra. Therefore by using coding technique high spatial resolution can be realized. Another way to view this is that the fast changing of the pulse waveform provides a constant DC signal for pre-excitation to allow a high spatial resolution to be realized.

It is obvious that M sets of code are needed for M-bit simplex code based scheme, but two sets of code are needed for the complementary code based scheme for the codes with the same length. Since the signal in a fiber optic system is unipolar, each code is divided into two codes to generate the bipolar signal for the complementary code. Due to the larger number of code sequence needed, simplex code needs longer acquisition time and large memory space compared to the complementary code of the same length.

The above equations describing the decoding process show that for the same length of code word, the decoding complexity for complementary code is less than that of the simplex code. The decoding complexity for the simplex code is M-L, while the decoding complexity for the complementary code is about $12Llog_2L+5L$ thanks to the FFT used in decoding. Here M is the length of the code word and L is the number of the point measured by the oscilloscope. Since in a practical sensing system L is much larger than M, the calculation steps for the two technology is similar. However, a complementary code with $M^2/2$ bit code length is needed if we want to achieve the same SNR enhancement as an M bit simplex code. In this case, since $M^2/2$ may be larger than L when M is a large number, the number of the calculation step become $24M^2log_2M+5M^2$. We can see that in this case the decoding complexity for complementary code is higher than that of the simplex code if we want to achieve the same SNR enhancement. However, the result show that for the same SNR enhancement requirement complementary code based technique requires less acquisition time, less memory space requirement than simplex code, and the realization of the tradeoff among all these parameters is easier for complementary code based scheme than that based on simplex code because of different rate of increase for acquisition time, memory space and decoding complexity for the two schemes.

In our experiment the PPG clock is set at 10GHz thus the pulse width of the pump signal is 100ps, which corresponds to an ideal spatial resolution of 1cm. The PPG is used to control the PEOM to generate either simplex-coded pulses or complementary-coded pulses with different code length. The temperature is maintained to be the same during the experiment. The measured Brillouin gain spectra are shown in Figure 5-10. S15 stands for 15bits simplex code, S31 stands for 31bits simplex code, C16 stands for 16 bits complementary code, and C32 stands for 32bits complementary code. According to Figure 5-10, we can see clearly that the simplex code provides much more effective improvement in the SNR compared with complementary code with the same code length. The Brillouin spectrum with a single pulse is not provided since the SNR is poor and the Brillouin gain spectrum cannot be obtained. Though Simplex code can provide better SNR enhancement, longer acquisition time, large memory space requirement and longer signal decoding time are required.

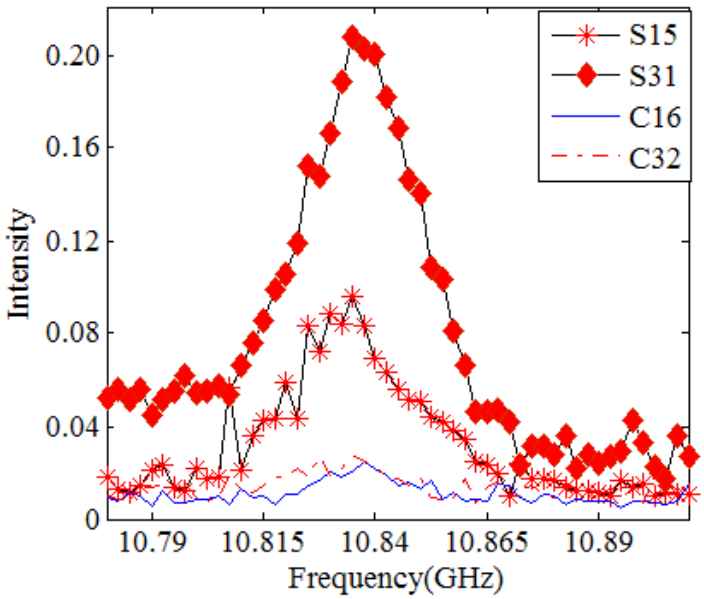

Figure 5-10 Measured Brillouin gain spectra at different code length for simplex and complementary codes.

To reduce the acquisition time, memory space requirement, complementary code based scheme is used in the following experiments. In order to better understand the effect of complementary code on the decoded Brillouin gain spectra, we measured the Brillouin spectra for complementary code with different code length while keeping other conditions to be the same. The results are shown in Figure 5-11. It is obvious that the SNR increases greatly with the increase of the code length. However, the SNR enhancement is not significant when the length of code word is increased from 128bits to 256 bits indicating that the pump power is close to saturation and the backscattered light power cannot be increased infinitely by increasing the code length.

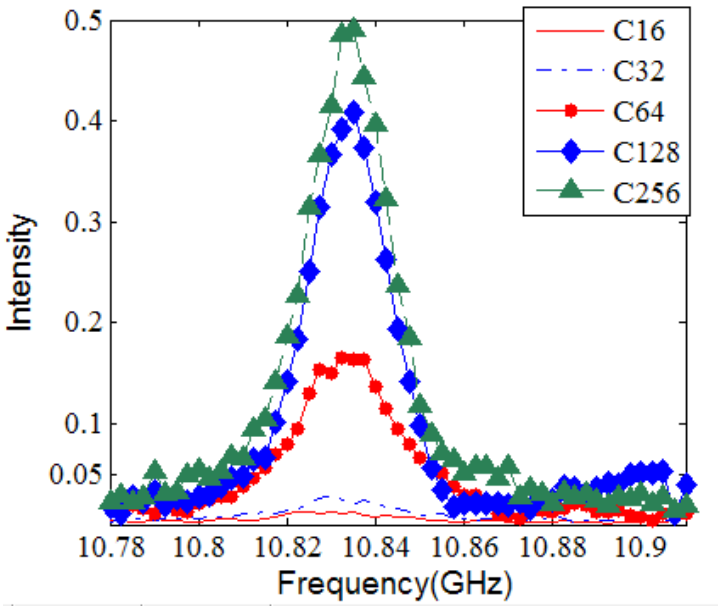

Figure 5-11 Measured Brillouin gain spectra at different complementary code code length. C16, C32, C64, C128 and C256 stand for 16-bits, 32-bit, 64-bit, 128-bit and 256-bit complementary code, respectively.

Finally, to demonstrate the spatial resolution of the complementary code based BOTDA sensing system, strain was applied to a 20-cm section of the fiber under test while keeping the rest of the fiber at loose condition. Experiments were carried out using 16-bit complementary code pulses at room temperature (22℃), and the strains applied to the fiber section is about 2000 micro-strains. The data were collected and decoded through offline processing using a computer program. When the coded pump pulse starts to enter the stressed section, the temporal Brillouin gain signal decays rapidly with the damping constant, which is determined by the fall time of the pulse and the phonon relaxation time. Two Lorentzian shaped peaks appear in the stressed section of

the fiber. Similar scheme as that used in [74] is employed for data filtering. Figure 5-12 shows the Brillouin gain spectrum as the function of the distance, which indicates that the Brillouin frequency of the loose fiber is 10.839GHz at room temperature, while the stressed section has the equivalent Brillouin frequency shift of 10.878GHz.

In our experiment, the clock of the PPG is set at 10GHz. So the time duration for each bit is 100ps. After the decoding process, we can recover the impulse response of a single pulse with 100ps pulse width. Theoretically our system can measure the temperature or strain distribution at a spatial resolution of 1cm. To verify this 1cm spatial resolution, we heat 1cm fiber with a TEC to 82℃. The hot spot is 30 meters away from the start point of the FUT, which has a total length of 50m. It was put under room temperature of 22℃. In the measurement we use a set of complementary code with a code length of 1024. The frequency of the RF generator is controlled by the computer and was scanned from 10.78GHz to 10.92GHz with 2MHz step. For each frequency step the signal is recorded by the RTO after 100 times of average. After the average process the results is recorded by the computer and the decoding process is applied. The spectral distribution along the fiber is plotted and shown in Figure 3. From the figure, we can clearly see the frequency shift which is about 80MHz

located 30m away from the start point of the FUT. The frequency shift coefficient for temperature can be calculated as 1.33MHz/℃.

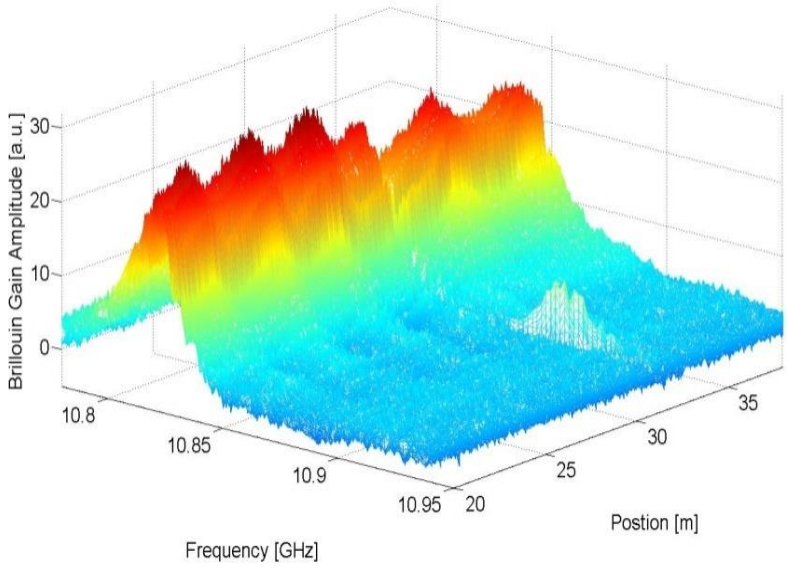

Figure 5-12 Experiment result: Spectral distribution along the fiber

To show the spatial resolution of our fiber, we plot the Brillouin signal at the frequency of the hot spot, which is 10.91GHz in our experiment. From the right subplot of Figure 4, the rising edge of the Brillouin signal from 10% to 90% is 1cm. This confirms the spatial resolution of 1cm. The falling edge is longer than the rising edge, which is 1.7cm.

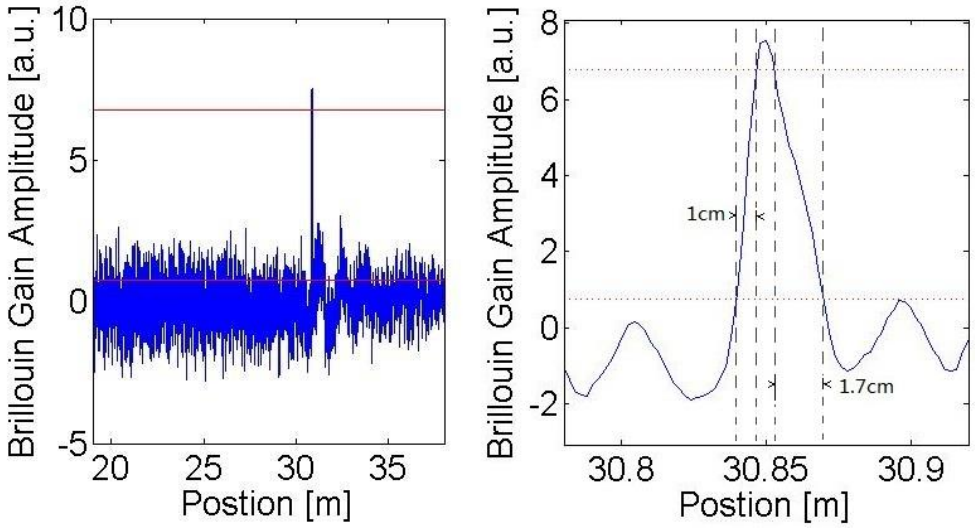

Figure 4 Brillouin signal at the frequency 10.87GHz

We theoretically and experimentally analyzed and compared the performance of BOTDA systems employing simplex code and complementary coded pump pulses. Both schemes demonstrate significant enhancement to SNR performance of the BOTDA systems. The results show that the two schemes have similar acquisition time, memory space requirement in order to realize the same SNR enhancement comparing with BOTDA based on single phase modulated pump pulse. By using complementary coded pulses with individual pulse duration of 0.1 ns, 1-cm high resolution BOTDA system based on phase modulated pump pulse has been realized.

While using complementary code, it is important to ensure that the pulses representing “1” and ‘-1’ are identical to each other. Otherwise a large amount of

noise will be introduced to the Brillouin signal since the autocorrelation outside the peak can not cancel each other completely. A large DC component can also result from the imperfect shape of the pulses.

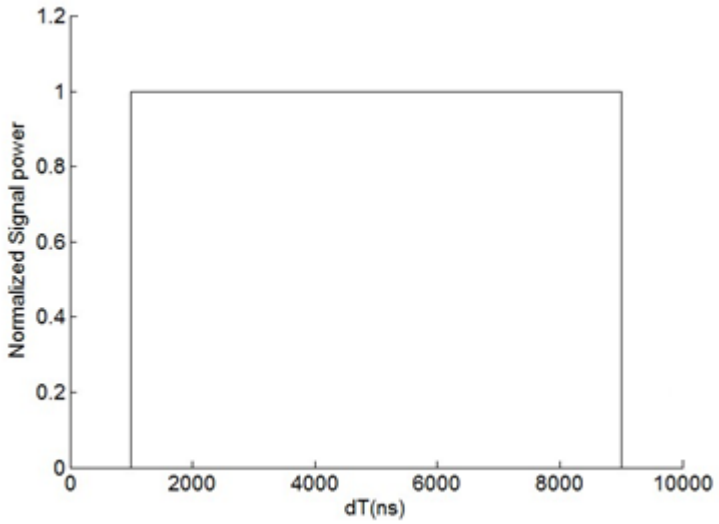

Figure 5-13 Simplified impulse response from a fiber

A simulation is carried out to show the effect of the imperfect code sequences on the experimental results. The fiber is assumed to be uniform and the effect of the acoustic lifetime is ignored so the impulse response of the fiber can be simplified as a square function as shown in Figure 5-13. We then calculate the signal received when perfect code sequences are sent into the fiber and use the decoding process to obtain the amplifier Brillouin probe signal. We also calculate the received signal and decoded signal when the code sequences are imperfect. The decoding is done by the equation $R_i(t) = r(t) \otimes C_i(t)$. The

obtained results for codes sequences with different amplitude for “1”s and “-1”s is shown in Figure 5-14. When the ratio indicated is the ratio between the amplitude for “1” and the amplitude for “-1”.

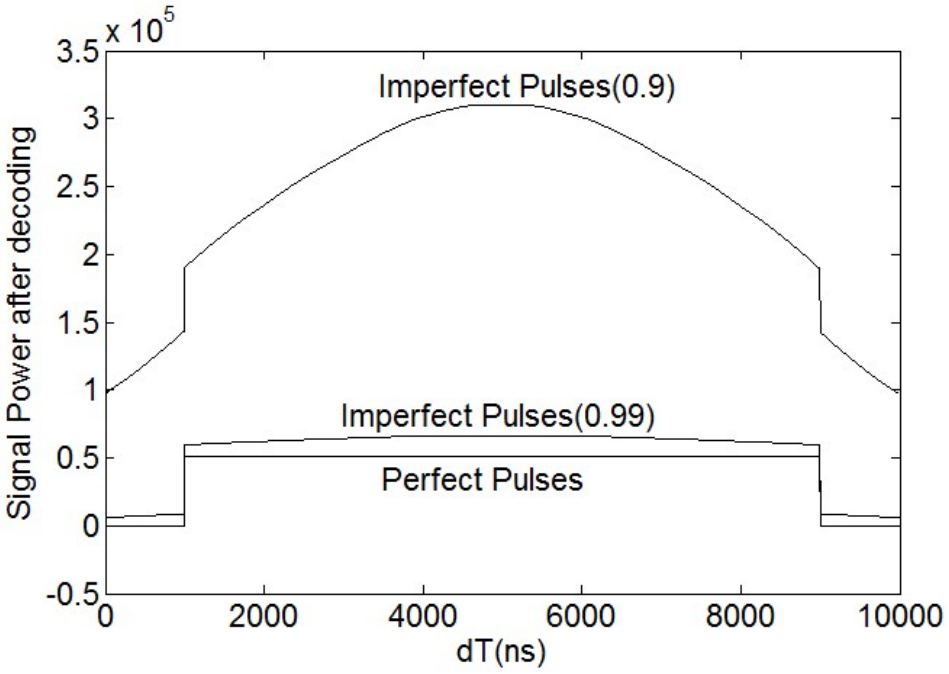

Figure 5-14 Signal after decoding

From Figure 5-14 we can see when the pulses representing the “1”s and the “-1”s of the code sequences are perfectly square and have the same amplitude, the signal can be fully recovered as the impulse response of the fiber, with a code gain depending on the length of the code being used. However, when the amplitude of the “1” and “-1” is different, although they are still square pulses, the decoded signal will be distorted. When the different between the amplitude is

1% the results is slightly distorted and is still acceptable when used to calculate the Brillouin gain spectral distribution. When the different is large, about 10% in our case, the distortion is so significant that it is difficult to be used to calculate the spectral distribution along the fiber.

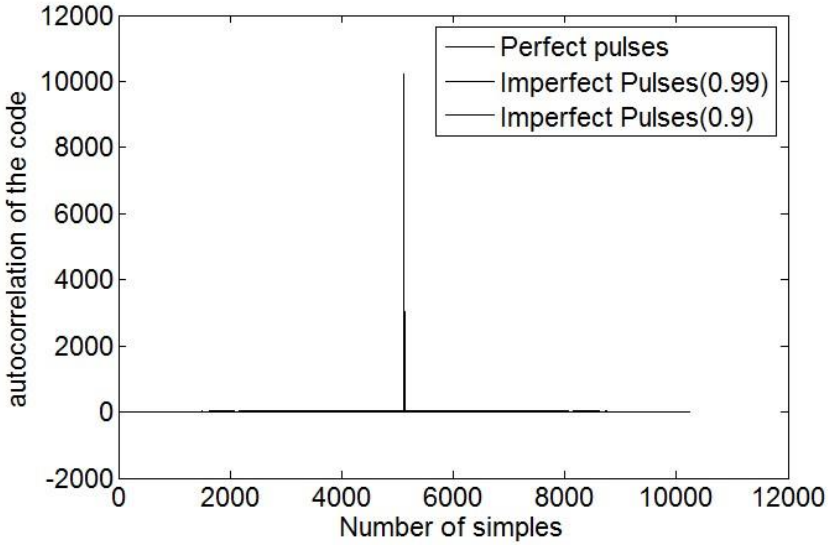

Figure 5-15 Autocorrelation of different codes

To understand why there is such a big distortion, we calculate the autocorrelation of the three sequences used above using A*A+B*B. The results are shown in Figure 5-15 and Figure 5-16. From Figure 5-15 we can see the autocorrelation of the three code sequences are very similar. The value at the local point is very high, which means even when the pulses are distorted, we can still get a big coding gain. This can be seen from Figure 5-14, even the results from a distorted code sequence maintain the basic shape of the impulse response

and has a large coding gain.

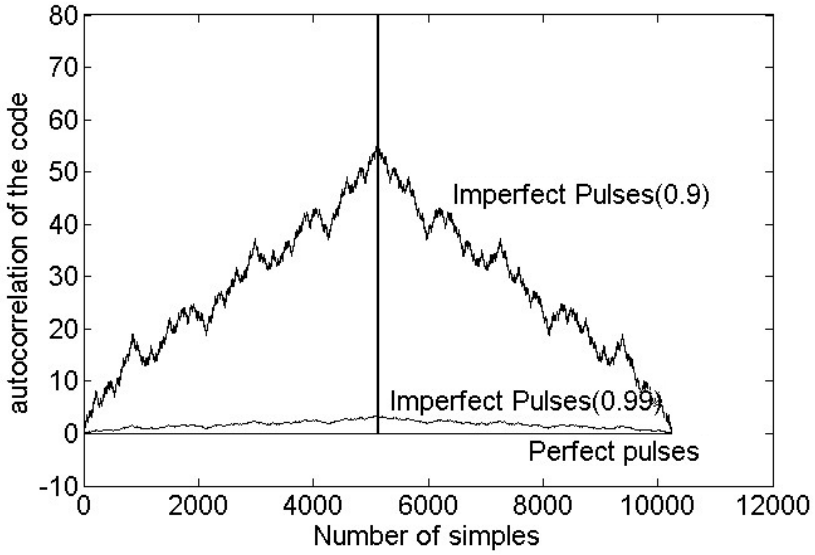

Figure 5-16 Autocorrelation of different codes (details about the noise floor)

A more detailed result is shown in Figure 5-16. Here we pay more attention to the lower amplitude portion of the autocorrelation results. From Figure 5-16 it is clear that the autocorrelation cancels each other outside the local point. This good autocorrelation ensures that the decoded signal only contains the local information at each point. When the code sequences are imperfect, the autocorrelation outside of the local point can not fully cancel each other. If this code is used in the experiment, which is always the case, the value in the decoded signal contains a little bit of signals from the points far away from the point being calculated and a large error is introduced into this point. Although in Figure 5-16, the residual value outside the local point is very small compare to

the value of the local point shown in Figure 5-15, the effect is still significant since the number of the points is large and their integration is comparable with the peak value in Figure 5-15. Unfortunately, in the experiment it is very difficult to tune the amplitude for the pulse represent “1” and “-1” to be at the same value. The difference may come from the imperfect signal generated by the function generator or the imbalance of the modulator used to generate the pulse. There is always a distortion of the decoded signal. We have to tune it carefully to ensure the different is as small as possible to reduce this distortion.

Besides the imbalance of the amplitude for the “1”s and “-1” of the code sequence, the distortion of the pulse will make the case even worse. We introduce some small differences in the shape of the pulses for “1”s and “-1”s, and calculate the decoded signal. The result is shown in Figure 5-17. The pulses representing “-1” is distorted slightly compare to the pulses representing “1”. From this figure we can see the distortion of the pulses causes larger error to the result compare to the effect of amplitude difference. We can also see from the figure that the distortion is worse for longer code length. This will limit the length of the code that can be used in the BOTDA system. For applications where longer codes are needed, better signal source with smaller signal distortion is essential.

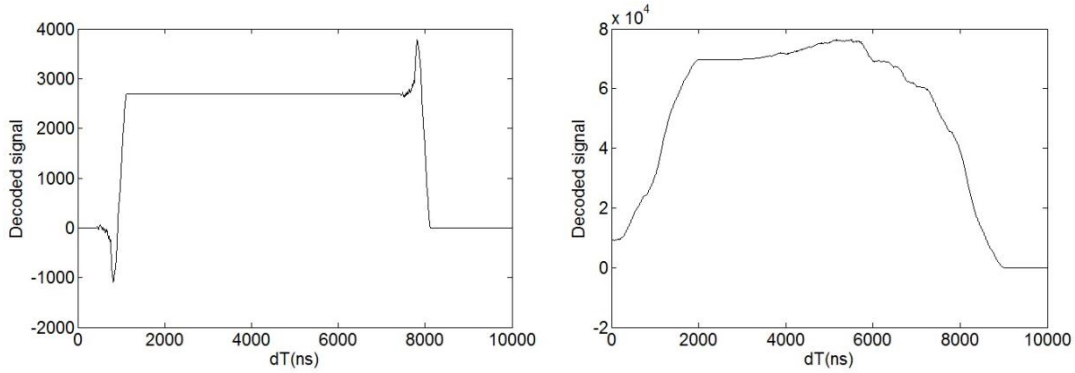

Figure 5-17 Decoded signal for 128bits signal and 1024bits signal with distorted pulses

5.4 Improve the Quality of the Brillouin Signal

As discussed in Chapter 4, distributed sensing with either high spatial resolution or long sensing range is very challenging. On one hand very short pulses is needed to realize high spatial resolution. With very short pulses there are two consequences. Firstly the Brillouin signal will be very weak since the strength of the signal is linearly proportional to the width of the pump pulse. Secondly the linewidth of the Brillouin signal will become so wide that the measured Brillouin spectrum will have significant amount of uncertainty and the measurand (Temperature or Strain) can not be measured very accurate. On the other hand, the sensing range of the distributed sensing system based on Stimulated Brillouin scattering is limited by the pump depletion, modulation instability, and other nonlinear effect in the fiber.

These problems become even more seriouly when we try to combine high

spatial resolution and long sensing range together. With high spatial resolution, we will have a very small Brillouin signal. With long sensing range, the signal is decaying due to the pump depletion and there is a very strong DC component in the Brillouin signal which is difficult to be removed. Now we combine all these problems together, which means we will have a very small signal over a strong DC component and the signal itself is decaying. In addition, we always have the problem of noise in any BOTDA system.

The back scattered signal for one frequency step is shown in Figure 5-18. The signal is from a 25km long G.652D fiber. During the experiment the pump pulse is 20ns corresponding to a 2m spatial resolution. The frequency of the probe signal is set at 10.83GHz lower than the pump signal, which is the Brillouin shift of the G.652D fiber. The reflected signal is then detected by a 125MHz photodiode and measured by an Agilent scope (DCA-J 86100C).

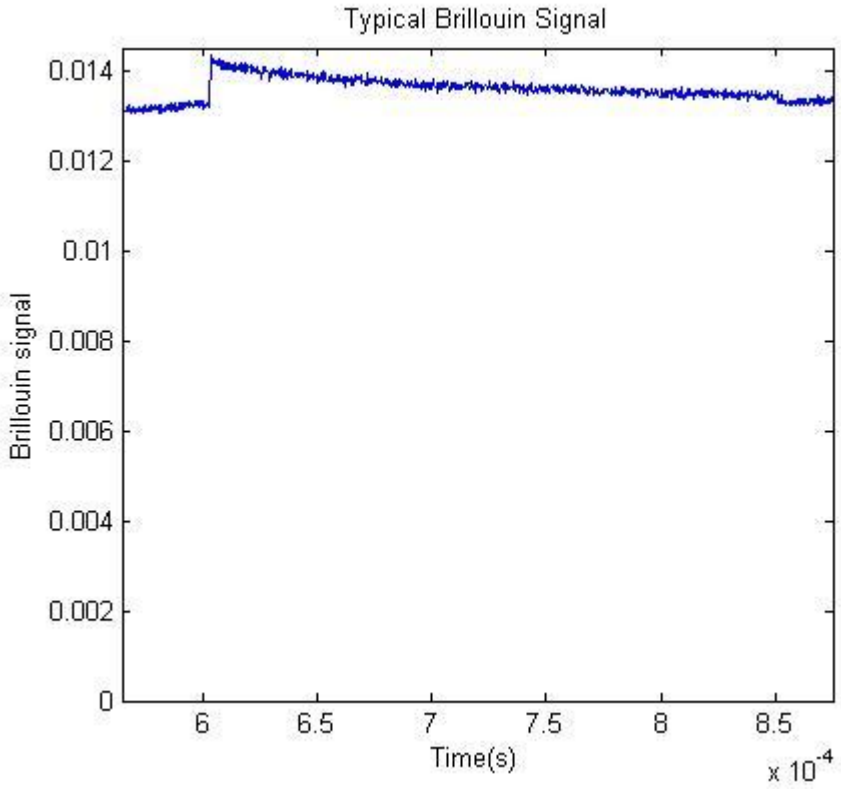

Figure 5-18 Brillouin signal from 25km G652D fiber

From Figure 5-18 we can see the SNR at the end of the fiber is very small. If we want to measure this signal correctly we need to improve the SNR at this critical point. At the same time, we have to reduce the DC components so that this signal can be detected by the real time scope with high accuracy.

When we try to further reduce the width of the pump pulse to achieve a higher spatial resolution, the Brillouin signal become even weaker and it cannot be detected properly.

In order to improve the Brillouin signal at the critical point, we used

complementary coding technology and Raman Amplifier in the experiment. As shown in Section 0. By using the Complementary coding technology, the SNR of the Brillouin signal has been enhance and the strength of the signal are also amplified due to the coding gain. To compensate the depleted pump power, a Raman amplifier is added to the setup.

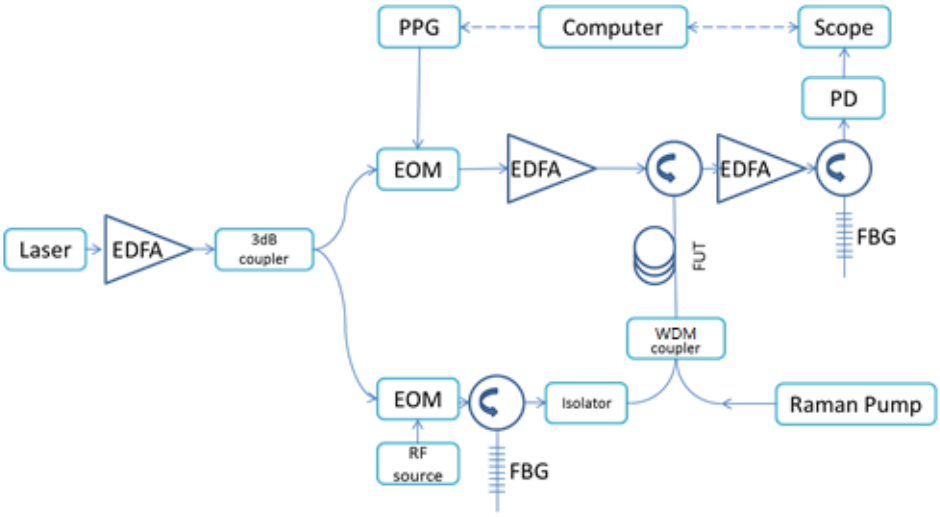

Figure 5-19 BOTDA setup with Raman assistant

The setup is shown in Figure 5-19. It is similar with the setup being used before except a Raman pump is added to the setup. The light from the Raman pump is counter-propagating with the Brillouin pump. So when the power of the Brillouin pump decayed due to the depletion, it can be amplified by the Raman pump. This gain can compensate part of the depleted power. Using this setup we can measure the signal as shown in Figure 5-20. During the experiment 512bits

of complementary code is used and the pulse width of each bit is 100ps, which is corresponding to a spatial resolution of 1cm.

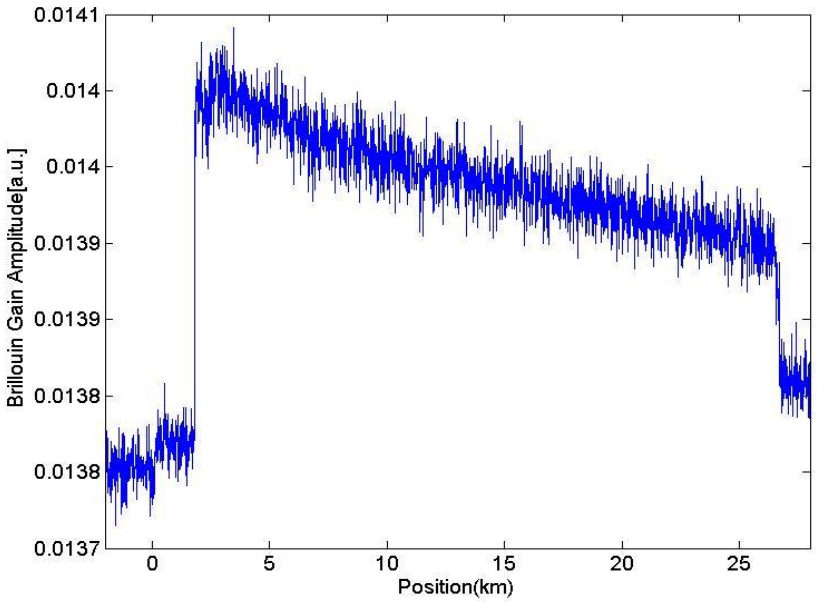

Figure 5-20 Brillouin signal after carefully adjust the system

From Figure 5-20 we can see the SNR at the critical point is much better than before and the signal strength is also better. At the same time, there is a strong noise which is introduced by the Raman amplifier. Because of the large noise, the 1cm spatial resolution sensing still cannot be fully demonstration till now. Effort should be paid to tune the system and reduce the noise coursed by the Raman pump to realize 1cm spatial resolution over 25km fiber.

In conclusion, by using Raman amplification and complementary coding

technology, we can excite Brillouin signal using 100ps pulses train over a 25km fiber. In future this setup can be used to realized 1cm spatial resolution over 25km fiber. The number of the sensing points of this sensing system is approximately 2.5million, which is the largest to our knowledge.

CHAPTER 6. CONCLUSIONS AND FUTURE WORK

In this Chapter, conclusions are given and suggestions for future work are presented.

6.1 Summary

Distributed optical fiber sensing techniques enable the measurement of temperature or strain distribution simultaneously along the fiber with high spatial resolution. In this thesis distributed sensing system based on Brillouin scattering was studied. The main noise sources of the system were identified. Characteristics of the backscattered signal were analyzed carefully in order to identify methods to improve the performance of the system. By using complementary coding of the pump signal, high spatial resolution distributed sensing over long sensing fiber had been realized. The coding and decoding process of the complementary code had been studied and it was shown that signal to noise ratio of the system can be improved greatly.

Major achievements of the thesis work are summarized as follows:

- The distributed sensing systems were studied in detail and the main challenges of realizing distributed sensing with high spatial resolution over long distance were addressed. A detailed study of the acoustic lifetime of different type of optical fibre has been presented for the first time.

- A BOTDA system with phase modulated pulse sequence is proposed

and demonstrated. Significant SNR enhancement is demonstrated experimentally through pump phase modulation using Simplex code.

- Using complementary code, distributed sensing with 1cm spatial resolution was realized. The performance of the sensing system, especially the SNR of the signal, is enhanced greatly due to the coding gain of this technique. Coding and decoding process of complementary code were investigated and key factors limiting the performance of this coding technique were identified.

- Wavelength selective coupling and wavelength selective polarization have been proposed and demonstrated for PCF fibres. They can potential be used for distributed sensing systems.

6.2 Recommendations for Future Work

In chapter 5, the work on the use of coding technique to enhance the performance of the Brillouin sensing systems was reported. The signal power of the sensing system was enhanced by the coding gain of the complementary code so that the signal can be detected even when the signal is very small due to the high spatial resolution and the long sensing range. The coding technique can also be used for selectively sensing part of the fiber by using code sequence at

both ends of the fiber for both the pump and the probe signals, similar to that of BOCDA systems. In this case the Brillouin gain at a specific part of the fiber can be enhanced while it will be reduced in other parts. By changing the delay of the code sequences used, the part of fiber where the gain is enhanced can be varied. This is particularly useful since in some applications, we are only interested in the temperature or strain distribution at some specific parts of the fiber instead of the whole length of the fiber. In these cases the measurement time can be greatly reduced by measuring the signal from the selected part instead of the whole fiber.

There are other advantages when selectively measuring the temperature or strain distribution along certain part of a fiber. In Chapter 4, we analyzed the difficulties for realizing distributed sensing over long distance with high spatial resolution. In addition to the limitation of the signal quality, measurement time is another issue. One possible way to overcome the conflict between time consuming and high spatial/long distance is that we can combine high spatial resolution and low spatial resolution approaches together. A fast scan with low spatial resolution can be applied to the whole sensing fiber to locate the hot spot roughly. Later a more detailed scan can be applied part of the fiber which contain the hot spot. Using the combination of these two types of system, the

measurement time can be reduced and the signal processing can be easier since for both types of scan fewer amounts of data will be processed. This can also reduce the requirements of the signal processing part of the system and reduce the cost of the whole system. In chapter 6 some preliminary work about PCF is reported. By design the structure of the PCF, the characteristics of the fiber can be tuned. A new type of PCF can be designed for specified Brillouin sensing, such as PCF with Brillouin frequency more sensitive to temperature and less sensitive to strain or more sensitive to strain but less sensitive to temperature. Types of PCF with high Brillouin gain can also be used to enhance the performance of Brillouin sensor. As discussed in Chapter 4, Brillouin sensing system with high spatial resolution and long sensing range can be limited by the poor signal quality, using a fiber with high Brillouin gain and low loss will enhance the quality of the signal greatly and may result in a system with much better performance.

LIST OF REFERENCE

[1] K. C. Kao and G. A. Hockham, “Dielectirc-fiber surface waveguides for optical frequencies,” Proceedings of the Institution of Electrical Engineers-London, Volume 113, pp.1151-1158, 1966.

[2] B. Culshaw, “Optical fiber sensor technologies: opportunities and-perhaps pitfalls,” Journal of Lightwave Technology, Volume 22, pp.39-50, 2004.

[3] M. K. Barnoski and S. M. Jensen, “Fiber waveguides: a novel technique for investigating attenuation characteristics,” Applied Optics, Volume 15, Issue 9, pp.2112-2115, 1976

[4] J. P. Dakin, D. J. Pratt, and G. W. Bibby, J. N. Ross, “Distributed optical Raman temperature sensor using a semiconductor light source and detector,” Electronics Letters, Volume 21, pp.569-570, 1985.

[5] L. Brillouin, “La Viscosité Des Liquides Et Son Interprétation Théorique,” Journal De Physique et Le Radium, Volume 3, Issue 9, pp.326-340, 1922.

[6] L. Mandelstam and J. Tamm, “Elektrodynamik der anisotropen Medien in der speziellen Relativitätstheorie,” Mathematics and Statistics, Volume 95, Issue 1, pp.154-160, 1926.

[7] E. Gross, “Change of Wave-length of Light due to Elastic Heat Waves at Scattering in Liquids,” Nature, Volume 126, Issue 3171, pp.201-202, 1930.

[8] R. Lucas and P. Biquard, “Propriétés Optiques des Milieux Solides et Liquides Soumis Aux Vibrations Élastiques Ultra Sonores,” Journal De Physique, Volume 3, pp.464-477, 1932.

[9] P. Debye and F. W. Sears, “On the Scattering of Light by Supersonic Waves,” Proceedings of The National Academy of Sciences, Volume 18, Issue 6, pp.409-414, 1932.

[10] E. P. Ippen and R. H. Stolen, “Stimulated Brillouin scattering in optical fibers,” Applied Physics Letters, Volume 21, Issue 11, pp.539-541, 1972.

[11] T. C. Rich and D. A. Pinnow, “Evaluation of Fiber Optical Waveguides Using Brillouin Spectrosocpy,” Applied Optics, Volume 13, Issue 6, pp.1376-1378, 1974.

[12] A. Kobyakov, S. Kumar∗, D. Q. Chowdhury, A. B. Ruffin, M. Sauer, and S. R. Bickham, “Design concept for optical fibers with enhanced SBS threshold,” Optics Express, Volume 13, No. 14, pp.5338-5346, 2005.

[13] J. B. Coles, B. P. P. Kuo, N. Alic, S. Moro, C. S. Bres, J. M. C. Boggio, P. A. Andrekson, M. Karlsson, and S. Radic, “Bandwidth-efficient phase modulation techniques for Stimulated Brillouin Scattering suppression in fiber optic parametric amplifiers,” Optics Express, Volume 18, Issue 17, pp.18138-18150, 2010.

[14] N. A. Olsson and J. P. Van Der Ziel, “Fiber Brillouin amplifier with electronically controlled bandwidth,” Electronics Letters, Volume 22, Issue 9, pp.488-490, 1986.

[15] P. Bayvel and I. P. Giles, “Linewidth narrowing in semiconductor laser pumped all-fiber Brillouin ring laser,” Electroinics Letters, Volume 25, Issue 4, pp.260-262, 1989.

[16] P. Bayvel and I. P. Giles, “Evaluation of performance parameters of single-mode all-fiber Brillouin ring lasers,” Optics Letters, Volume 14, Issue 11, pp.581-583, 1989.

[17] R. W. Tkach, A. R. Chraplyvy, and R. M. Derosier, “Performance of a WDM network based on stimulated Brillouin scattering,” IEEE Photonics Technology Letters, Volume 1, Issue 5, pp.111-113, 1989.

[18] K. Y. Song, M. G. Herráez, and L. Thévenaz, “Observation of pulse delaying and advancement in optical fibers using stimulated Brillouin scattering,” Optics Express, Volume 13, Issue 1, pp.82-88, 2004.

[19] Y. Okawachi, M. S. Bigelow, J. E. Sharping, Z. M. Zhu, A. Schweinsberg, D. J. Gauthier, R. W. Boyd, and A. L. Gaeta, “Tunable All-Optical Delays via Brillouin Slow Light In an Optical Fiber,” Physics Review Letters, Volume 94, Issue 15, pp.153902-(1-4), 2005.

[20] J. Rohren, and L. Q. Gothard, Encyclopedia of Physical Science, P. 155.

[21] K. Kageyama, H. Murayama, K. Uzawa, I. Ohsawa, M. Kanai, Y. Akematsu, K. Nagata, and T. Ogawa, “Doppler effect in Flexible and Expandable Light Waveguide and Development of New Fiber-Optic Vibration/Acoustic Sensor,” Journal of Lightwave Technology, Volume 24, Issue 4, pp.1768-1775, 2006.

[22] F. C. Li, H. Murayama, K. Kageyama, and T. Shirai, “Doppler effect-based fiber-optic sensor and its application in ultrasonic detection, Optical Fiber Technology, Volume 15, Issue 3, pp.296-303, 2009.

[23] C. V. Raman and K. S. Krishnan, “A new type of Secondary Radiation,” Nature, Volume 121, pp.501-502, 1928.

[24] F. C. Li, H. Murayama, K. Kageyama, and I. Ohsawa, “Multiple damage assessment in composite laminates using a Doppler-effect-based fiber-optic sensor,” Measurement Science and Technology, Volume 20, Issue 11, pp.1-10, 2009.

[25] R. A. Serway, “Physics for scientists and engineers,” Third Edition, Saunders, pp.1150, 1990.

[26] F. W. Sears, M. W. Zemansky and H. D. Young, University Physics, Sixth Edition, Addison-Wesley, pp.843–844, 1983.

[27] H. Hertz, “Ueber den Einfluss des ultravioletten Lichtes auf die electrische Entladung,” General and Introductory Physics, Volume 267, Issue 8, pp.983-1000, 1887.

[28] R. A. Serway, Physics for Scientists & Engineers, third edition, pp.1150, 1990.

[29] R. W. Boyd, Nonlinear Optics, fourth edition, Academic press, 2008.

[30] Smekal, “Zur Quantentheorie der Dispersion,”, Naturwissenschaften, Volume 11, Issue 43, pp.873-875, 1923.

[31] G. Landsberg, and L. Mandelstam, “Eine neue Erscheinung bei der Lichtzerstreuung in Krystallen," Naturwissenschaften, Volume 16, Issue 28, pp.557, 1928.

[32] S. F. Mafang, “Brillouin Echoes for Advanced Distributed Sensing in Optical Fibers,” These No. 4958 (2011), École Polytechnique Fédérale de Lausanne.

[33] D. K. Gifford, B. J. Soller, M. S. Wolfe, and M. E. Froggatt, “Distributed Fiber-Optic Temperature Sensing using Rayleigh Backscatter,” in Proc. ECOC 2005, pp.005, We4, 2005.

[34] Y. Koyamada, M. Imahama, K. Kubota, and K. Hogari, “Fiber-Optic Distributed Strain and Temperature Sensing With Very High Measurand Resolution Over Long Range Using Coherent OTDR,” Journal of Lightwave Technology, Volume 27, Issue 9, pp.1142-1146, 2009.

[35] J. P. Dakin, D. J. Pratt, G. W. Bibby, J. N. Ross, “Distributed optical fiber Raman temperature sensor using a semiconductor light source and detector,” Electronics Letters, Volume 21, Issue 13, pp.569-570, 1985.

[36] L. Thévenaz, “Brillouin Distributed Time-Domain Sensing in Optical Fibers: State of the Art and Perspective,” Frontiers of Optoelectronics in China, Volume 3, Issue 1, pp.13-21, 2010

[37] A. J. Rogers, “Distributed optical-fiber sensors,” Journal of Physics D: Apply Physics, Volume 19, pp.2237-2255, 1986.

[38] D. Culverhouse, F. Farahi, C. N. Pannell, and D. A. Jackson, “Potential of stimulated Brillouin scattering as sensing mechanism for distributed temperature sensor,” Electronics Letters, Volume 25, Issue 14, pp.913-915, 1989.

[39] T. Kurashima, T. Horiguchi, and M. Tateda, “Distributed-temperature sensing using stimulated Brillouin scattering in optical silica fibers,” Optics Letters, Volume 15, Issue 18, pp.1038-1040, 1990.

[40] X. Bao, D. J. Webb, and D. A. Jackson, "22-km distributed temperature sensor based on Brillouin gain in an optical fiber", Optics Letters, Volume 18, Issue 7，pp.552-554, 1993.

[41] X. Bao, D. J. Webb, and D. A. Jackson, "32-km distributed temperature sensor using Brillouin loss in an optical fiber", Optics Letters, Volume 18, Issue 18, pp.1561-1563, 1993.

[42] T. Horiguchi, T. Kurashima, and Y. Koyamada, “1 m spatial resolution measurement of distributed Brillouin frequency shift in signle-mode fibers,” in Tech. Dig. Symp. Opt. Fiber Meas., NIST special Publication 864, pp.73-76, 1994.

[43] M. Nickles, L. Thevenaz, and P. A. Robert, “Measurement of the distributed-Brillouin-gian specturem in optical fibers by using a single-laser source,” in Tech. Dig., OFC 1994, paper WF1, pp.89-90, 1994.

[44] X. Bao, A. Brown, M. De Merchant and J. Smith, "Characterization of the Brillouin-loss spectrum of single-mode fibers by use of very short (<10-ns) pulses", Optics Letters, Volume 24, Issue 8, pp.510-512, 1999.

[45] V. Lecoeuche, D. J. Webb, C. N. Pannell, and D. A. Jackson, “Transient response in highresolution Brillouin-based distributed sensing using probe pulses shorter than the acoustic relaxation time,” Optics Letters, Volume 25, pp.156-158, 2000.

[46] L. Zou, X. Bao, Y. Wan, and L. Chen, “Coherent probe-pump-based Brillouin sensor for centimetre-crack detection,” Optics Letters, Volume 15, pp.370-372, 2005.

[47] A. W. Brown and B. G. Colpitts, “Dark-Pulse Brillouin optical Time-Domain Sensor with 20-mm Spatial Resolution,” Journal of Lightwave Technology, Volume 25, Issue 1, pp.381-386, 2007.

[48] M. A. Soto, G. Bolognini, and F. Di Pasquale, “Long-range simplex-coded BOTDA sensor over 120 km distance employing optical preamplification,” OPTICS LETTERS, Volume 36, Issue 2, pp.277-279, 2011.

[49] X. Bao and L. Chen, “Recent Progress in Optical Fiber Sensors Based on Brillouin scattering in Ottawa University,” Photonics Sensors, Review, Volume 1, Issue 2, pp.102-117, 2011.

[50] L. Thévenaz and S. F. Mafang, "Distributed fiber sensing using Brillouin echoes" in 19th International Conference on Optical Fiber Sensors, Perth, Australia, pp.70043N-(1-4), 2008.

[51] K. Hotate, and T. Hasegawa, “Measurement of Brillouin gain spectrum distribution along an optical fiber using a correlation-based technique -

proposal, experiment and simulation," IEICE Trans. Electronics, E83-C, 405-412, 2000.

[52] K. Y. Song, Z. He, and K. Hotate, "Distributed strain measurement with millimeter-order spatial resolution based on Brillouin optical correlation domain analysis," Optics Letters, Volume 31, Issue 17, pp.2526-2528, 2006.

[53] T. Kurashima, T. Horiguchi, and Y. Koyamada, "New technique to shift lightwave frequency for distributed fiber optic sensing," Proc. SPIE 1797, pp.18-30, 1992.

[54] K. Shimizu, T. Kurashima, T. Horiguchi, and Y. Koyamada, "New technique to shift lightwave frequency for distributed fiber optic sensing," Proceeding of SPIE 1797, pp.18-30, 1993.

[55] T. Kurashima, T. Horiguchi, H. Izumita, S. Furukawa, and Y. Koyamada, "Brillouin Optical-Fiber Time Domain Reflectometry," IEICE Transactions on Communications, Volume E76-B, Issue 4, pp.382-290, 1993.

[56] K. Shimizu, T. Horiguchi, and Y. Koyamada, "Measurement of distributed strain and temperature in a branched optical fiber network by use of Brillouin optical time-domain reflectometry," Optics Letters, Volume 20, Issue 5, pp.507-509, 1995.

[57] H. G. Shiraz and T. Okashi, "Fault Location in Optical Fibers Using Optical Frequency Domain Reflectometry," Journal of Lightwave Technology, Volume LT-4, Issue 3, pp.316-322, 1986.

[58] D. Garus, K. Krebber, F. Schliep, and T. Gogolla, "Distributed sensing technique based on Brillouin Optical-fiber Frequency-domain analysis," Optics Letters, Volume 21, Issue 17, pp.1402-1404, 1996.

[59] D. Garus, T. Gogolla, K. Krebber, and F. Schliep, "Brillouin optical-fiber frequency-domain analysis for distributed temperature and strain measurements", IEEE Journal of Lightwave Technol., Volume 15, Issue 4, pp.654-662, 1997.

[60] K. Hotate, and M. Tanaka, "Distributed fiber Brillouin string sensing with 1-cm spatial resolution by correlation-based continuous-wave technique", IEEE Photonics Technology Letters, Volume 14, Issue 2, pp.779-781, 2002.

[61] T. Yari, K. Nagai, M. Ishioka, K. Hotate, and Y. Koshioka, “Aircraft Structural Health Monitoring using on-board BOCDA system,” Proc. Of SPIE, Volume 6933, pp.69330S, 2008.

[62] M. Imai, R. Nakano, T. Kono, T. Ichinomiya, S. Miura, and M. Mure, “Crack Detection Application for Fiber Reinforced Concrete Using BOCDA-Based Optical Fiber Strain Sensor,” Journal of Structural Engineering, Volume 136, Issue 8, pp.1001-1008, 2010. G. P. Agrawal, Nonlinear Fiber Optics, 2nd ed. (Academic, Boston, Mass., 1995).

[63] T. R. Parker, M. Farhadiroushan, V. A. Handerek, and A. J. Rogers, “A Fully Distributed Simultaneous Strain and Temperature Sensor Using Spontaneous Brillouin Backscatter”, IEEE Photonics Technology Letters, Volume 9, Issue 7, pp.979-981, 1997.

[64] G. P. Agrawal, Nonlinear Fiber Optics, 2nd ed. (Academic, Boston, Mass., 1995).

[65] L. Thévenaz and J-C. Beugnot, "General analytical model for distributed Brillouin sensors with sub-meter spatial resolution" in 19th International Conference on Optical Fiber Sensors, Edinburgh, United Kingdom, pp.75036A-4, 2009.

[66] M. A. Soto, G. Bolognini, F. Di Pasquale and L. Thévenaz, “Long-range Brillouin optical time-domain analysis sensor employing pulse coding techniques”, Measurement Science and Technology, Volume 21, Issue 9, pp.094024(1-7), 2010.

[67] M. D. Jones, “Using Simplex Codes to Improve OTDR Sensitivity”, IEEE Photonics Technology Letters, Volume 15, Issue 7, pp.822-824, 1993.

[68] P. K. Sahu, M. A. Soto, J. Lee, G. Bolognini, N. Park, and F. Di Pasquale, "Analysis of Brillouin-Based Distributed Fiber Sensors Using Optical Pulse Coding," in Optical Fiber Communication Conference and Exposition and The National Fiber Optic Engineers Conference, OSA Technical Digest (CD) (Optical Society of America), paper OMT1, 2008.

[69] M. A. Soto, G. Bolognini, F. Di Pasquale, and L. Thévenaz, “Simplex-coded BOTDA fiber sensor with 1m spatial resolution over a 50 km range”, Optics Letters, Volume 35, Issue 2, pp.259-261, 2010.

[70] M. A. Soto, G. Bolognini, and F. Di Pasquale, “Analysis of optical pulse coding in spontaneous Brillouin-based distributed temperature sensors”, Optics Express, Volume 16, Issue. 23, pp.19097-19111, 2008.

[71] M. Nikles, L. Thevenaz, and P. A. Robert, “Brillouin gain spectrum characterization in single-mode optical fibers”, Journal of Lightwave Technology, Volume 15, Issue 10, pp.1843-1851, 1997.

[72] L. Thévenaz , “Brillouin distributed temperature and strain sensing” in COST Madeira School.

[73] A. Othonos, K. Kalli, D. Pureur, and A. Mugnier, “Fiber Bragg Gratings”, Springer Series in Optical Sciences, Volume 124, pp.189-269, 2006.

[74] S. M. Foaleng, M. Tur, J. C. Beugnot, and L. Thévenaz, “High Spatial and Spectral Resolution Long-Range Sensing Using Brillouin Echoed,” Journal of Lightwave Technology, Volume 28, Issue 20, pp.2993-3003, 2010.

[75] M. Nikeles, L. Thévenaz, and P. A. Robert, “Simple distributed fiber sensor based on Brillouin gain spectrum analysis,” Optics Letters, Volume 21, Issue 10, pp.758-760, 1996.